

2021

Innovative magnetorheological devices for shock and vibration mitigation

Xiaojing Zhu

Follow this and additional works at: <https://ro.uow.edu.au/theses1>

University of Wollongong

Copyright Warning

You may print or download ONE copy of this document for the purpose of your own research or study. The University does not authorise you to copy, communicate or otherwise make available electronically to any other person any copyright material contained on this site.

You are reminded of the following: This work is copyright. Apart from any use permitted under the Copyright Act 1968, no part of this work may be reproduced by any process, nor may any other exclusive right be exercised, without the permission of the author. Copyright owners are entitled to take legal action against persons who infringe their copyright. A reproduction of material that is protected by copyright may be a copyright infringement. A court may impose penalties and award damages in relation to offences and infringements relating to copyright material.

Higher penalties may apply, and higher damages may be awarded, for offences and infringements involving the conversion of material into digital or electronic form.

Unless otherwise indicated, the views expressed in this thesis are those of the author and do not necessarily represent the views of the University of Wollongong.

Recommended Citation

Zhu, Xiaojing, Innovative magnetorheological devices for shock and vibration mitigation, Doctor of Philosophy thesis, School of Mechanical, Materials, Mechatronic and Biomedical Engineering, University of Wollongong, 2021. <https://ro.uow.edu.au/theses1/1104>

Research Online is the open access institutional repository for the University of Wollongong. For further information contact the UOW Library: research-pubs@uow.edu.au



UNIVERSITY
OF WOLLONGONG
AUSTRALIA

Innovative magnetorheological devices for shock and vibration mitigation

Xiaojing Zhu

Supervisors:

Senior Prof. Weihua Li

Prof. Haiping Du

Dr. Shuaishuai Sun

This thesis is presented as part of the requirement for the conferral of the degree:

Doctor of Philosophy of the Engineering

University of Wollongong

School of Mechanical, Materials, Mechatronic and Biomedical Engineering

June 2021

Abstract

Vibration and impact protection have been a popular topic in research fields, which could directly affect the passengers' and drivers' comfort and safety, even cause spines fracture. Therefore, an increasing number of vehicle suspensions and aircraft landing gears are proposed and manufactured. Magnetorheological fluids (MRFs), as a smart material, are growly applied into the above device owing to its unique properties such as fast response, reversible properties, and broad controllable range, which could improve the vibration/impact mitigation performance.

MRF was utilized to achieve adaptive parameters of the vehicle suspensions by controlling the magnetic field strength of the MRF working areas. Generally, the magnetic field is provided by a given current, subsequently, it would consume massive energy from a long-term perspective. Thus, a self-powered concept was applied as well. This thesis reports a compact stiffness controllable MR damper with a self-powered capacity. After the prototype of the MR damper, its property tests were conducted to verify the stiffness controllability and the energy generating ability using a hydraulic Instron test system. Then, a quarter-car test rig was built, and the semi-active MR suspension integrated with the self-powered MR damper was installed on a test rig. Two controllers, one based on short-time Fourier transform (STFT) and a classical skyhook controller was developed to control the stiffness. The evaluation results demonstrate that the proposed MR damper incorporated with STFT controller or skyhook controller could suppress the response displacements and accelerations obviously comparing with the conventional passive systems.

Landing gears, gun recoil systems, are generally employed to mitigate the impacts during crash landing events or the gun recoils in wars, protecting human being from spine fractures and devices from structural failures. Similar to the vehicle suspensions, both the

passive and active landing gears have them inherit limitations. Therefore, MR dampers are applied in semi-active landing gears which could adapt to various impacts. For conventional MR damper, the MRF is normally accommodated in two chambers connected by a narrow bypass and a piston. When shocks occur, the piston will push the MRF into another chamber to mitigate the impact. Nevertheless, this design requires massive MRF. Besides, if the impact velocities are too large, the velocity of the MRF in the bypass will be excessive large due to a huge pressure difference, which will trigger an enormous damping force, being detrimental to passengers and the aircrafts. Therefore, an MR damper with a novel structure was proposed in this thesis. The unique structure design reduces the use of MRF, while avoiding the risk of excessive MRF speed. Additionally, a control algorithm was proposed to be applied on the new MR damper to obtain a stable damping force under different impact velocities and scenarios. The experimental results illustrate that the new damper could offer a stable damping force over the sink rate from 2m/s to 5m/s.

Acknowledgments

First of all, I would like to express my sincere appreciation to my principal supervisor, Senior Prof. Weihua Li, for accepting me as a PhD student of UOW and for his support and help over the past few years. It is Professor Li who helped me adapt to the new life-style of Australia and guided me on the path of research. As an expert in my research field, I can always benefit a lot from his wise opinions no matter on the improvement of the research proposal or the suggestions in the process of research. In addition, he is not only my academic guide, but also my mentor in my life. His working attitude also inspires me, which keeps me humble and hungry. His selfless guidance and encouragement helped me become a better person.

In the meanwhile, I would also like to thank my co-supervisors, Professor Haiping Du, and Dr Shuaishuai Sun, who gave me lots of valuable help and suggestions in my PhD study. I also want to express my gratitude to my wife, Suying Wang, and my daughters, Wangyu Zhu and Keyu Zhu, who understand and support me to pursue the doctoral degree without any complaints. It is your trust and encouragement that keep me motivated at all times. Additionally, I would like to extend my gratitude and respect to my friends and colleagues, Donghong Ning, Jian Yang, Xin Tang, Dan Yuan, Lei Deng, Bo Yang, Matt Christie, Zisu Ma, Zhuonan Hao, Xinyu Chen, Shida Jin, thank you for your help and company. Finally, I would like to thank all of you who helped me grow up. Every experience I had with you is truly meaningful.

Certification

I, Xiaojing Zhu, declare that this thesis submitted in fulfilment of the requirements for the conferral of the degree of Doctor of Philosophy, from the University of Wollongong, is wholly my own work unless otherwise referenced or acknowledged. This document has not been submitted for qualifications at any other academic institution.

Xiaojing Zhu

20th March 2021>>

TABLE OF CONTENT

Abstract	i
Acknowledgments	iii
Certification	iv
Table of Content	v
List of Figures	ix
List of Tables	xv
Chapter 1. Introduction	1
1.1 Research Background and Motivation	1
1.2 Research Objectives	3
1.3 Novelty and Significance	错误!未定义书签。
1.4 Outline	4
Chapter 2. Literature review	7
2.1 Magnetorheological (MR) fluid materials.....	7
2.2 MR Damper	13
2.2.1 Linear MR Damper	13
2.3 Semi-active Vehicle Suspension System	26
2.4 Energy-regenerative technology for MR damper.....	30
2.5 Landing gears	34
2.6 Classical semi-active control algorithms.....	39
2.7 linear feedback control	42

2.8 Modern intelligent control algorithm	42
2. 9 Conclusions	45
Chapter 3. Development of a stiffness variable MR damper with self-powered generation capacity	47
3.1 Introduction	47
3.2 Design, analysis, and prototype of the self-powered variable stiffness MR damper	48
3.2.1 Structural design of the new damper	48
3.2.2 Working principle	51
3.2.3 Prototype of the new damper	52
3.3 Modelling and theoretical analysis	53
3.3.1 Modelling	53
3.3.2 Magnetic field simulation	57
3.4 Experimental testing and result discussion.....	58
3.4.1 Experimental setup	58
3.4.2 Stiffness testing.....	59
3.4.3 Testing of the self-powered generation capacity	64
3.5 Conclusion.....	69
Chapter 4. Experimental evaluation of the self-power variable stiffness damper on a quarter-car test rig.....	71
4.1 Introduction	71
4.2 Experimental evaluation of the self-powered variable stiffness damper on a	

quarter-car test rig	72
4.3 The mathematic model for quarter-car test system	73
4.4 Road excitations design.....	74
4.5 Evaluation under sweep excitation.....	76
4.6 Control strategy Development.....	77
4.6.1 The control algorithm preparation	77
4.6.2. Skyhook control algorithm	80
4.6.3 STFT control algorithm	83
4.7 Conclusion.....	89
Chapter 5. Design, modelling, and testing of semi-active impact absorber.....	91
5.1 Introduction	91
5.2 Design, analysis, and prototype of the impact absorber	92
5.2.1 Structure prototype of the impact absorber.....	92
5.2.2 Magnetic field simulation	94
5.3 Numerical evaluation	100
5.3.1 Block diagram building	100
5.3.2. The development of the control equation	102
5.3.3 Simulation results	103
5.4 Experimental tests	106
5.4.1 Property test of the proposed linear impact absorber	106
5.4.2 Constant current impact tests	107
5.4.3 Controlled current impact tests	111

5.5 Conclusion.....	115
Chapter 6. Conclusion and future work	116
6.1 Summary of the semi-active MR suspension with self-powered capacity.....	116
6.2 Summary of the semi-active MR landing gears	117
6.3 Future work of the semi-active MRF vehicle suspension	118
6.4 Future work of the semi-active MRF landing gear	120
References	121
Publications during the PhD candidature	135

LIST OF FIGURES

Figure 2.1 State variation of MR fluid (© 2005 Lord Corporation).	9
Figure 2.2 MR damper (Avraam, 2009). Model no: RD-8041-1	13
Figure 2.3 (a) Mono tube MR damper, (b) twin-tube MR damper,	16
Figure 2.4 (a) Internal coil MR damper and (b) external coil MR damper.	16
Figure 2.5 (a) Flow mode MR damper, (b) shear mode MR damper, (c) squeeze mode MR damper, and (d) mixed mode MR damper.	17
Figure 2.6 (a) Single coil MR damper, (b) double coil MR damper, and (c) multi coil MR damper.	18
Figure 2.7 (a) Inner bypass MR damper and (b) MR damper with external bypass.	18
Figure 2.8 Schematic structure of integrated MR fluid damper.	19
Figure 2.9 Schematic structure of valve mode MR fluid damper [59].	20
Figure 2.10 Schematic structure of mixed-mode MR fluid damper [59].	20
Figure 2.11 Schematic of multimode MR isolator [61].	21
Figure 2.12 Schematic of the bypass-type MR fluid damper [59].	22
Figure 2.13 Schematic configurations of the bypass-type MR fluid shock dampers with internal coils: (a) double-ended MR shock damper and (b) single-ended MR shock damper. [63].	23
Figure 2.14 Schematic configuration and photo of the porous bypass-type MR fluid damper with external coils: (a) schematic structure and (b) photo [64].	24
Figure 2.15 The prototype MR fluid damper with three-stage piston [67].	25
Figure 2.16 Expedition MR fluid damper with two-stage piston [48].	26

Figure 2.17 MacPherson type suspension model [86].	29
Figure 2.18 Linear quarter car model with 2-DOF [90].	30
Figure 2.19 Schematic structure of a self-powered MR fluid damper [23].	31
Figure 2.20 (a) Schematic of EMI system and (b) prototype of large-scale EMI system. [92].	32
Figure 2.21 Schematic diagram of the self-powered MRF damper-based vibration control system [13].	33
Figure 2.22 Schematic diagram of a smart passive system and the generator [22].	33
Figure 2.23 Sectional view of self-powered, self-sensing MR damper [94].	34
Figure 2.24 The schematic diagram of the active landing gear [98].	35
Figure 2.25 The configuration of the new damper [99].	36
Figure 2.26 Schematic diagram of MR landing gear in half-vehicle [99].	36
Figure 2.27 The shock strut and landing gear diagram [100].	37
Figure 2.28 Schematic configuration of MR damper with two cores [101].	37
Figure 2.29 Schematic diagram of the MR absorber [102].	38
Figure 2.30 Dynamic model of the landing gear [102].	38
Figure 2.31 Skyhook control model.	40
Figure 2.32 Groundhook control model.	40
Figure 2.33 Hybrid control model.	41
Figure 3.1 Structure schematic of the new damper.	49

Figure 3.2 Schematic of the MR damping cylinder: (a) MR damper with a conventional piston [123] and (b) Inner bypass MR damper cylinder used in the new damper ..	50
Figure 3.3 Working principle of the stiffness variation	52
Figure 3.4 Prototype of the new damper	53
Figure 3.5 Dynamic model of the variable stiffness damper	55
Figure 3.6 Magnetic field simulation	57
Figure 3.7 Average flux density through activation regions of the innovative MR damper	58
Figure 3.8 Instron test system installed with the prototype	59
Figure 3.11 Equivalent stiffness of the damper	61
Figure 3.12 Property comparison between the passive MR damper and self-powered MR damper (a) 20mm amplitude (b) 30mm amplitude	62
Figure 3.13 Comparison between the experimental results and simulation results	64
Figure 3.14 Rectifier circuits of the self-powering component (a) parallel connection (b) series connection	66
Figure 3.15 The effect of the rectifier circuit on the power generation. (a) Directly generated voltage and rectified voltage of G1, (b) Rectified voltage of G1 and G2 connecting in series and parallel	68
Figure 3.16 Self-generating capability under different amplitude	68
Figure 3.17 Modelling results of the self-powering component	69
Figure 4.1 Quarter car test system for the novel suspension evaluation	72
Figure 4.2 Mathematic model for quarter-car test system	73

Figure 4.3 Road excitations generator	75
Figure 4.4 The random road signal	75
Figure 4.5 The frequency spectrum of the random road signal	76
Figure 4.6 Transmissibility comparison under different cases	77
Figure 4.7 MyRIO pin configurations of connectors (a) A, B and (b) C	79
Figure 4.8 NI MyRIO-1900 and PID controllers	79
Figure 4.9 (a) Prototype and (b) circuit diagram of the MOSFET	80
Figure 4.10 Flow diagram of skyhook control.....	81
Figure 4.11 The LabVIEW program of the skyhook controller	82
Figure 4.12 Comparison among three above cases.....	83
Figure 4.13 The ideal transmissibility graph of the two working modes.....	84
Figure 4.14 The measured transmissibility graph	84
Figure 4.15 The flow diagram of STFT control strategy	85
Figure 4.16 The LabVIEW program of the STFT control algorithm	86
Figure 4.17 Acceleration comparison between the controlled MR damper and passive MR damper.....	87
Figure 4.18 The control signal and self-powered energy of the MR damper under random excitation.....	88
Figure 4.19 Displacement response comparison between passive suspension and controlled MR suspension (a) Time domain, (b) Frequency domain	89
Figure 5.1 The structural comparison between the new MR damper and the conventional one.....	93

Figure 5.2 The prototype of the impact absorber	94
Figure 5.3 Magnetic field simulation	95
Figure 5.4 The magnetic flux density	96
Figure 5.5 The averaged magnetic flux density	96
Figure 5.6 Yield Stress vs. Magnetic field strength	97
Figure 5.7 B-H curve.....	98
Figure 5.8 Comparison for yield stress	99
Figure 5.9 Comparison for B-H curve	99
Figure 5.10 Yield stress calculation	100
Figure 5.11 Yield force simulation	102
Figure 5.12 Viscous part	102
Figure 5.13 The acc-velocity-displacement relationship	103
Figure 5.14 Displacements under different currents with 2m/s impact velocity	104
Figure 5.15 Real-time velocities under different currents with 2m/s impact velocity ..	104
Figure 5.16 Forces under different currents with 2m/s impact velocity	105
Figure 5.17 MTS test system	107
Figure 5.18 Force-displacement plots under different currents	107
Figure 5.19 The experimental setup for impact tests.	108
Figure 5.20 Displacement-time plot.....	109
Figure 5.21 Force-time plot	109
Figure 5.22 (a) The proposed MR damper; (b) The conventional damper	111

Figure 5.23 Real-time (a) Force (b) Current (c) Displacement of the control process with 4m/s impact velocity.	113
Figure 5.24 The effect of control gain k	114
Figure 5.25 The control gain k selection.....	114
Figure 5.26 The mean peak force versus impact velocity.....	115
Figure 6.1 Prototype of the MOSFET switch circuit in improved Skyhook control strategy	119
Figure 6.2 Operation flow diagram of the improved Skyhook control strategy	120

LIST OF TABLES

Table 2-1 Different types of operation mode	10
Table 2-2 Various MR non-linear models	11
Table 2-3 Classification of MR fluid damper	14
Table 3-1 Parameters for MR damper.....	50
Table 3-2 Parameters used in modelling of self-powering component.....	56
Table 3-3 Estimated model parameters of the MR damper	63
Table 4-1 Symbol declaration	74
Table 4-2 RMS value	89
Table 5-1 Typical properties of MRF-140CG (From Lord company).....	97
Table 5-2 Parameters of effective area.....	101

Chapter 1

Introduction

1.1 Research Background and Motivation

Suspension of vehicle systems supports the whole weight of the vehicle, offers the ability of directional control during maneuvering and also provides the ability to reduce the vibration generated by the road disturbances. Therefore, suspension of vehicle is a key component that has great influence on the performance of vehicle. In addition, a classical suspension of vehicle consisted of two parts: a spring and a damper [1]. The suspension dissipates energy by the damper and stores energy in the spring. Usually, the process of energy dissipation may lead uncomfortable or harsh ride, although it is helpful for the stability of vehicle. The demand to decrease the negative effect of the process has promoted the development of many advanced suspensions. Controllable suspension system is reckoned as a promising way of optimizing the compromise between the handling of the vehicle and the ride comfort [2].

Particularly, active and semi-active vehicle suspensions are two typical intelligent suspensions which are controllable to improve the ride comfort and the handling of the vehicle. Although active suspension may reduce vibration more, the disadvantages of possible instability, complex control algorithms, and large power consumption limit its common use [3-6]. More interest has recently been given to the semi-active vehicle suspension because it requires less power, uses cheaper hardware, and has sufficiently good performance. In fact, a great deal of research on semi-active control of vehicle suspensions has already been reported. The semi-active vehicle suspension offers both the stability of the uncontrollable passive suspension system and the effective control performance of the active suspension without the need of large energy consumption [7-

9].

Magnetorheological (MR) fluid, which can be reversibly changed its rheological characteristics such as plasticity, elasticity and viscosity by the application of a controllable magnetic field, has been widely employed in the field of vibration control [10-13]. MR fluid is significantly fast responsive to magnetic field, with an estimated time of the response which is less 10 ms [14, 15], and needs relatively low energy to support. In recent years, MR fluid is used for the MR damper as a working liquid becoming one of the most promising components for semi-active vehicle suspensions [16-18], due to excellent dynamical features of MR fluid such as large yield stress, fast response, low power consumption, and robust characteristics within various environments. However, the MR damper still requires external energy supply to assure the generation of magnetic field for the MR fluids, though the external power consumption is relatively small and approximately several watts for one MR damper. While considering there are at least four MR dampers in one car during their long-time operation, the total consuming energy cannot be ignored. It will add the fuel consumption of the vehicles. Additionally, the external power cables will also reduce the reliability of vibration control system [19]. Hence, many researchers investigated the potential harvesting energy if all potential power is regenerated by suspension vibration. The simulation performed by Segel and Lu [20] demonstrated that approximately 200W of power is dissipated by four dampers when a passenger car is running on a road. Additionally, the self-powered MR damper has exhibited promising features and studied by some researchers currently [13, 21-25].

Besides self-powered MR dampers mentioned above, variable stiffness MR vehicle suspension is an innovative semi-active vibration control systems and performs better than constant stiffness controllable system [26]. Many research have been carried out to

develop the concept of the controllability of variable MR vehicle suspension [27, 28]. Although the better performance of the variable stiffness has been proved, compact devices capable of self-power generation and varying stiffness for practical applications have rarely been researched and manufactured.

Based on this motivation, this work proposes a new stiffness variable MR vehicle suspension with self-power generation capability. The performance of the self-powered vehicle suspension on vibration attenuation has been evaluated on a quarter car test rig. The vibration reduction evaluation of the self-powered vehicle suspension is evaluated under two kinds of excitations, i.e. harmonic excitation and random excitation. The experimental results indicate that the self-powered vehicle suspension outperforms the uncontrolled suspension and the commercialized suspension, which verified its capability for providing better ride comfort.

1.2 Research Objectives and Aims

To clarify the main aims of this research, the specific objectives are as follows:

- Design and prototype an MR vehicle suspension which could provide a variable stiffness and self-power generation capability.
- Optimise the stiffness variable MR vehicle suspension with self-powered generation capacity to be suitable for both on-road and off-road situation.
- Evaluate the optimized suspension on a quarter car test rig under two kinds of excitations, i.e. harmonic excitation and random excitation.
- Design and manufacture a landing gear integrated with a novel MR damper to achieve a less velocity dependent property.
- Evaluate the shock mitigation performance under various impact velocities of the MR landing gear combined with a bang-bang current control algorithm.

1.3 Novelty and Significance

This thesis focuses on shock and vibration mitigation based on MR devices. Regarding the vibration mitigation part, a unique integration of self-generated capacity and stiffness-variable property was proposed. In addition, STFT control algorithm was employed in the proposed MR device (MR vehicle suspension) to improve the mitigation performance further. The entire combination of the MR devices and control methods is innovative in vibration mitigation field. In relation to the shock suppression, an MR damper which features a novel structure was prototyped, which provides another original alternative to achieve stable force during variable shocks used in vehicles or aircrafts.

1.4 Outline

This thesis consists of six chapters. Chapter 1 briefly introduces the research background and motivation, objectives, the scope, and the outline.

Chapter 2 presents a literature review which is generally divided into 9 parts. The first part introduces the smart material, MR fluids, that are utilized in this thesis. The working principle, working modes, and the proposed models to predict the mechanical properties are introduced. The second part details the damper based on MRF, and the classification according to different standards are listed in detail for illustration. The third part introduces the semi-active vehicle suspensions integrated with MR dampers, which is the focus of the Chapter 3 and 4 in this thesis. Then, the fourth part explains the principle of the self-powered techniques employed in MR damper, this technique is also utilised in this thesis. The work of helicopter landing gears is introduced in the fifth part from the passive landing gear to the semi-active ones, various control algorithms are applied on the landing gears as well. From the sixth part to eighth part, massive commonly used control strategy is described. The last part is a summary for the literature review.

Chapter 3 focuses on the fabrication of the new MR damper with controllable stiffness.

First of all, the mathematical models of the MR damper were built, and the magnetic field simulation was conducted to validate the feasibility of the self-powered concept and the controllable stiffness. After the fabrication of the MR damper, property tests were conducted to further prove the above desirable properties.

Chapter 4 described the investigations based on the stiffness-controllable MR damper proposed in Chapter 3, mainly to verify the feasibility of the MR damper in the real scenarios. First and foremost, the new MR damper was assembled on a quarter-car test rig. Then the transmissibility of different working modes of the suspension was measured by giving a sweep sinusoidal signal. That helped to adjust the stiffness of the system to avoid the resonance. In addition, a designated random vibration signal was employed to simulate the road excitations. The road test was conducted under several cases, the passive mode, the continuous self-powered mode, the skyhook controller (switch the on/off state of the self-powered component) mode, and the STFT mode. By the comparison of the experimental results under different working mode, the effectiveness of the control algorithm is verified. Moreover, an improvement based on skyhook controller is discussed for further study.

Chapter 5 proposed a novel linear multiple coils MR damper which could be employed on aircraft and helicopter landing gears. After designing the structure of the MR damper, the magnetic field simulation was built to validate that the given current could activate the MRF. Then, by employing the MTS tension and compression system, the property tests were conducted. In addition, for a fixed current, the relationship between peak damping force and impact velocities was obtained, the results show that the peak damper force increases as the impact velocities enlarge. To obtain a stable peak force under various shock velocities. A control method based on bang-bang current control was developed with an adjustable control gain. By multiple experiments, the control gain for

different impact velocities was attained. The new MR damper integrated with the proposed control algorithm was validated to be effective and efficient.

Chapter 6 summarized the main findings of this thesis and discuss the future work in this research field.

Chapter 2

Literature Review

Suspension of vehicle is a key component that has great influence on the performance of vehicle. For conventional passive suspensions of vehicle with constant parameter values, it is difficult to meet all the demand of different road disturbance, meanwhile for conventional active suspensions, the disadvantages of possible instability, complex control algorithms, and large power consumption limit their common use. With the development of automobile industry and the enhancement of customer demand, the semi-active technology applied on vehicle suspension is increasingly becoming wider, especially the application of magnetorheological technology with variable stiffness. However, the MR Suspension still requires external energy supply to assure the generation of magnetic field. Hence, many researchers investigated the potential self-powered MR suspensions if all potential power is regenerated by suspension vibration. This chapter reviews the studies related to the MR semi-active vehicle suspension system with variable stiffness and regeneration energy capacity, including MR material, device structure, energy-regenerative technology, and corresponding control strategies.

Compared with the vertical vibration caused by uneven roads that the vehicle suspensions experience, the vertical impacts, for example, crash landings of the helicopters, is worth investigating and discuss as well. Various landing gears are proposed in recent years, nevertheless, the impact mitigation capacity of the passive landing gears are limited due to the fixed parameters once manufactured. Therefore, MR technique has been increasingly applied into the landing gear systems.

2.1 Magnetorheological (MR) fluid materials

Magnetorheological (MR) fluid is unraveled by Jacob Rabinow in 1948 as a class of

“smart fluid”, due to its capability of producing MR effect widely employed to control vibration [29]. The MR effect is basically discovered as a significant change of MR fluid’s yielding shear stress continuously controlled by the intensity of magnetic fields. MR fluid consisted of micron magnetic particles such as iron or cobalt particles, and carrier fluid as well such as silicone oil or hydraulic oil [30, 31]. When magnetic field is unapplied, the magnetic particles such as iron or cobalt particles in MR fluid can move easily and smoothly, as shown in Figure 2.1(a). However, when exposed to the application of magnetic field, the magnetic particles could not move freely and restrictedly form a chain-like structure along with the line of magnetic induction. Actually, in this case, the magnetic particles are polarized and then attracted one to another along with the line of magnetic field, as illustrated in Figure 2.1(b). Specifically, MR fluid is able to change from a free-flowing liquid state into a semisolid state with restricted fluid movement in significantly fast response (an estimated time of the response which is less 10 ms) when under an application of magnetic field. Hence, comparing to conventional materials, MR fluid can present rheological transition and viscoelastic properties within milliseconds under the application of magnetic field with the help of its soft morphology and controllable rheology. Additionally, the energy consumption for semi-solid state of MR fluid is not a concern since MR fluid is able to reach high yield stress (50 kPa or more) with a magnetic field that can easily be created by an electromagnet applied at modest current and relative low voltage (1–2 A and 2–24 V).

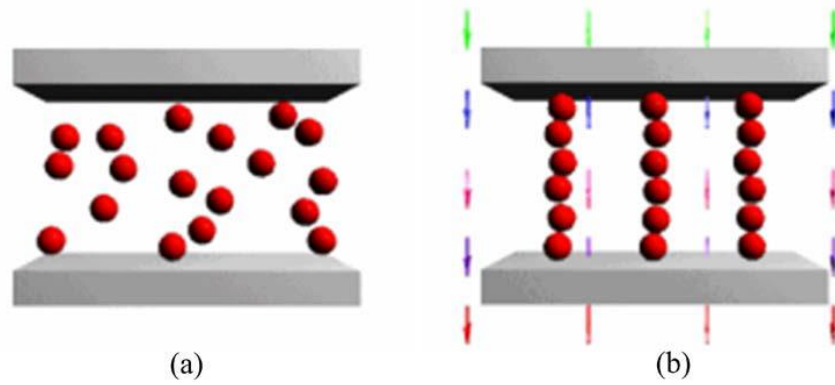


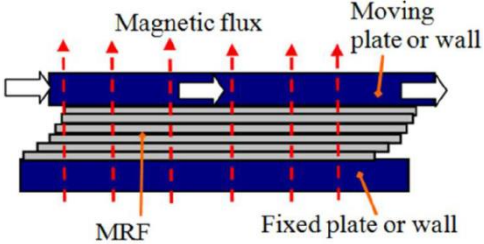
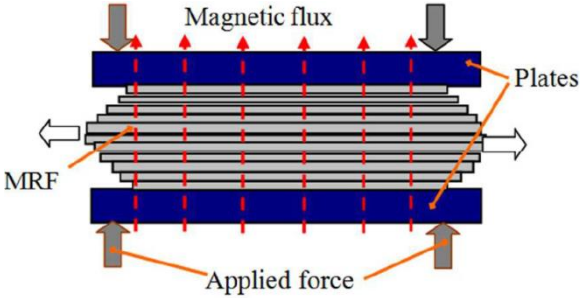
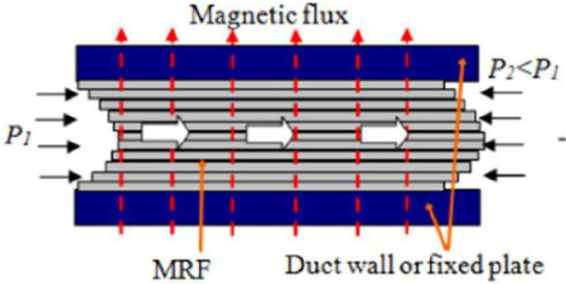
Figure 0.1 State variation of MR fluid (© 2005 Lord Corporation).

In free-flowing liquid state, MR fluid exhibits independent behavior of magnetic field with the plastic viscosity determined by the viscosity of the carrier fluid and micron magnetic particles volume fraction. In the semisolid state, MR fluid exhibits dependent behavior of magnetic field characterized by the variable yield stress which is dependent on the strength of applied magnetic field. Only when the shear stress exceeds the yield shear stress, MRFs come back to free flow state with nearly unchanged plastic viscosity [32, 33]. In addition, the temperature range of MR fluid's operation can be pretty large from -40°C to 150°C [34].

Moreover, based on the significant advantages of MR fluid, MR fluid is widely employed in rotary brakes, dampers, shock absorbers, clutches, rotary brakes, grinding devices, polishing and prosthetic devices, and so on. Concretely, all devices using MR fluid can be categorized in four modes: squeeze, shear, magnetic gradient pinch and valve, as illustrated in Table 2-1 [35-38]. Particularly, the valve mode is the most widely used mode for MR fluid, while the shear mode is basically suitable for dampers providing small forces or in compact brakes and clutches. In some MR fluid devices, two modes of MR fluid are combined together and applied inside the MR devices at the same. To develop MR fluid devices, MR fluid model plays a significant role as exact models can predict the performance of these MR fluid devices. MR fluid establishes nonlinear

behavior when exposing external magnetic fields. Various nonlinear models have been employed to characterize MR fluid, such as the Biviscous model, the Bingham plastic model, the and Herschel–Bulkley model, as shown in Table 2-2 [34, 39-44].

Table 0-1 Different types of operation mode

Types of modes	Figures	References
Shear [35]		Nguyen and Choi (2012)
Squeeze [35, 36]		Nguyen and Choi (2012) Farjoud et al. (2009)
Valve [35]		Nguyen and Choi (2012)

Pinch mode

Avraam (2009) [37]

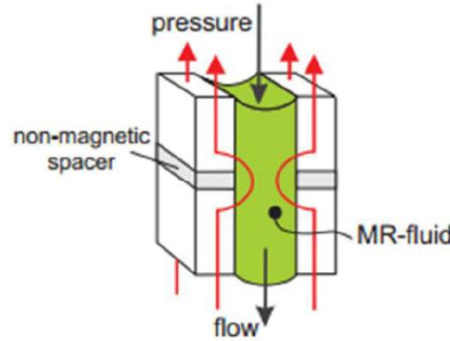
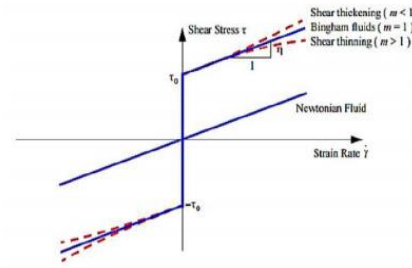


Table 0-2 Various MR non-linear models

Model name	Equation	Figure	Reference
Bingham plastic model [34, 39, 40]	$\tau = \tau_y(H) \text{sgn}(\dot{\gamma}) + \eta \dot{\gamma}, \tau > \tau_y$ $> \tau_y \tau = G \dot{\gamma}, \tau < \tau_y$ $H = \text{magnitude of applied field}$ $\dot{\gamma} = \text{fluid shear strain rate}$ $\text{sgn}(\cdot) = \text{signum function}$ $\eta = \text{plastic viscosity (at zero field)}$ $\tau = \text{shear stress}$ $\tau_y = \text{yielding shear stress}$ $G = \text{complex modulus of the material}$		Jolly et al. (1998), Wang and Liao (2011), and Weiss and Duclos (1994)
Biviscous model [34, 39, 41, 42]	$\tau = \begin{cases} \tau_y(H) + \eta \dot{\gamma}, & \tau > \tau_1 \\ \eta_r \dot{\gamma}, & \tau < \tau_2 \end{cases}$ $\tau_y(H) = \tau_1 \left(1 - \frac{\eta}{\eta_r}\right)$ $\eta_r \text{ and } \eta \text{ correspond to the elastic and viscous fluid properties}$		Stanway et al. (1996), Wang and Liao (2011), and Wilson and Thomas (2006)

Herschel–Bulkley model $\tau = (\tau_y(H) + K|\dot{\gamma}|^{1/m})\text{sgn}(\dot{\gamma})$
 K and m are the fluid parameters

[34, 39, 41-44]



Wang and Gordaninejad (2005), Choi et al. (2005), and Wang and Liao (2011)

The Bingham model of MR fluid demonstrates and explains the Bingham plastic behavior of MR fluid. In Bingham model, MR fluid seems to be a rigid body under low stress and behaves as a viscous and restricted fluid under high stress. The equations of Bingham model are presented in Table 2-2. In addition, Bingham plastic model can be employed to explain the post-yield. Nevertheless, Herschel–Bulkley model can be utilized to interpret shear thinning behavior of the MR fluid [37].

Due to the significant advantages of MR fluid, the MR instrument is increasingly becoming promising in practical application in many fields, including mechanical engineering, civil engineering and automotive suspension system. Furthermore, many MR fluid devices are capable of meeting the demands of real-world applications and are currently produced in large volumes. For instance, Lord Corporation is the world's largest MR fluid devices manufacture, producing MR fluid damper of vehicle suspension, as presented in Figure 2.2. Based on the development of MR fluid devices, many research has been carried out to develop the concept of the controllability of variable MR vehicle suspension. Although the better performance of the variable stiffness has been proved, compact devices capable of self-power generation and varying stiffness for practical applications have rarely been researched and manufactured. Therefore, how to design an effective compact model, which can regenerate energy and vary stiffness to fulfil the requirement of ride comfort and maneuverability, is an important starting point of the research. The following are some existing structure designs and applications for MR

damper.

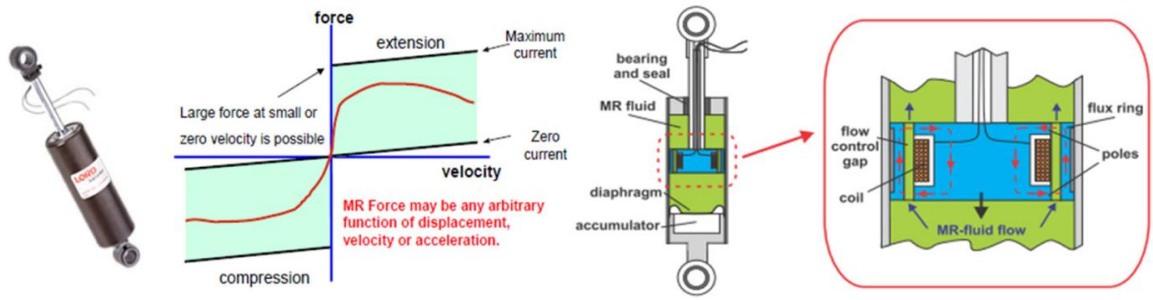


Figure 0.2 MR damper (Avraam, 2009). Model no: RD-8041-1

2.2 MR Damper

Basically, there are different types of MR fluid-based devices such as MR dampers, MR valve, and MR brake. The MR damper is commonly used in automobile and civil structure. Based on the movement of piston, MR dampers are categorized into rotary damper and linear damper. A rotary MR damper provides design compactness and substantial weight reduction thus requiring compacter room than a linear MR damper for device installation. Additional, a rotary MR damper also employs a smaller quantity of MR fluid, contributing significantly for cost reduction. However, linear MR damper has the capability to use relatively simple structure to change its damping stiffness by varying the magnetic field strength inside the damper. Coupling with embedded control system, linear MR dampers have gained popularity and proved its potential to enhance the performance of suspension systems. Therefore, linear MR dampers for automotive suspension systems are among the most popular MR fluid devices, as illustrated the details in the fellow part.

2.2.1 Linear MR Damper

An MR damper, which works as a vibration isolator, is a key component of semi-active vehicle suspension and it can be controlled by applying controllable magnetic field. Basically, a normal linear MR damper contains a piston rod, a piston head, magnetic coils, a damper housing, MR fluid, and an air gap. Piston rod coupled with piston head, while

magnetic coils are wrapped on piston head and then the coil-induced magnetic flux can flow through the MR fluid, as presented in Figure 2.3 [37]. If external power is applied to the magnetic coils during the movement of piston head, then it creates a magnetic field in the gap through which the MR fluid moves and raises the yield stress of the MR fluid in the circular gap. The increment of the yield stress increases the pressure drop down the length of the piston head and changes the velocity profile of the MR fluid in the gap. During the past two decades, the linear MR fluid damper gains significant developments and there are many different types of linear MR fluid dampers, as shown in Table 2-3 (Figure 2.3- Figure 2.7). Several typical linear MR dampers have comparative advantages, becoming increasingly popular.

Table 0-3 Classification of MR fluid damper

Based on design and configuration	Types	Figures
Parlak et al. (2013) [45]	Mono tube	Figure 2.3(a)
Avinash et al. (2014) [46]	Twin tube	Figure 2.3(b)
Wang et al. (2014) [47]	Double ended	Figure 2.3(c)
Poynor (2001) [48]	Hydraulic hybrid	Figure 2.3(d)

Based on layout of coils	Types	Figures
Sohn et al. (2015) [49]	Internal coil	Figure 2.4(a)
Hong et al. (2015) [50]	External coil	Figure 2.4(b)

Based on control valve	Types	Figures
-------------------------------	--------------	----------------

Kim et al. (2016c) [51]	Single flow mode Flow mode	Figure 2.5(a)
Wereley et al. (2007) [52]	Shear mode	Figure 2.5(b)
Olabi (2012) [53]	Squeeze mode	Figure 2.5(c)
Alghamdi and Yazid et al. (2014) [54]	Mixed mode	Figure 2.5(d)

Based on coil stage of the piston	Types	Figures
Ali and Ramaswamy (2009) [55]	Single coil	Figure 2.6(a)
Hu et al. (2016) [56]	Double coil	Figure 2.6(b)
Singh and Wereley (2014) [57]	Multi coil	Figure 2.6(c)

Based on bypass design	Types	Figures
Bai et al. (2015) [58]	Inner bypass	Figure 2.7(a)
Alghamdi and Olabi (2012) [53]	External bypass	Figure 2.7(b)

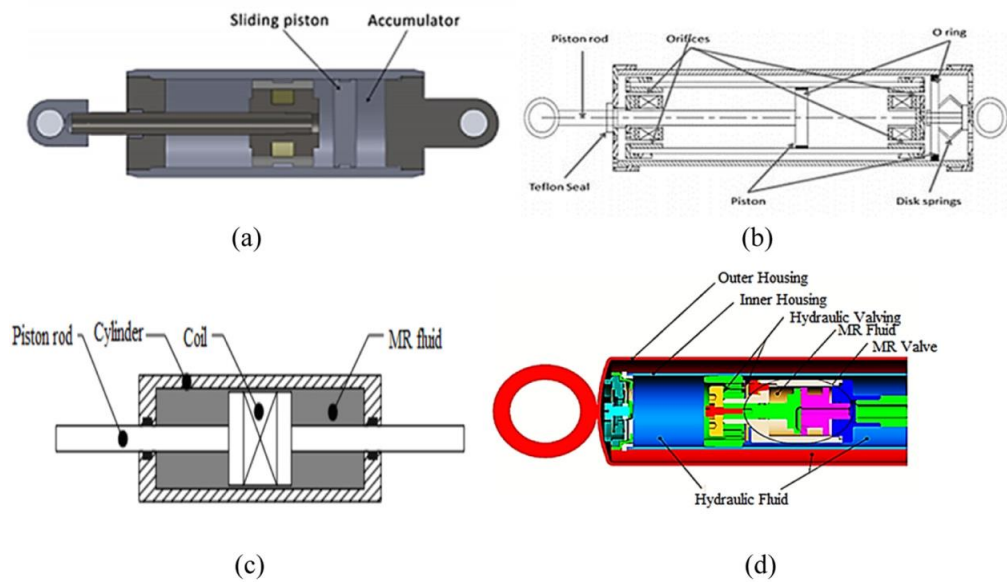


Figure 0.3 (a) Mono tube MR damper, (b) twin-tube MR damper, (c) double-ended MR damper, and (d) hydraulic hybrid.

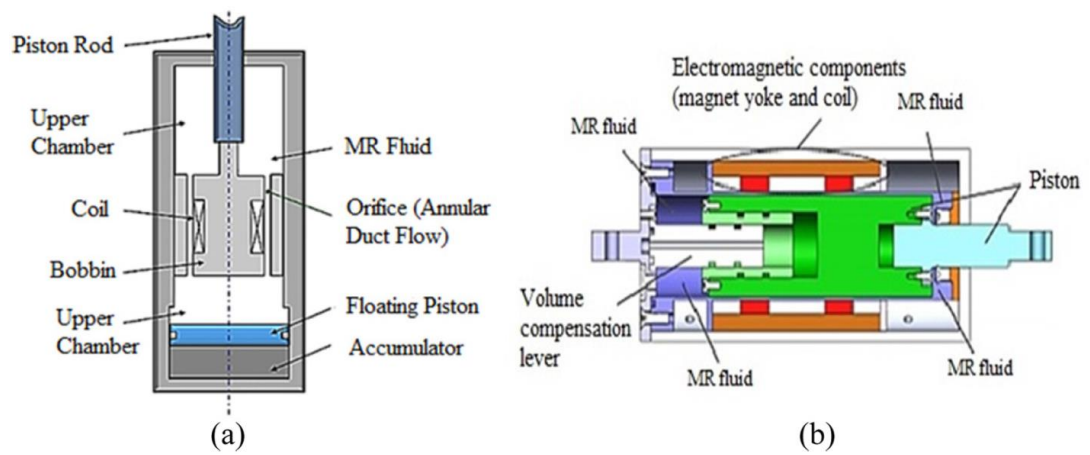


Figure 0.4 (a) Internal coil MR damper and (b) external coil MR damper.

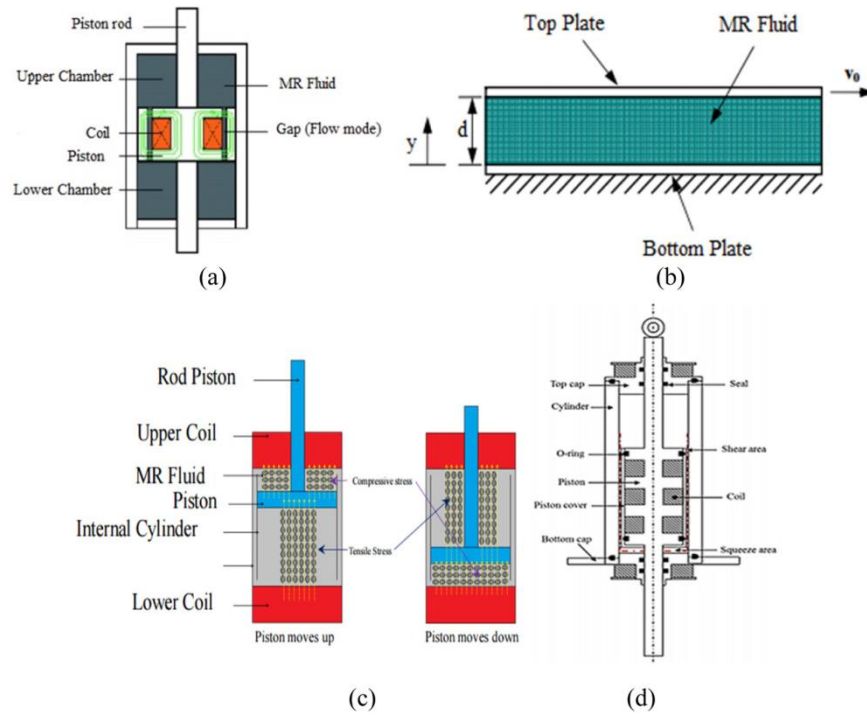


Figure 0.5 (a) Flow mode MR damper, (b) shear mode MR damper, (c) squeeze mode MR damper, and (d) mixed mode MR damper.

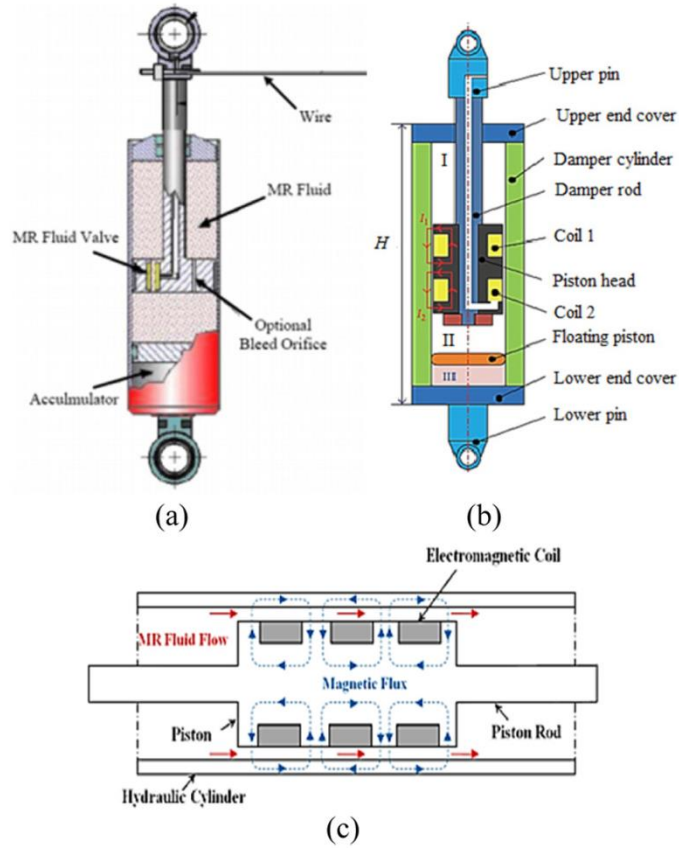


Figure 0.6 (a) Single coil MR damper, (b) double coil MR damper, and (c) multi coil MR damper.

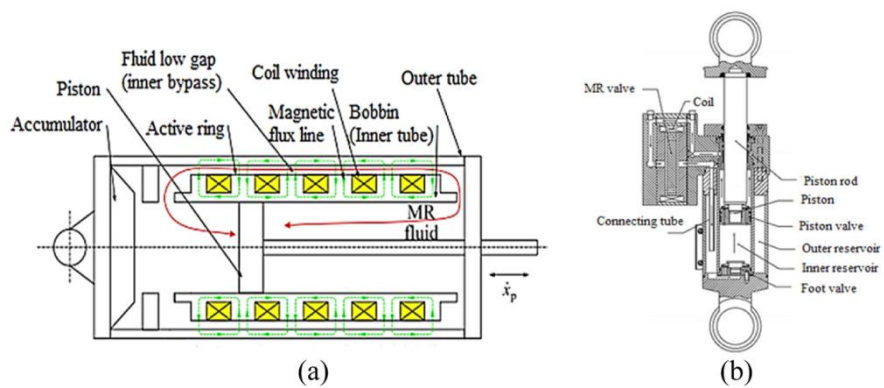


Figure 0.7 (a) Inner bypass MR damper and (b) MR damper with external bypass.

Double-ended structure.

A double-ended structure is a special arrangement of elements from the mono-tube structure, as shown in Figure 2.3 (c). The two sides of the piston rod have the same diameter and passes through both ends of the double-ended MR damper. This arrangement can subtract a rod-volume compensator, meanwhile the gas chamber can be removed, and then as a result no spring effect could be created by itself. Double-ended MR dampers have been employed for gun recoil applications, impact and shock loading, and seismic protection [47].

Integrated MR dampers with internal coils.

Figure 2.8 demonstrates an integrated MR damper's basic schematic structure with internal coils. The MR control valve is arranged inside the moving piston, and the piston rod is a hollow structure for coil wires to pass through and separate them from MR fluids. This sort of MR dampers could conduct in three fluid modes (i.e. mixed mode, using valve mode and direct shear mode; single flow mode; and multimode, using valve mode, direct shear mode, and squeeze mode) because of the available relative motion of magnetic core and outer housing.

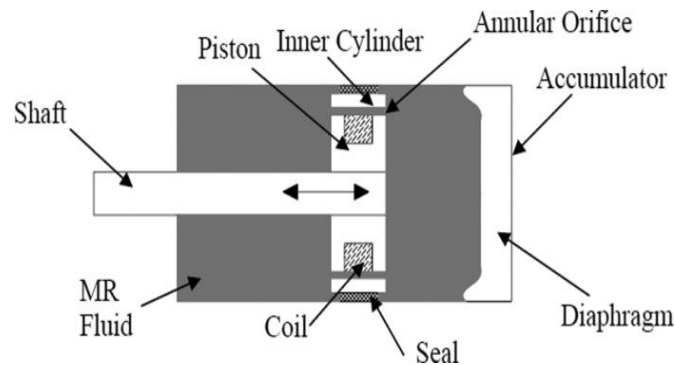


Figure 0.8 Schematic structure of integrated MR fluid damper.

Figure 2.9 illustrates the basic schematic structure of a single valve mode integrated MR damper, employing a fixed annular orifice between an additional inner cylinder and the magnetic coil bobbin rounded by a Teflon seal in the piston. Due to aluminous outer

housing, the structure is characterized by high seal requirement but low weight and has the flux line passing through the inner cylinder in their return path.

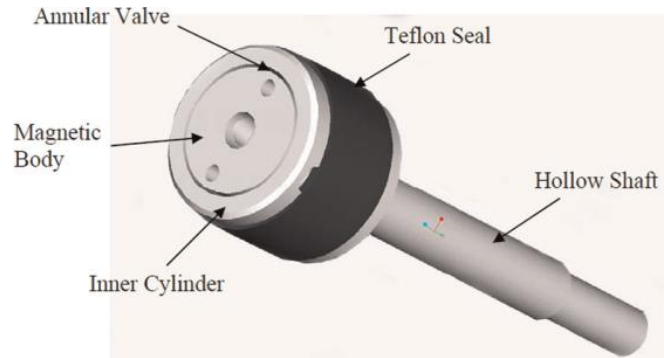


Figure 0.9 Schematic structure of valve mode MR fluid damper [59].

Figure 2.10 shows the schematic structure of a mixed-mode–integrated MR damper. There is an annular gap between the low-carbon steel outer housing and the core bobbin. This design has less requirements on sealing but relatively increased weight because it utilizes low-carbon steel outer housing as a part of magnetic circuit [59].

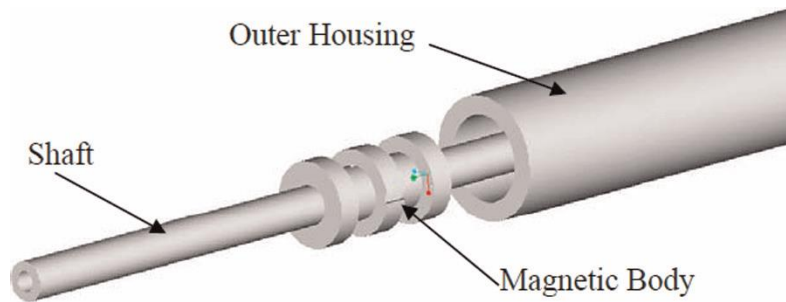


Figure 0.10 Schematic structure of mixed-mode MR fluid damper [59].

Moreover, this mixed-mode–integrated MR damper can be designed and manufactured as commercially available air cylinder or hydraulic cylinder and an assembled customized low-carbon steel piston head sleeve coupling with slots and cushion rings [60]. Figure 2.11 presents the structure of a multi-mode MR fluid isolator. The electromagnetic coil attached to the top elastomer through the linking screw is wrapped around the bobbin.

During the movement of the top elastomer, the outer cylinder works as a magnetic flux return for generating valve and shear damping. The squeeze mode damping is produced by the axial motion of the elastomer and the bobbin that forces radial flow of the fluid in the gap between the bottom of the bobbin and the outer cylinder. This structure can raise damping force and reduce unwanted lockup state between small-amplitude excitations, which often exists in a single-valve-mode MRF isolator, and the magnetic pole gap against relatively high-frequency [61].

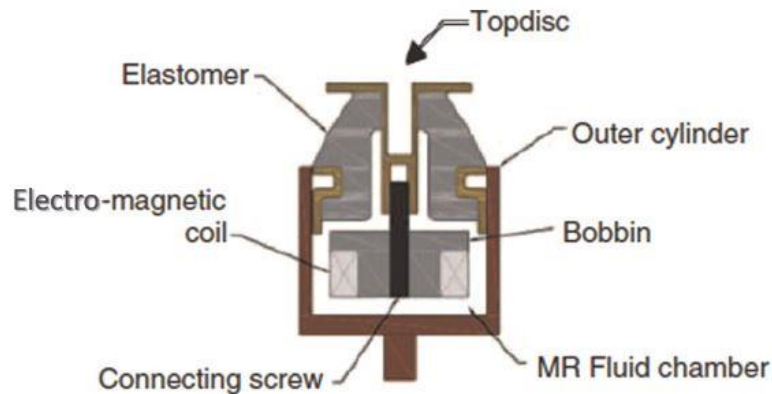


Figure 0.11 Schematic of multimode MR isolator [61].

Basically, integrated MR dampers with internal coils are usually characterized with a compact structure and good protection of wires. However, due to the internal coil in MR fluids, inconvenient assemble and maintenances, and inflexible replacement of MR fluid control valve, the disadvantages of the devices are harsh design requirement, hard heat dissipation, increased weight of the piston head. Although, it is obvious that most MR dampers employ the integrated design of piston/valve mono-tube structure as a result of the efficiency in providing high on-state force and low off-state force in a compact robust package [62] .

MR dampers with bypass valves.

The MRF control valve is embedded into the MRF cylinder coupling with a bypass duct, and the resistant flow is created outside the MRF cylinder as presented in Figure 2.12. In practical design, the mono-tube or double-ended MRF cylinder is utilized in convenient conjunction coupling with a bypass duct. It is noticed that the bypass-type MR dampers are conducted in single-valve mode since the flow channel and outer housing are always fixed. Additionally, there are bypass-type MR dampers with internal and with external coils accordingly.

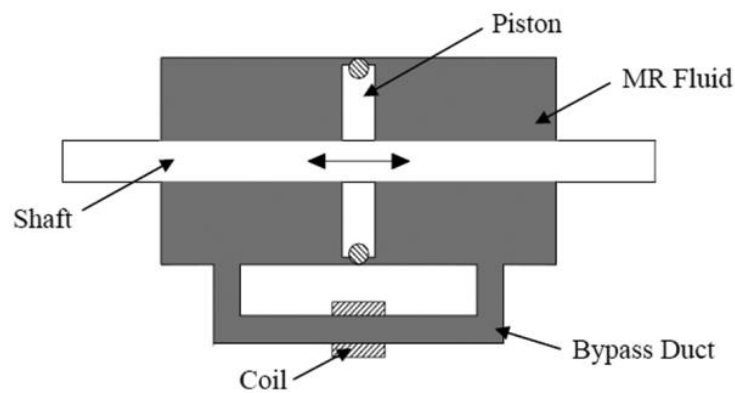


Figure 0.12 Schematic of the bypass-type MR fluid damper [59].

Figure 2.13 illustrates single-ended damper and double-ended damper, which are two different bypass-type MR shock dampers with internal coils for high impulsive force systems having mostly large stroke and large excitation amplitude such as aircraft landing gear units, gun recoils [63], and off-road vehicle suspension.

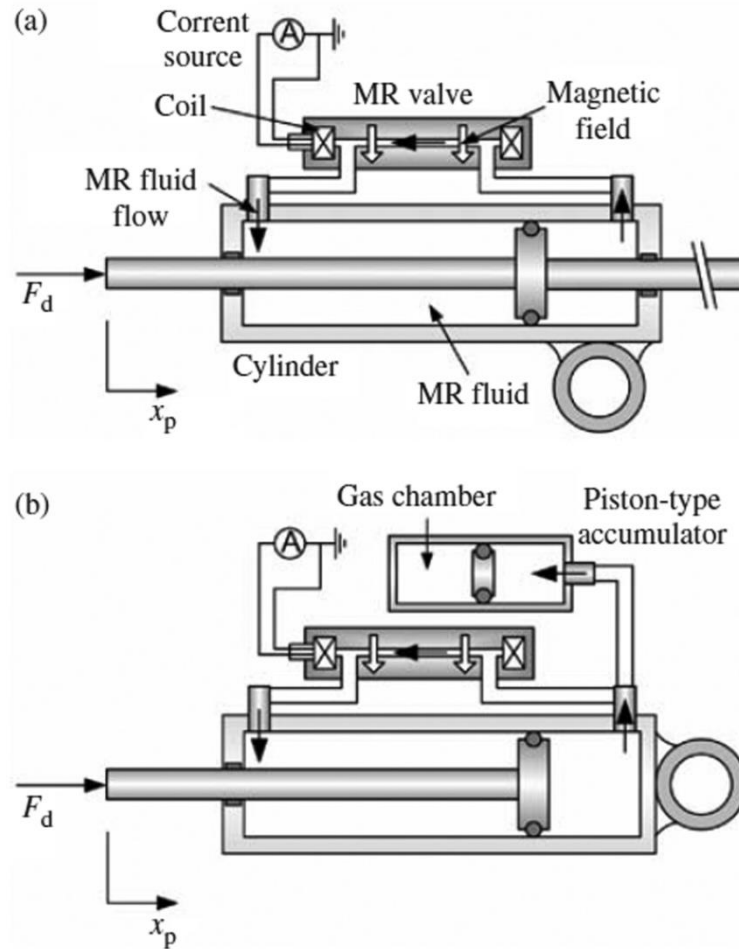


Figure 0.13 Schematic configurations of the bypass-type MR fluid shock dampers with internal coils: (a) double-ended MR shock damper and (b) single-ended MR shock damper. [63].

Figure 2.14 presents a bypass-type MR damper with external coils, containing porous media and being externally wrapped by a stationary magnetic coil in order to make a compact energy absorber with the capability of creating large damping force and a wide force range [64]. The main advantage of bypass-type MR dampers is their simple structure design and assembly and convenience in maintenance [59]. It is obvious that according to different application requirements, this facilitates realization of modular design based on available hydraulic cylinder and not on special modification of piston/piston rod. Additionally, modular disk-type bypass MRF valves were designed in order to offer high force in large-scale seismic applications. In full-scale civil engineering,

three bypass-type MR dampers with different force capacity (2, 20, and 200 kN) were designed and manufactured [65, 66]. However, the main disadvantage of bypass-type MR dampers could be its less compact structure and more requirements for wire protection, compared with the integrated MR damper with internal coils and the hollow piston [60].

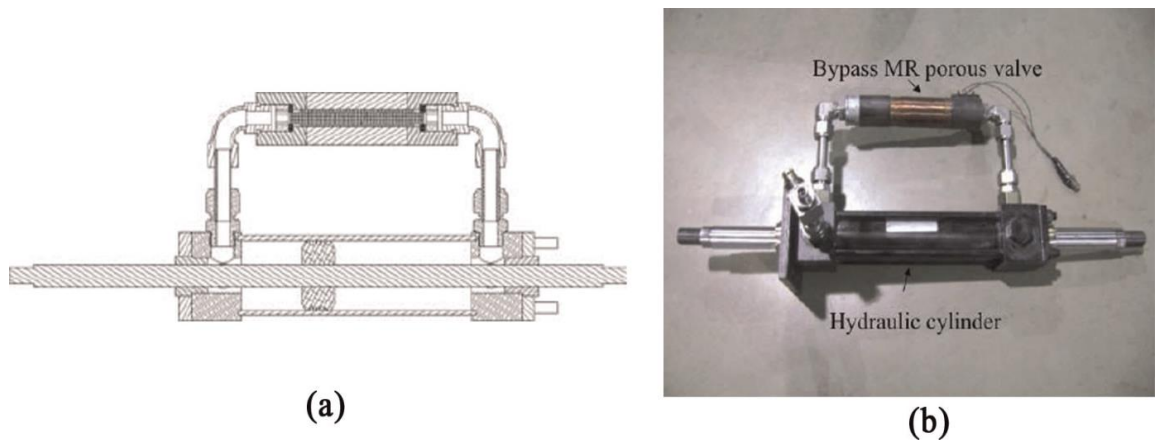


Figure 0.14 Schematic configuration and photo of the porous bypass-type MR fluid damper with external coils: (a) schematic structure and (b) photo [64].

Multistage piston/coil configurations.

Generally, the force of an MR damper is dependent on the area of the activation region such as the band-shaped volumes of on-state MR fluid activated by magnetic field. In bid to raise damping force, increasing the activation region is a way required. Although a larger size of the activation region can be utilized for MR dampers with a single-stage piston to increase the damping force, the available damping force cannot be significantly raised due to strong sensitivity to the fluid gap. Therefore, multistage pistons for MR dampers are developed, which could be less sensitive to the fluid gap due to an increase in the area of activation regions that the additional coils create with the same cross-sectional geometry [48].

Figure 2.15 illustrates a civil engineering applications of a 20-ton high force MR damper with a multistage piston, in which the electromagnetic coils with a totally approximately 1.5 km of copper wire are wrapped in three sections on the piston, causing in four effective

activation regions as the fluids flowed past the piston [67].

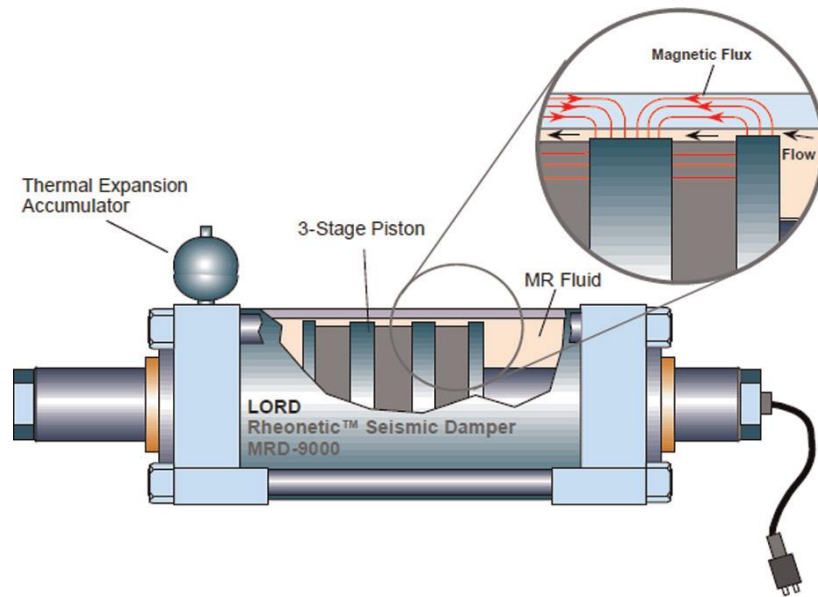


Figure 0.15 The prototype MR fluid damper with three-stage piston [67].

Figure 2.16 shows a monotube MR damper (for Ford Expedition in studying roll-over dynamics) with a two-stage piston, which has the capacity of 185-psi nitrogen accumulator and 4.1-in total stroke [48, 68]. The multistage piston/coil MR dampers are often favorable in enlarging damping force under a constraint volume and compensating for larger gap size in applications [69]. Importantly, some considerations should be noted in the design of multistage piston MR dampers. Firstly, the coils are alternately wound such that the magnetic fields are additive and do not cancel each other [48, 70]. Secondly, parallel connections of electromagnetic coils are preferred to achieve faster response due to smaller reluctance generated [67]. Thirdly, the increase of achievable damping force with respect to additional coil could reach a limitation due to magnetic saturation and volume requirements [71].

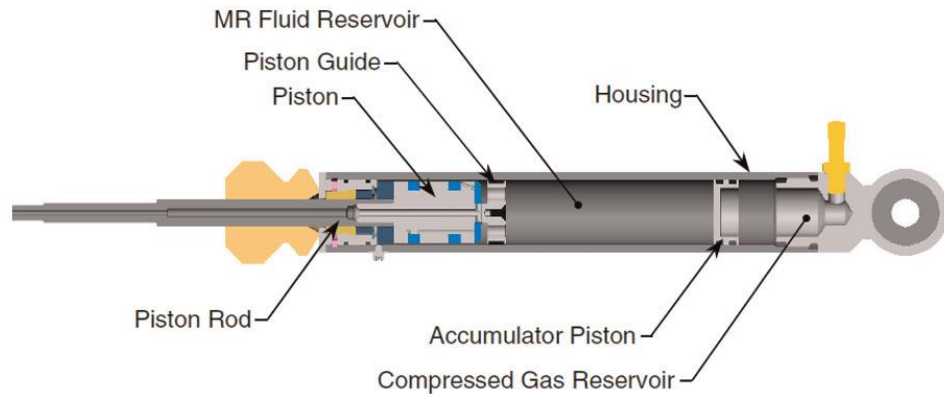


Figure 0.16 Expedition MR fluid damper with two-stage piston [48].

2. 3 Semi-active Vehicle Suspension System

Generally, vehicle suspension can be classified into three modes: passive, active and semi-active suspension. Although passive system is relatively simple and cost-effective, this configuration still has a significant limitation that is the damping force cannot be variable to cope with uncertain disturbances. Additionally, an inevitable vibration can be encountered and cannot be removed, when the frequencies of the vibration closely reach the natural resonance frequencies of passive suspension system around 2 Hz [72].

When the suspension system has an external active force generation as a controllable energy input component, for example electric motor, air pump, and hydraulic pump, it is called active suspension. Active suspension can vary the damping force between sprung mass and unsprung mass based on the road disturbances information collected by sensors. Relatively better control performance can be offered by an active suspension with a wide frequency range compared to its passive counterpart. To meet the real-time demand, the active damper is often coupled with a passive damper. Basically, the power consumption of the whole system can be quite high, about 5-10 kW [73]. Therefore, energy consumption and expensive hardware cost should be considered when designing the active suspension system. In contrast to this, the power consumption of the semi-active

vehicle suspension is around 10-20 W at vehicle speed 25 mph [74]. In addition, semi-active system can provide both the effective control performance of active system without high power consumption and the reliability of passive system.

Comparing with active suspension, the semi-active suspension with lower energy consumption can offer a similar performance of vibration control [75, 76]. Although the concept and actual real-world application of semi-active suspension is later than active one, it has been considered as the most widely utilized controllable suspension system [77].

In 1973, the skyhook control and the concept of vehicle semi-active suspension firstly be presented by Karnopp et al. [78]. In 1983, TOYOTA Corp. revealed a new car, Soarer 280GT, which coupled with the semi-active suspensions in three operating modes. In 1988, according to Supersonic suspension technology, NISSAN Corp. employed semi-active suspensions in the car Maximas. Subsequently, in 1989, FORD Corp. used semi-active control coupled with active control and employed this control strategy in the car Thunderbird [79]. Nowadays, many car models utilized semi-active suspension including Porsche 911, BMW 7 series, and Benz S-class, etc. [73].

The semi-active suspension technology is most widely applied by the following two types [73]:

I. The Continuous Damping Control (CDC) presented by ZF Sachs Corp. was initially employed on the car model, Phaeton, produced by Volkswagen Corp. This technology can continuously change the hole of the damper to adjust damping force in real-time, meanwhile the highest response frequency can reach 1000 Hz [80]. Currently, in Audi A6 all-road Quattro vehicle technique, CDC is employed to combine with air suspension structure; at the same time, likely adaptive control strategy involving Hydractive technology has been presented by Citroen Corporation [81].

II. MagneRide technology was proposed by Delphi Corporation. This technique based on MR fluid is initially utilized by GM Corp. on car model of Cadillac Seville STS in 2002. After about a decade of development, MR dampers have become standard components that have been widely used in mid- to high-end models of General Motors, Volkswagen, Ferrari, and Land Rover. Delphi [82] states that the transforming time of MR fluid from low viscosity Newton model into high viscosity bingham model can reach millisecond level.

In order to more accurately describe the dynamic characteristics of a suspension, many mathematical models of vehicle suspension have been proposed in existing literature [83-85]. The most widely used model of vehicle suspension models involves the following two models:

(1). MacPherson suspension model

Basically, the real suspensions' structure are almost developed on the basis of MacPherson type suspension, therefore, a MacPherson suspension model that owned nonlinearity should be built. The classic MacPherson suspension system consists of A-type below transverse arm and joint, in which damper traveller also plays the role of the kingpin as a central axis for steering knuckle turning around. The structure of typical MacPherson suspension has been researched and built by much research [86-88], presented in Figure 2.17 as follows:

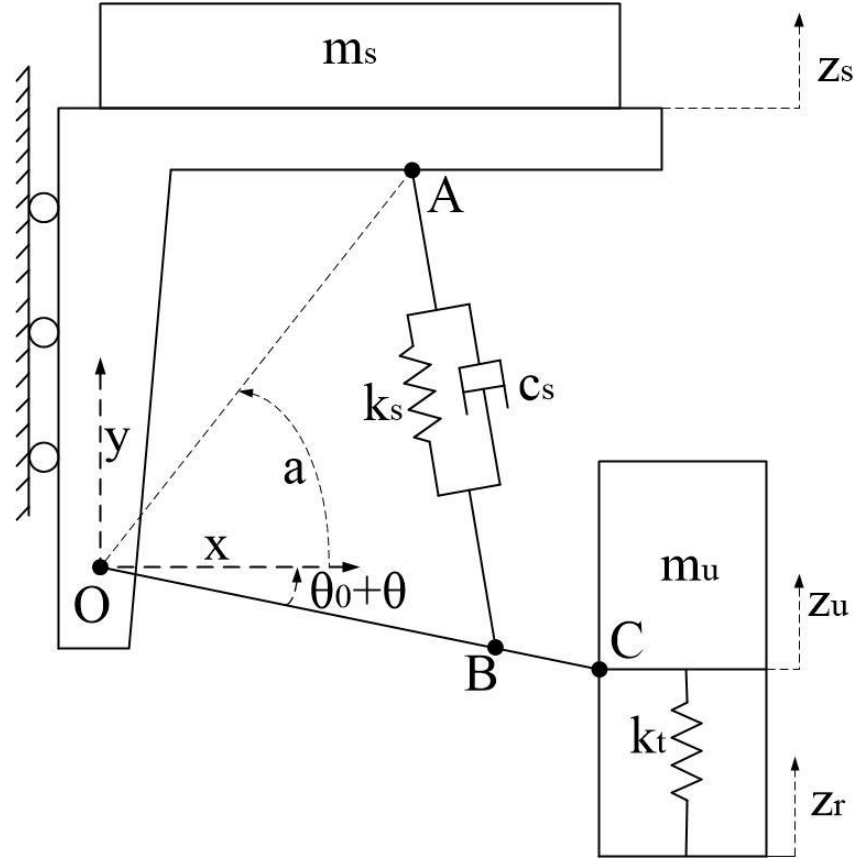


Figure 0.17 MacPherson type suspension model [86].

The 2 degree of freedom (DOF) of this system are the displacement of spring mass(z_s), and the below transverse arm's angle (θ). The initial position angle between X-axis and below transverse arm is defined as θ_0 , meanwhile the increment angle to the initial position during below-transverse movement in system is defined as θ . The counter clockwise is initially defined as the forward direction. In bid to capture the system dynamic equation, the Lagrange method [89] should be employed to build Lagrange motion equation.

(2). Linear quarter-car model

A linear quarter-car with 2-DOF is a quite simple model to imitate the vertical motion of a chassis and wheel without considering roll vibration modes [90, 91]. The model is illustrated in Figure 2.18, which is widely utilized for suspension analysis.

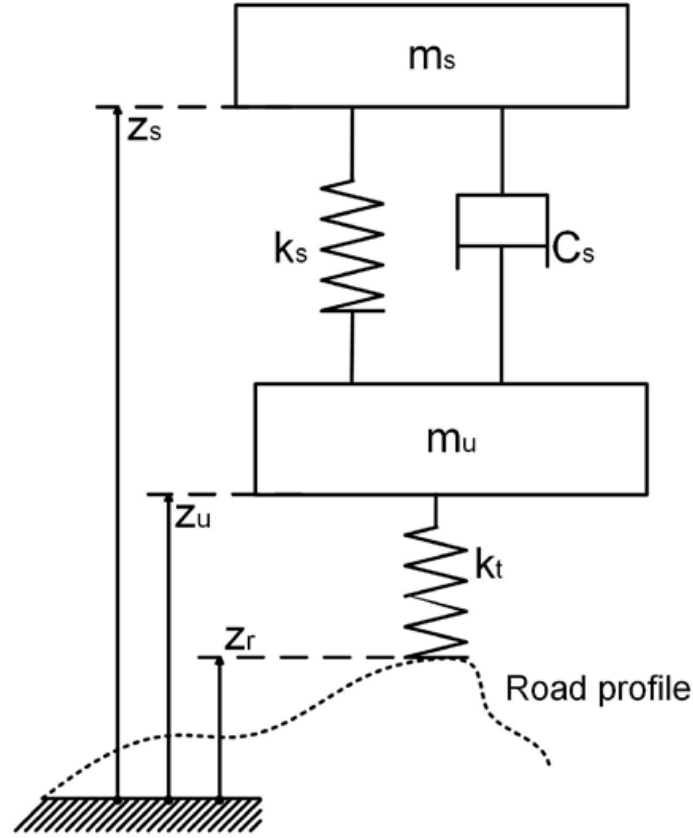


Figure 0.18 Linear quarter car model with 2-DOF [90].

In Figure 2.18, m_s represents a quarter of the suspension mass; m_u is defined as the unsprung mass; z_s and z_u are defined as the displacements of sprung mass and unsprung mass, respectively; and then z_r represents the road profile; k_t is defined as the tyre stiffness, while k_s is defined as the stiffness of the spring between the chassis and the tyre; c_s is defined as the damping of a passive damper offering a damping force which is proportional to the velocity $\dot{z}_s - \dot{z}_u$. Finally, the state-space equation of the quarter car system can be regarded as a special application of the McPherson nonlinear model.

2.4 Energy-regenerative technology for MR damper

Although the external power consumption to assure the generation of magnetic field for the MR fluids is relatively small and approximately several watts for one MR damper, it

still requires external energy supply. While considering there are at least four MR dampers in one car during their long-time operation, the total consuming energy cannot be ignored. It will add the fuel consumption of the vehicles. Additionally, the external power cables will also reduce the reliability of vibration control system. Hence, many researchers investigated the potential harvesting energy if all potential power is regenerated by suspension vibration. The simulation performed by Segel and Lu [20] demonstrated that approximately 200W of power is dissipated by four dampers when a passenger car is running on a road. Additionally, the self-powered MR damper has exhibited promising features and studied by some researchers currently. Usually, in practical applications the electromagnetic coils in MR damper systems are needed to be activated by either a current amplifier or a power supply.

An energy-harvesting device is employed to an MR damper to realize the achievement of self-powered effect by Choi and Wereley [23].

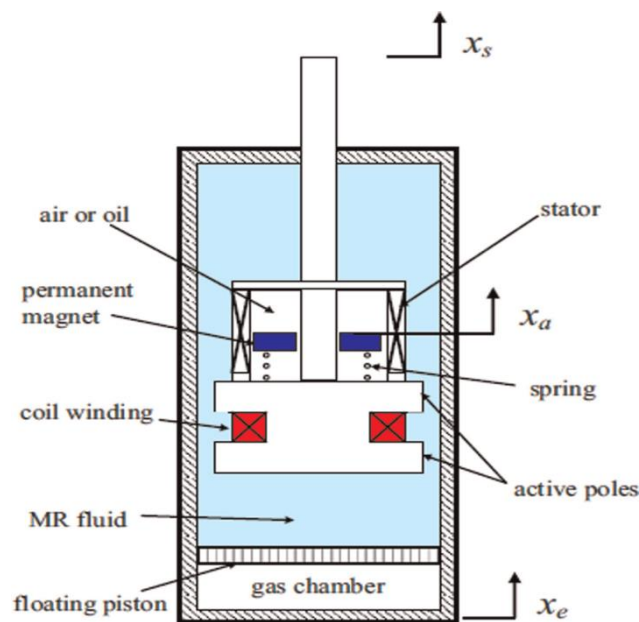


Figure 0.19 Schematic structure of a self-powered MR fluid damper [23].

This device is constructed out of a permanent magnet, a stator, and a spring, which

contributed as a dynamic vibration absorber (DVA) (Figure 2.19) in order to not only provide power to the MR dampers without external power supply by transforming mechanical energy into electrical power but also achieving significant reductions in system cost, volume, weight, control complexity decrement and maintenance.

Simulation presents that this self-powered MR damper within a single-degree-of-freedom (1DOF) engine mount system can offer good performance of vibration isolation coupling with neither a sensor nor a control processor. Therefore, this self-powered MR damper can be utilized at remote locations where supplying power is relatively impractical.

The self-powered MR damper can also be achieved by embedded electromagnet induction (EMI) device into an MR damper system. The EMI device (Figure 2.20) is constructed out of a permanent magnet and a solenoid coil, while the EMI device can function as a velocity sensor or a power source in an MR damper system because the kinetic energy of reciprocal relative motion is transformed into the electric energy and as a result, the damping characteristics of the MR damper is varied by itself [92].

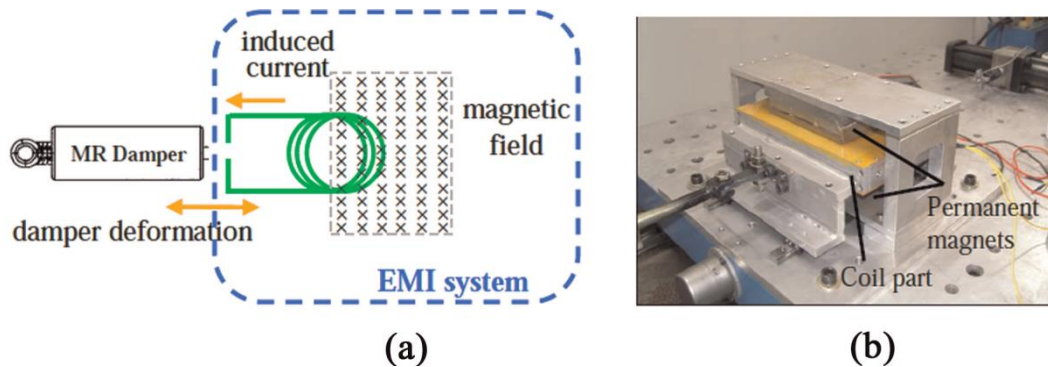


Figure 0.20 (a) Schematic of EMI system and (b) prototype of large-scale EMI system.

[92].

Specifically, an adaptive passive control system constituted by an MR damper and EMI device for reducing vibration of building structures influenced by ground accelerations was proposed [93]. A vibration power generator based on EMI principle was built and coupling with a linear MR damper in parallel in a system as shown in Figure 2.21 [22].

A passive system for large-scale civil constructions involving MR damper and an EMI system was proposed as presented in Figure 2.22, which has self-adaptability without any sensors or controller since power output is proportional to the input load such as earthquake [13].

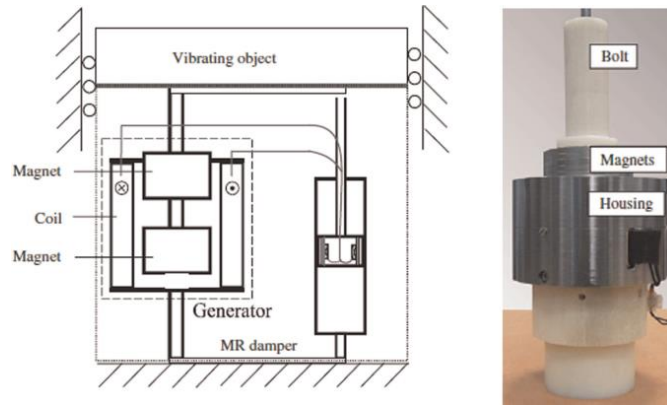


Figure 0.21 Schematic diagram of the self-powered MR damper-based vibration control system [13].

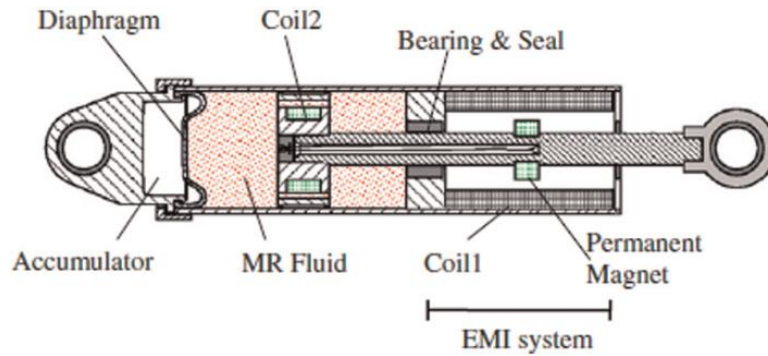


Figure 0.22 Schematic diagram of a smart passive system and the generator [22].

Additionally, a prototype of self-sensing, self-powered MR damper constituted of an MR damper, a power generation device employing stator and mover, a velocity sensor utilizing EMI, and an interaction and mounting part was developed as illustrated in Figure 2.23 [94].

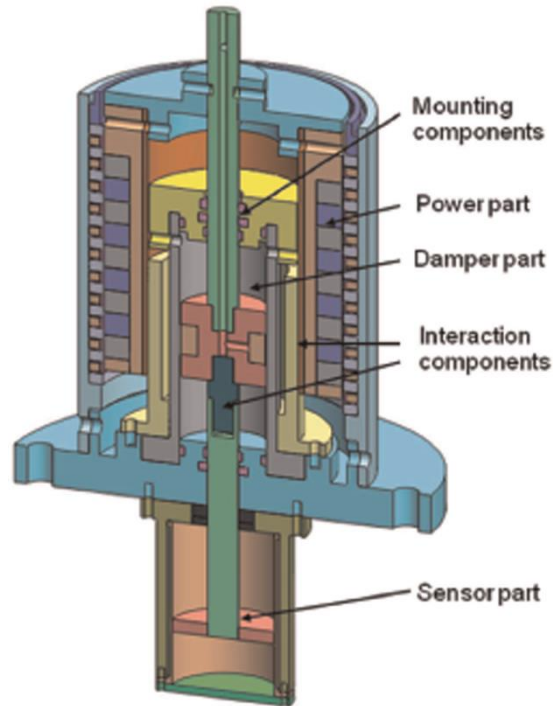


Figure 0.23 Sectional view of self-powered, self-sensing MR damper [94].

2.5 Landing gears

Landing gear systems are widely employed in aircrafts to protect the fuselage structure and the passengers on board from injury even spine fracture during crash landing scenarios. The development of landing gear analysis originates from 1950s [95]. Massive simulation and experimental work have been done. Initially, the landing gears are generally work in passive mode during landing events. Ross and Edson [96] are one of the first group to focus on actively controlled landing gears. They indicate the advantages of using active landing gear systems when running on uneven runways. Kushida et al. [97] designed a robust landing gear employing an active/passive hybrid momentum exchange impact damper and the performance is verified by both simulation and experiments, in the meanwhile, the time response is considered. Wang[98] proposed an active landing gear system (as shown in Figure 2.24) to improve the performance on impact loads and vertical movement. A mathematical model is established with PID

control strategy, and the simulation results indicate that the proposed active landing gear system is feasible and effective.

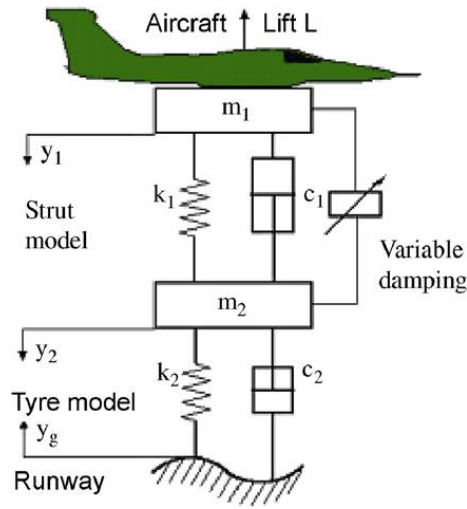


Figure 0.24 The schematic diagram of the active landing gear [98].

MRF is also increasingly introduced into landing gears due to its changeable rheological properties. Lee and his colleagues [31] applied MR dampers into the landing gears to attenuate the excessive shock and continuous vibration during landing and taxiing events. In addition, a simplified skyhook control logic was utilized to suppress the shock and vibration. And the simulation outcomes via hardware-in-the-loop-simulation supported the viewpoint that the introduction of MR damper and skyhook controller is feasible and effective.

According to energy conservation, a new control logic was proposed by Yoon and his partners [99] for landing gear systems which integrates the MR damper. This control logic can forecast the maximum structure stroke and obtain the optimal damper force, then by adjusting the MR effect to retain the damper force in various landing events. In their research, after drop simulation, this new control logic is proved to give a better performance than that of conventional skyhook control. Specifically, the landing efficiency increases by 16%, and the jerk impact declines by 42% during the impact. The

configuration of the new MR damper is shown in Fig 2.25. Besides, Fig 2.26 demonstrates the employed scenario of the new MR landing gear.

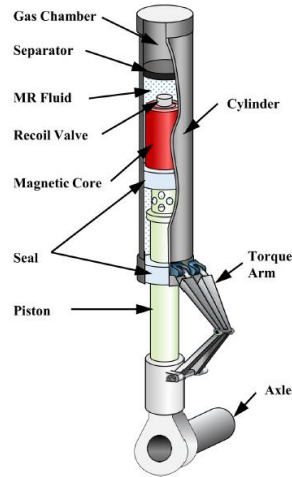


Figure 0.25 The configuration of the new damper [99].

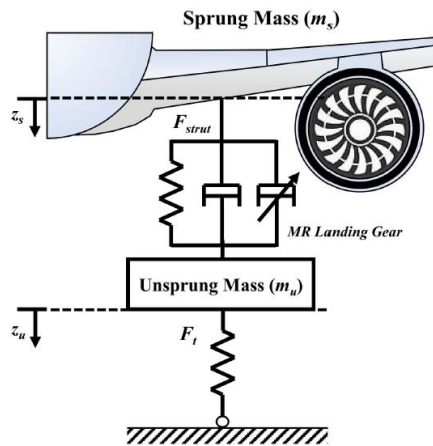


Figure 0.26 Schematical diagram of MR landing gear in half-vehicle [99].

Choi and Wereley [100] put forward an ER and MR fluid-based landing gear systems, whose main component is ER/MR shock structure. The shock struts and theoretically landing gear diagram are shown in Figure 2.27. The ER/MR struts model was firstly developed on the basis of experimental data, then by employing a sliding mode controller which is robust against external excitations and parameters (sprung mass, damping and

so on) modify, the whole landing gear system was built and validated to be effective on shaving the acceleration and displacement.

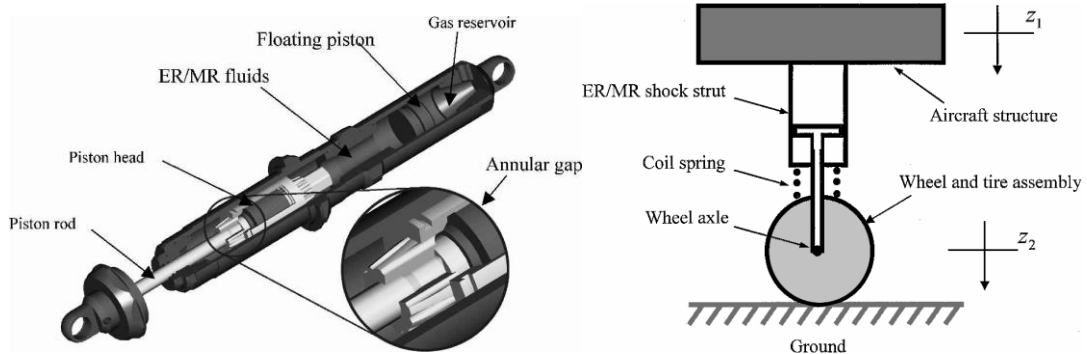


Figure 0.27 The shock strut and landing gear diagram [100]

Han et al. [101] presented a landing gear system based on a two-core type (Fig 2.28) of a semi-active MR damper. The unique design of two orifices could provide asymmetry property by a recoil valve. Besides, a hybrid control algorithm that integrates skyhook control and force control actions, which is validated to be capable in boosting the landing efficiency, decreasing the maximum stroke and landing force.

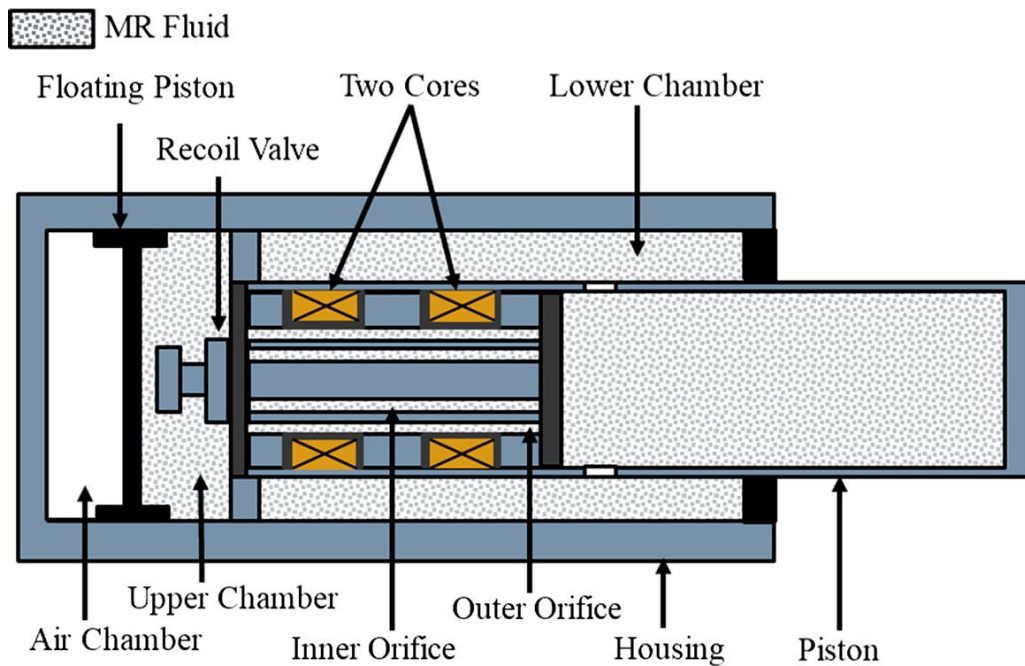


Figure 0.28 Schematic configuration of MR damper with two cores [101].

Dong and Xiong [102] studied a landing gear system incorporated with a MR absorber. Besides, a human simulated intelligent control (HSIC) is applied to control the MR absorber performance. Furthermore, a genetic algorithm is developed to obtain the optimal parameters of HSIC. Under various sink rate and sprung mass, a simulation was built, the results demonstrate that the MR absorber could diminish the peak impact force. Moreover, the HSIC exhibits strong robustness and wide adaptivity than the classic skyhook control. Figure 2.29 and 2.30 show the schematic diagram of the MR absorber and the dynamic model of the proposed landing gear.

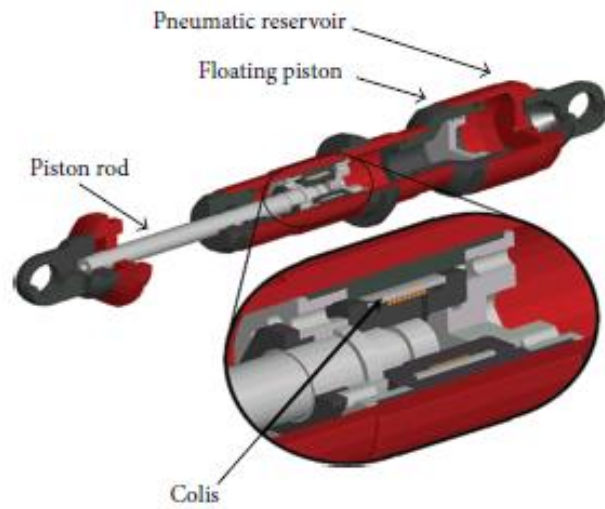


Figure 0.29 Schematic diagram of the MR absorber [102].

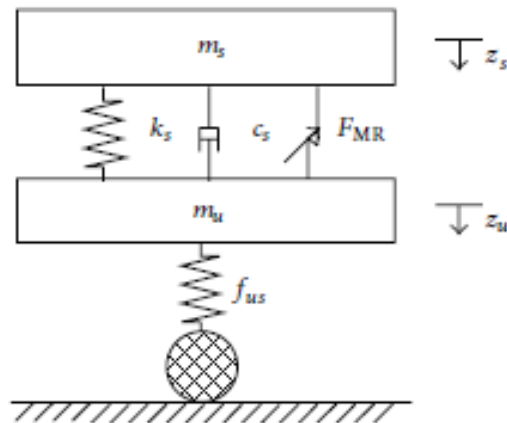


Figure 0.30 Dynamic model of the landing gear [102].

Gharapurkar et al. [103] presented a switching technique which could tune the system from 1 degree of freedom (DOF) to 3 DOF. In this way, the sequential connecting of the wheels of the main landing gear and nose landing gear with the ground can be reflected. Two control algorithms, namely, linear quadratic regulator, and H-infinity were applied to control the MR damper, the simulation results show that the robustness of H-infinity strategy can improve the bounce response including overshoot, settling time than LQR control no matter in general landings or in crash landings.

2.6 Classical semi-active control algorithms

- Skyhook control

Skyhook controller, as a classical control algorithm, has been attracting massive attention after it was first proposed by Karnopp in 1973 [104]. This method investigated the situation that the damper is placed between the sprung mass and the inertial coordinates. Comparing with the passive suspension, the skyhook damper could manipulate the sprung load directly. The absolute velocity is independent from the movement of the wheels, which offers an excellent damping performance.

In skyhook control applied in semi-active suspensions, the damper effects when the absolute velocity of the vehicle seats and the relative velocities of the vehicle wheels are at the same direction. On the other hand, the damper will be off. The model of skyhook control is shown in Fig. 2.31.

So far, the skyhook controller has been widely applied in automotive magnetorheological semi-active suspensions owing to its simple principle and low implementation requirement. Lee and Choi [105] designed a MR damper applied in vehicle suspension system with a skyhook damping switch controller to mitigate vertical vibration. Eventually, the simulation and road tests were conducted to verify the feasibility.

University of Virginia, USA [106] and Chongqing University intelligent structure center adopts continuous Skyhook damping control to conduct a real vehicle road test on the magneto-rheological semi-active suspension.

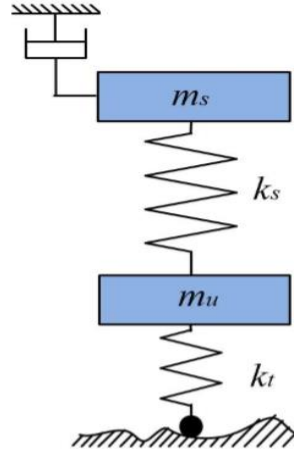


Figure 0.31 Skyhook control model

- Groundhook control

As a counterpart of skyhook control, the damper in groundhook control is placed between the unsprung and the inertial coordinates. So that the damper could adjust the absolute speed of the unsprung mass without considering of the motion of the system. The model of groundhook control is shown in Fig. 2.32.

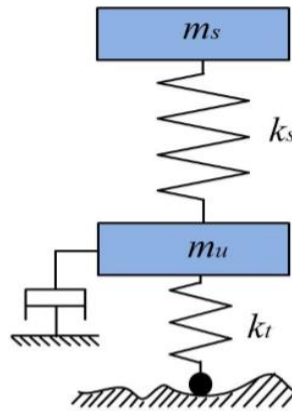


Figure 0.32 Groundhook control model

As a compare with the skyhook controller, the groundhook control is not commonly employed. Via the experiments conducted by the Virginia Institute of Technology [107], the groundhook control is validated to be effective to suppress the non-sprung vibration to stabilized the steering during driving. Nevertheless, it added a large additional mass to the sprung mass, which would reduce the comfort of drivers.

- Hybrid control

As mentioned above, neither the skyhook controller nor the groundhook controller can simultaneously reduce the vibration of the sprung and non-sprung mass. Hence, Goncalves [108] proposed a hybrid control strategy acting on the quarter-car model and MR damper. The experimental results show that the proposed control methodology could shave the peak value of the displacement and acceleration under transient input. Nonetheless, the application range is limited due to the superior difficulty of weighting coefficient determination. The model of the hybrid controller is illustrated in Fig 2.33.

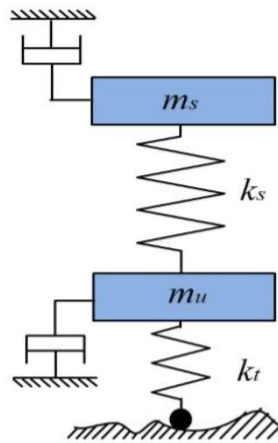


Figure 0.33 Hybrid control model

- Short-time Fourier Transform (STFT) control

STFT control was developed based on short-time Fourier transform to analyse the sinusoidal phase and frequency phase of a particular section of a time-varying signal [109]. The controller could analyse the resonance frequency of the system and avoid it by

switching on/off the rectified power supply of the damping system. However, STFT can only use one selected window function, once the function is fixed, the resolution of STFT is unchangeable. Subsequently, the time and frequency resolution cannot be optimized at the same time [110], causing issues in real-life scenarios. In addition, STFT is a unique control method which can change from one dimension to multi-dimension by introducing other variables.

2.7 linear feedback control

- Linear quadratic Gaussian (LQG) control

LQG is a kind of linear optimal control algorithm originates from LQR control, in this theory, Kalman filter [111] is employed to estimate the system state suitably. The input of LQG control is supposed to be white noise with Gaussian distribution, and the index of the system is expressed as quadratic. Generally, the Riccati equation is derived consisting of weighted values like acceleration, tire dynamic load, then a feedback weighting matrix is obtained. By adjusting the weighting matrix, the road excitation response could be improved.

- Robust control

To ensure the effectiveness of the suspension under diverse working situations, robust control is also widely employed in vehicle suspension systems. Palkovics et al. [112] proposed an active suspension with controllable vertical stiffness using robust controller. This concept is quite conservative, especially used in semi-active suspensions.

2.8 Modern intelligent control algorithm

- Sliding mode variable structure control

Sliding mode variable structure control theory is a comprehensive method of control system. The basic concept is that when the switching function determined by the state

vector of the system reaches a certain value as the motion of the system changes, the structure of the system is transformed into another structure. Yokoyama [113] designed a sliding mode controller which used the Skyhook control quarter-car magneto-rheological suspension model as the reference model and verified the effectiveness of this control strategy through simulation. Choi et al. [114] established a sliding mode intersection structure controller based on the vehicle model and carried out a hardware-in-the-loop simulation.

Although the sliding mode control is highly robust to external disturbances, the ideal sliding mode interface is not easy to determine. Therefore, the conditions for practical application in suspension system control are not mature yet.

- Fuzzy control

The fuzzy control takes some state value of the system as input and blurred the input according to a certain fuzzy rule. The obtained control value is used as the output result to adjust the suspension damping. Fuzzy control was first proposed by Zadeh in 1965 [115] and is widely applied in vehicle suspension systems as an important intelligent control strategy. Tusset [116] studied the fuzzy control strategy of nonlinear vehicle suspension for MR damper and verified its effectiveness by simulation. Later, Khajavi [117] proposed a fuzzy logic semi-active system designed for a specific vehicle. Hashiyama et al. [118] used Genetic Algorithm (GA) to design a fuzzy controller for vehicle suspension semi-active systems. Computer simulation results show that the fuzzy control combined with GA is more effective than the conventional method. Nizar [119] set the speed of the body and the speed of the suspension as the input of the controller and used nine fuzzy rules to control the vertical vibration acceleration and the tire deformation of the vehicle. The results showed that the fuzzy control can make the vehicle vertical acceleration lower comparing with passive control. Further, Rashid et al. [120]

proposed a hybrid fuzzy method component which used a PID controller to analyze quarter-car system.

Fuzzy control design does not require knowledge of the precise mathematical model of the controlled object. The control inference for fuzzy control uses inexact inference which is suitable for solving nonlinear, time-varying and lags systems that are hard to be solved using old control method. However, designing an excellent fuzzy controller requires a certain amount of manual adjustment experience as a basis of the control strategy and a large number of experiments to adjust the controller parameters. So it needs time for its development in engineering applications in the direction of adaptive and self-learning.

- Adaptive control

The adaptive control method is separated into self-correction control and model reference adaptive control [121]. The combination of on-line identification of controlled object parameters and the controller parameter setting constitutes the former control method. Regarding the model reference adaptive control, it achieves that the vibration output of the controlled vehicle can still track the selected ideal reference model although the external excitation condition and the vehicle parameters change.

- Neural network control

The neural network has been investigated in depth by suspension scholars and is considered to be a high robustness and adaptive intelligent control methodology. Guo et al. [122] studied the neural network semi-active control of quarter-car vehicle suspension vibration with magneto-rheological damper, applying neural network direct adaptive and neural network indirect adaptive control algorithms. The results show that the neural network controlled semi-active suspension has obvious damping effect. However, neural network control is slow in convergence, difficult to be utilized for real-time control and easy to diverge. Therefore, this control only succeeds in theoretical simulation, and the

wide application still needs a further exploration.

2. 9 Conclusions

MR fluid is a significantly ideal material of semi-active suspension and smart landing gears, due to excellent dynamical features such as large yield stress, fast response, low power consumption, and robust characteristics within various environments. However, the semi-active MR vehicle suspensions still require external energy to power the MR damper. A self-powered MR vehicle suspension can avoid all energy consumption and hence offer a more versatile solution to this problem. Furthermore, limited work has been presented on including variable stiffness in these MR suspension systems, which can drastically improve performance due to the ability to avoid system resonance. To investigate this, this work proposes a new stiffness variable MR vehicle suspension with self-power generation capability. In addition, for impact mitigation application, the MR fluid could be utilized in landing gear system to offer a slow force increment as the impact velocities boost.

Therefore, the overview on MR fluid, MR damper, semi-active vehicle suspension, energy- regenerative technology for MR damper, landing gear system with MR damper, and related control algorithms is presented.

For the structure design of a new stiffness variable MR vehicle suspension with self-power generation capability and a linear landing gear system integrated with MR damper to maintain the peak impact load, the following conclusions could be drawn from the chapter:

- 1.** MR fluid is a significantly ideal material of semi-active suspension. Firstly, MR fluid is able to change from a free-flowing liquid state into a semisolid state with restricted fluid movement in significantly fast response (an estimated time of the response which is less 10 ms). Secondly, the energy consumption for semi-solid state of MR fluid is not a

concern since MR fluid is able to reach high yield stress (50 kPa or more) with a magnetic field that can easily be created by an electromagnet applied at modest current and relative low voltage (1–2 A and 2–24 V). Thirdly, the temperature range of MR fluid's operation can be pretty large from -40°C to 150°C.

2. In order to develop a compact practical prototype of stiffness variable MR vehicle suspension with self-power generation capability, the following types of MR dampers can provide useful ideas of structure design.

(1) Double-ended structure can subtract a rod-volume compensator, meanwhile the gas chamber can be removed, and then as a result no spring effect could be created by itself.

(2) Bypass-type MR shock dampers with internal coils for high impulsive force systems having mostly large stroke and large excitation amplitude. However, the main disadvantage of bypass-type MR dampers could be its less compact structure and more requirements for wire protection.

(3) In multistage piston/coil configurations structure, due to an increase in the area of activation regions that the additional coils create with the same cross-sectional geometry, this damper can realize high damping force.

3. In order to achieve better impact/vibration mitigation performance, various control algorithms are often employed such as fuzzy control and skyhook control, which has been validated via both simulation analysis and experimental results.

Chapter 3

Development of a Stiffness-variable MR Damper with Self-Powered Generation Capacity

3.1 Introduction

Vehicle suspension system supports the whole weight of the vehicle, provides the capability of directional control during maneuvering and is also responsible for reducing the vibration generated by the road disturbances. Therefore, suspension of vehicle is a key component and has great influence on the performance of vehicle. Currently, passive damper has been widely utilized in suspension system for vibration reduction. The performance of the passive damper, however, is limited because it cannot adapt its parameters according to different requirements. Semi-active and active devices have been considered as new methods to advance the suspension performance. Although active suspension generally provides better ride comfort than semi-active can, its limitations of high energy consumption, potential instability, complex component requirement and control algorithm reduce its popularity. In contrast, the semi-active vehicle suspension only requires low energy consumption, costs much less, and can provide comparable performance with active suspension. Therefore, more interest has recently been given to the semi-active suspension and it has been considered as high-end intelligent suspension to improve the ride comfort and handling of vehicles.

Comparing with the damping controllability, the stiffness controllability can control the natural frequency of the vehicle to avoid vibration resonance. In addition, suspension stiffness controllable can also overcome the suspension stiffness design conflict because soft stiffness is required to achieve a good ride comfort and the handling stability and off-road drive of vehicles need hard suspension stiffness. As a result, the stiffness controllable

suspension with self-powering function is a promising method to further improve the vehicle performance.

In order to overcome the limitation of our previously reported stiffness variable MR damper, a long stroke stiffness controllable MR damper is required. What is more, the self-powering capability is integrated into the advanced damper and makes it energy free. The intention is to design the new damper with the following features and innovations: variable stiffness, self-powered generation capability, compact structure and large stroke. The successful development, theoretical analysis and experimental testing of this new variable stiffness self-powered MR damper make the concept of energy free stiffness variable MR damper feasible.

3.2 Design, analysis, and prototype of the self-powered variable stiffness MR damper

3.2.1 Structural design of the new damper

A structural schematic of the proposed MR Damper is illustrated in Fig. 3.1. There were two main parts of the damper: variable stiffness part and self-powered generation part. Specifically, it mainly consists of a hollow shaft generator, a ball screw bearing, two springs with different stiffness and an inner bypass MR damping cylinder. In the variable stiffness part, the inner bypass MR damper was installed between the upper spring with low stiffness and the bottom spring with high stiffness. Meanwhile, the shaft of the generator was fixed to the nut of the ball screw to constitute self-powered generation part, which can convert mechanical vibration to electrical energy. The shaft of the ball screw was connected with the shaft of damping unit and can move into the hollow shaft of the generator. The most innovative structural development of the MR device is that both variable stiffness feature and self-powered generation are integrated into this compact device.

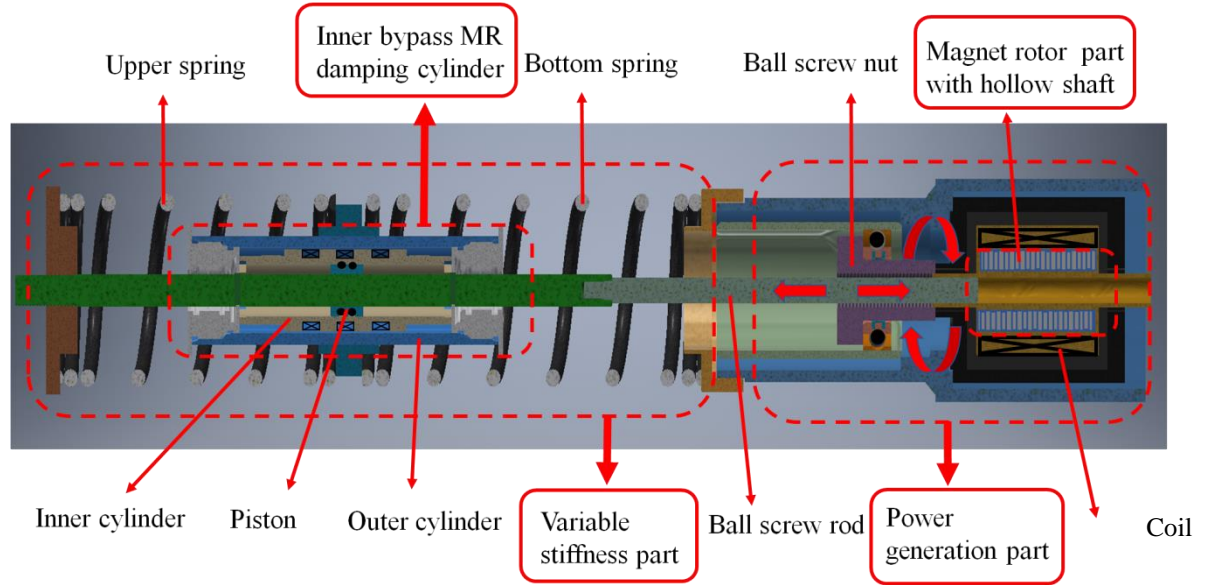


Figure 0.1 Structure schematic of the new damper

In order to enlarge the stroke of the damper, the MR damper's structure was designed as inner bypass type with multiple coils. The wire diameter of the coil is 0.4mm. There are 135 turns on each coil with opposite winding direction, as shown in Fig. 3.2 (b). Meanwhile, the hollow shaft generator could also contribute the compact structure of the new damper, allowing the ball screw rod travel through the hollow shaft. The application of the inner bypass-type MR dampers with internal coils can enlarge the stroke of the damper comparing with traditional piston structure. Specifically, Fig. 3.2 shows a stroke comparison between the conventional stiffness MR damper we developed previously in [38] and the inner bypass stiffness controllable MR damper presented in this paper. The strokes of the two dampers can be calculated by the parameters in Table 3-1. The stroke of the inner bypass MR damper can reach 105 mm, which is much larger than the stroke of 71 mm of the conventional damper.

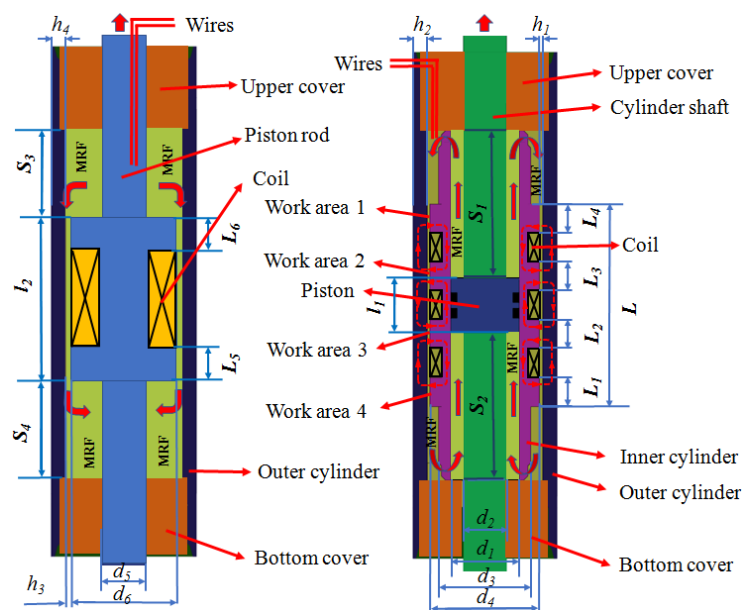


Figure 0.2 Schematic of the MR damping cylinder: (a) MR damper with a conventional piston [123] and (b) Inner bypass MR damper cylinder used in the new damper

Table 0-1 Parameters for MR damper

MRD parameters	unit	Values	MRD parameters	unit	Values
h_1		1mm	L_1		10mm
h_2		5mm	L_2		10mm
d_1		24mm	L_3		10mm
d_2		15mm	L_4		10mm
d_3		32mm	L		70mm
d_4		38mm	Turns of coil		135
d_5		15mm	S_1		52.5mm
d_6		30mm	S_2		52.5mm
h_3		1mm	S_3		35.5mm
h_4		4mm	S_4		35.5mm

l_1	16mm	l_2	50mm
-------	------	-------	------

3.2.2 Working principle

The overall working principle of the MR damper is that the power generated by the generator will be used to control the stiffness of the MR component so as to realize an energy free stiffness controllable suspension system.

The working principle of the variable stiffness part can be illustrated in Fig. 3.3, in which three different modes of the prototype are shown. For the first working mode, when the input coil current I , is zero, no magnetic field crossing MRF and the damping force will be small and allow the relative motion between the shaft and the cylinder. In this case, the MR damper is working in Mode 1 where the bottom spring k_2 and the upper spring k_1 work in series. When the current I increase to a medium level, the device will work in Mode 2. In this case, the damping force is larger and makes the sliding motion between the damper shaft and the damping cylinder harder. The spring k_2 will be compressed more and makes the overall damper stiffness larger. Moreover, if the damping force increases to a sufficient large level and stops the relative motion between the shaft and the cylinder, the MR damper will be working in Mode 3, because only the bottom spring k_2 will be deformed under external force compression. In conclusion, the stiffness of the new damper can be controlled in the range of the minimum value of $\frac{k_1 k_2}{k_1 + k_2}$ and the maximum stiffness of the bottom spring k_2 . In the new MR damper, the stiffness parameters of the two springs are $k_1=30220$ N/m and $k_2=34000$ N/m.

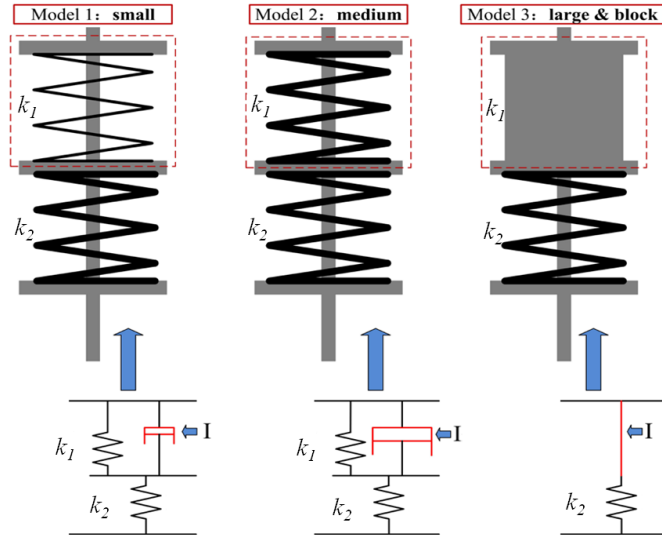
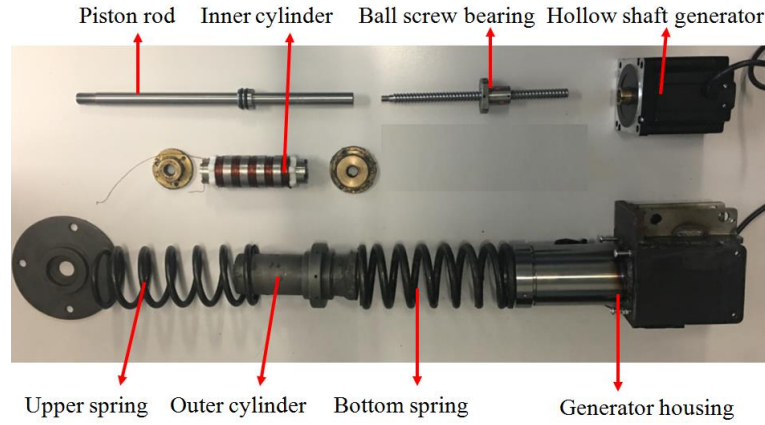


Figure 0.3 Working principle of the stiffness variation

The working principles of the power generation part as well as the variable stiffness MR damper are illustrated in Fig. 3.1. Firstly, the shaft of the MR damper will move up-and-down when the upper spring k_1 was excited by the harmonic excitation. Secondly, due to the rigid connection between the shaft of the MR damper and the rod of the ball screw bearing, the up-and-down motion of the shaft could force the rod to conduct a vertical movement without rotation. Then based on the mechanism of the ball screw bearing, the rod's vertical movement induces the rotation of the nut of the ball screw bearing. As the nut is fixed to the rotor of the generator, the magnet rotor will rotate and generate energy.

3.2.3 Prototype of the new damper

Fig. 3.4 shows the prototype of the new damper, which has been manufactured and assembled. In order to decrease the magnetic reluctance of the magnetic circuit, the materials of the inner cylinder and the outer cylinder are both low carbon steel, which features high magnetic conductivity. The MR fluid GH-MRF-45, produced by Beijing Hao Hua technology limited company, was used in the prototype. Meanwhile, the τ - B curve of the MR fluid is given in Appendix A.



(a) Components



(b) Prototype

Figure 0.4 Prototype of the new damper

3.3 Modelling and theoretical analysis

3.3.1 Modelling

In order to describe the property of the suspension system, two models, i.e. the variable stiffness dynamic model for the MR damper and the electricity generating model for the self-powering component, were built.

3.3.1.1 Dynamic model for MR damper

The dynamic model of the MR damper is shown in Figure 3.5, which is composed of a self-powered part and a variable stiffness part. The dynamic force generated by the self-powered part consists of a damping coefficient c_e and a friction f_e , which are working in parallel. The variable stiffness part consists of the MR damping cylinder, spring k_1 and

spring k_2 The spring k_1 connects in parallel with the MR damping cylinder and then the spring k_2 links with them in series. The Bouc-Wen model is employed herein to describe the dynamic performance of the MR damping cylinder.

The output force of the damper consists of three parts: the damping force from MR damper, the spring force from springs and the force generated by the generator. The resultant force can be calculated by:

$$F = k_1(z_s - z_i) + F_d + f_e \operatorname{sgn}(\dot{z}_s) + c_e \dot{z}_s \quad (3-3)$$

where c_e and f_e are damping and friction produced by the power generation part, z_i is unknown and should be calculated. The following equations are built to build the relationship between z_s and z_i .

$$\text{If : } F_d \geq k_2 z_i + m_i \ddot{z}_i$$

$$z_s = z_i \quad (3-2)$$

$$\text{If : } F_d < k_2 z_i + m_i \ddot{z}_i$$

$$m_i \ddot{z}_i = F_d + k_1(z_s - z_i) - k_2 z_i \quad (3-3)$$

where F_d represents the damping force of the MR damping cylinder. Based on the Bouc-Wen model, the force F_d can be expressed as follow:

$$F_d = c_0(\dot{z}_s - \dot{z}_i) + k_0(z_s - z_i) + az \quad (3-4)$$

where c_0 is viscous damping parameter, a is the evolutionary coefficient, k_0 is the stiffness coefficient.

The parameters in Eq.3-4 can be calculated as:

$$\dot{z} = -\gamma|(\dot{z}_s - \dot{z}_i)|z|^{n-1} - \beta(\dot{z}_s - \dot{z}_i)|z|^n + A(\dot{z}_s - \dot{z}_i) \quad (3-5)$$

$$a = a_a + a_b i \quad (3-6)$$

$$c_0 = c_{0a} + c_{0b}i \quad (3-7)$$

$$k_0 = k_{0a} + k_{0b}i \quad (3-8)$$

where A , γ , β are the hysteresis parameters, i is the control current

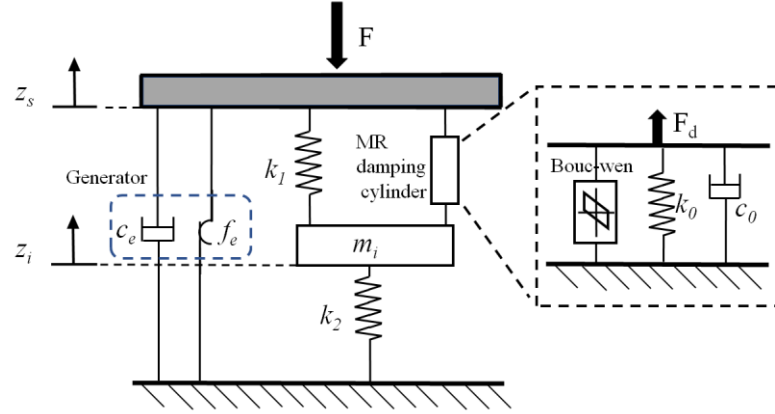


Figure 0.5 Dynamic model of the variable stiffness damper

3.3.1.2 Electricity generating model of the self-powered component

According to the rectifier circuit, the total resistance of the circuit can be calculated by:

$$R_t = R_{mr} + R_i + R_r \quad (3-9)$$

where R_{mr} is the resistance of the MR damper. R_r is the internal resistance of the rectifier, which can be regarded as zero Ohms when the switch turns on. R_i is the internal resistance of the generator.

Since the two groups of coils were parallel in the circuit, the voltages e_1, e_2 have the same value as the input voltage V_{in} . Therefore, the output voltage of the circuit working on the MR damper can be expressed as:

$$V_{out} = |V_{in} * \frac{R_{mr}}{R_t}| = |V_{in} * \frac{R_{mr}}{R_{mr} + R_i}| \quad (3-10)$$

where V_{in} is the voltage generated by the electromagnetic induction in the generator. The

equation between the rotation speed of the rotor and the generated voltage is given by:

$$V_{in} = 4\pi NBLn_m r \quad (3-11)$$

where B is the magnetic field intensity of the magnetic field generated by the magnet rotor. r is the radius of the generator rotor, L and N are the total length and the number of turns of the fixed coil windings. n_m is the rotation speed of the magnet rotor which is equal to the rotation speed n_s of the screw nut installed on the ball screw rod. The rotation speed of the screw nut is proportional to the vertical linear velocity of the ball screw rod.

The relationship between the linear motion speed of the ball screw rod and the rotation speed of the screw nut can be expressed as:

$$n_s = \frac{z_s}{P_h} \quad (3-12)$$

where z_s is the displacement of the ball screw rod, P_h is the ball screw lead.

According to the above equations, the relationship between the self-generated voltage and the velocity of the ball screw rod can be expressed as:

$$V_{out} = \left| 4\pi NBL \frac{z_s}{P_h} r \cdot \frac{R_{mr}}{R_{mr} + R_i} \right| \quad (3-13)$$

The circuit parameters are indicated in Table 3-2.

Table 0-2 Parameters used in modelling of self-powering component

Parameter	Value	Parameter	Value
R_1	10.2Ω	R_2	10.2Ω
R_{mr}	6.5Ω	B	$0.6T$
L	$0.09m$	N	235
P_h	$0.015m$	r	$0.0275m$

3.3.2 Magnetic field simulation

In order to complete the damping force calculation in Eqn. 3-10, the magnetic flux density across MRF should be calculated to determine the yield stress of the MRF under different current. The finite element method is applied in this section to analyse the magnetic field of the inner bypass MR damper and obtain the values of the magnetic flux density in the four activation regions under different current. Since the MR damper is a symmetrical structure, the magnetic field intensity of these four activation regions (Work Area 1, 2, 3 & 4) are symmetrical as well, as shown in Figure 3.6. The results of the magnetic flux density of work area 1 and Work area 4 are the same as well as the magnetic flux density of work area 2 and work area 3.

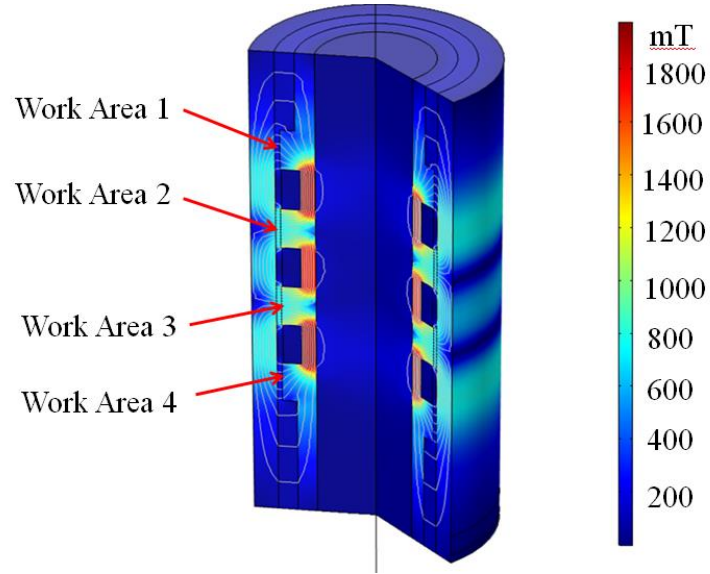


Figure 0.6 Magnetic field simulation

Fig. 3.7 presents the average flux through the four activation regions all increase with the 0.1A increment of input current I , which was set from 0A to 2A. The peak values of the magnetic flux density in the work area 1 and work area 2 are 260.8mT and 689.6mT respectively. In the multistage-coil structure of the MR damper, due to the additional coils

that create additional magnetic flux within the same cross-sectional geometry, the average magnetic flux density in activation regions of work area 2 and work area 3 are dramatically larger than that in activation regions work area 1 and work area 4.

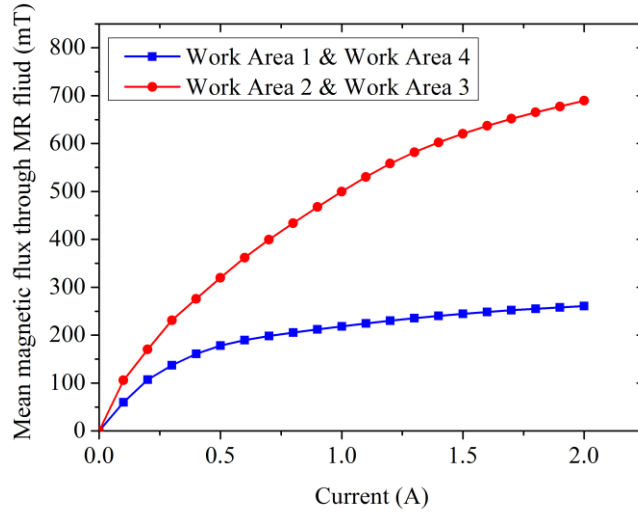


Figure 0.7 Average flux density through activation regions of the innovative MR damper

3.4 Experimental testing and result discussion

3.4.1 Experimental setup

In this section, experimental testing was conducted using a computer-controlled INSTRON test system (model 8033), as illustrated in Fig. 3.8, to demonstrate the dynamic performance of the new damper. There are three parts of the test system: the hydraulic grip, the self-powered variable stiffness MR damper and the hydraulic actuator. The hydraulic grip can fasten the top part of the MR damper and use the embedded sensors to collect the testing stroke and the generated force, meanwhile the hydraulic actuator can also grab the bottom of the damper and provide the controllable harmonic excitation to the MR damper. The tests to investigate the variable stiffness feature and the self-power generation capacity of the MR damper were conducted separately and detailed in the following two sub-sections.

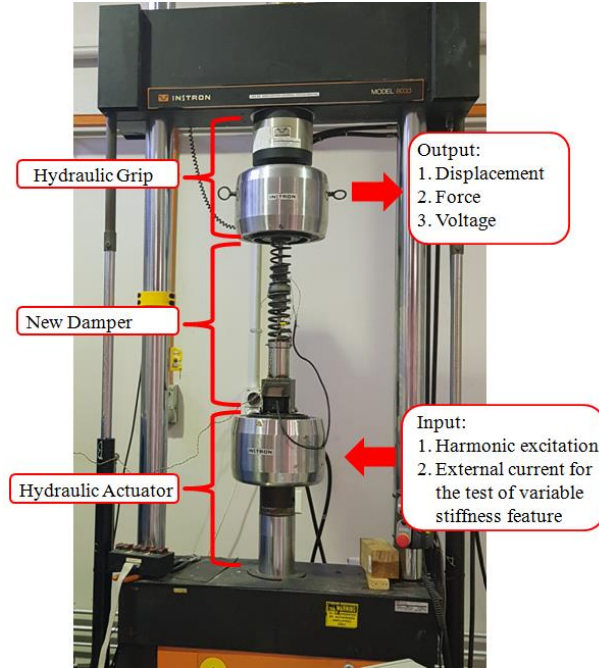


Figure 0.8 Instron test system installed with the prototype

3.4.2 Stiffness testing

To validate the variable stiffness characteristic, a harmonic excitation with a frequency of 0.15 Hz and different amplitudes (20 mm and 30 mm) was chosen as the excitation signal. The self-powering component is under open-loop scenario during the test. For each amplitude, different current levels changing from 0.0 A to 1.2 A with an interval of 0.4A was used to energize the MR damper.

During the experiment, the measured data from displacement sensor and force sensor was delivered to the computer for recording. Force-displacement relationship of the MR damper was used as the primary description method in the following analyses. The measured hysteresis loops indicating the variable stiffness are shown in Figure 3.9 and Figure 3.10. To analyse the working mechanism of the proposed MR damper, the hysteresis loop excited by 0.4 A current and 20 mm amplitude was taken as an example. It is seen that the force-displacement loop was hexagonal and that six letters from A to F were placed clockwise at the inflection points on the curve shown in Figure 3.9. From

point A to point D, the suspension is compressed while the suspension undergoes the opposite stretching process from D to A. The segmentation from point A to B indicates the friction and damping force of the whole system, including the friction and damping force of the generator, the friction force of the ball screw and the force generated by the variable stiffness component. During the segmentation from point B to point C, the top stiff spring was compressed. In this case, MR damper performs large stiffness. With the applied force increasing, the cylinder of the MR damper slides relatively with respect to its piston, which results in the compression of the lower soft spring. In this scenario, the two coil springs work in series and the MR damper demonstrates soft stiffness, as indicated by the segmentation CD. The segments DE, EF, FA are the stretch processes of the MR damper corresponding to segments AB, BC and CD.

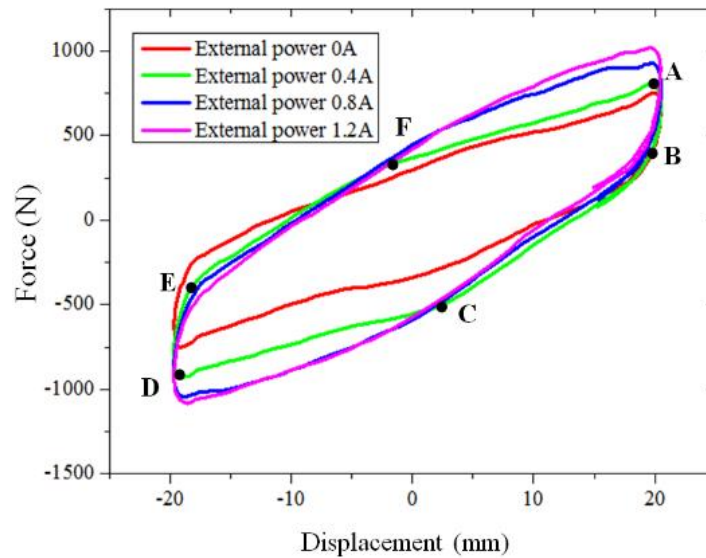


Figure 3.9 Force-displacement loops (20mm)

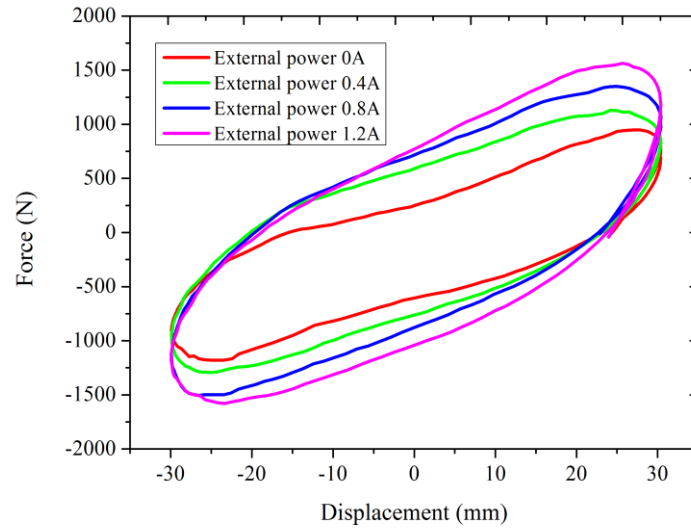


Figure 3.10 Force-displacement loops (30mm)

Figures 3.9 and 3.10 also indicate that the force-displacement loop tends gradually to be parallelogram rather than hexagon with the increasing current. This is because the damping force of the inside MR damping cylinder is large enough to hold the deformation of the top spring and thus the MR damper demonstrates large stiffness across the whole stroke. The equivalent stiffness of the MR damper can be calculated through the slope of various loops under 20mm and 30mm excitation amplitudes. The calculated results are shown in Fig. 3.11.

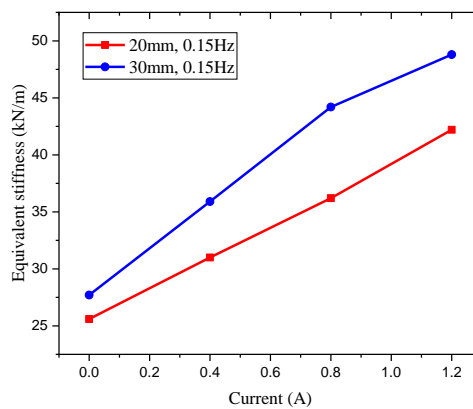
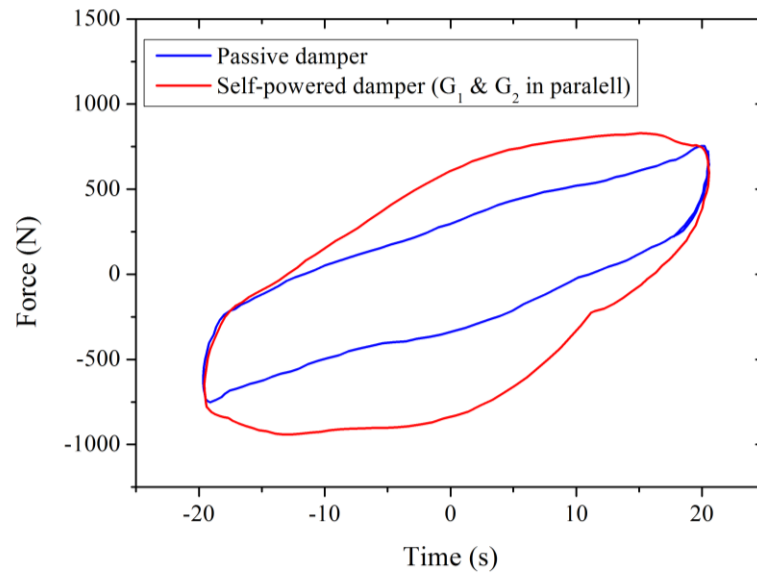
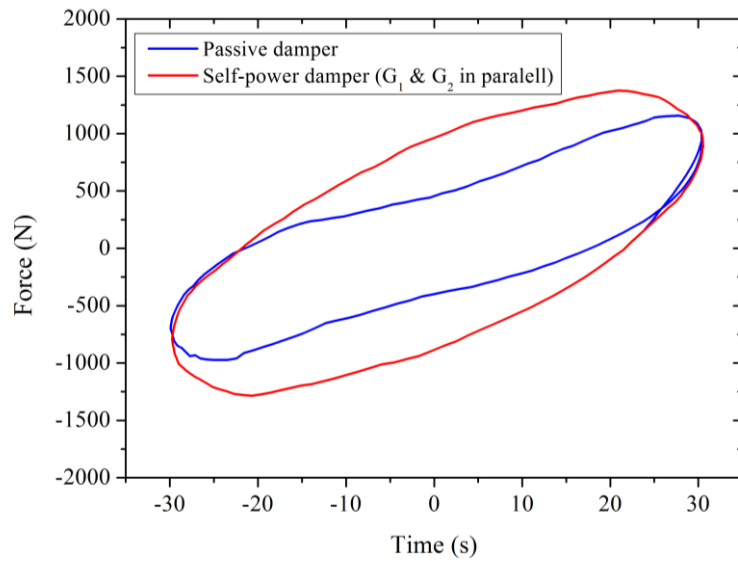


Figure 0.9 Equivalent stiffness of the damper

So as to further verify that the self-powered energy is sufficient to control the MR damper, the damping force generated from both of the self-powered MR damper and the passive MR damper are compared and presented in Figure 3.12. It is seen that the damping and stiffness of the self-powered MR damper are much larger than the passive MR damper, which means the self-generated power is enough to control the MR damper.



(a)



(b)

Figure 0.10 Property comparison between the passive MR damper and self-powered

MR damper (a) 20mm amplitude (b) 30mm amplitude

In order to verify the accuracy of the model built in section 3.3, the experimental data and the model simulation results under harmonic excitation of 20mm amplitude and 0.15Hz frequency are compared, as shown in Fig.3.13. All the parameters of the Bouc-Wen model can be determined through the parameter identification using the testing results of the MR damper. The parameter identification is conducted using Matlab/Simulink and the identified parameters are given in Table 3-3.

Table 0-3 Estimated model parameters of the MR damper

<i>Parameters</i>	<i>A</i>	<i>a_a</i>	<i>a_b</i>	<i>β</i>	<i>γ</i>	<i>c_{0a}</i>	<i>c_{0b}</i>
Values	16	250	128	808	893	100	10
<i>Parameters</i>	<i>k_{0a}</i>	<i>k_{0b}</i>	<i>k₁</i>	<i>k₂</i>	<i>m_i</i>	<i>c_e</i>	<i>f_e</i>
Values	70	-75	28.02 N/mm	42.43 N/mm	3.5 kg	23	150N

The fitting results between the modelling result and the experimental results are given in Figure 3.13. This figure shows that the established model can predict the dynamic performance of the MR damper accurately.

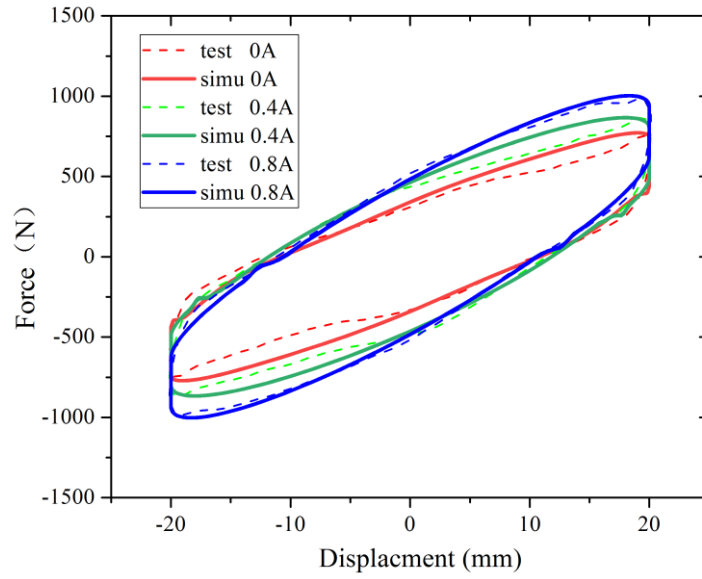
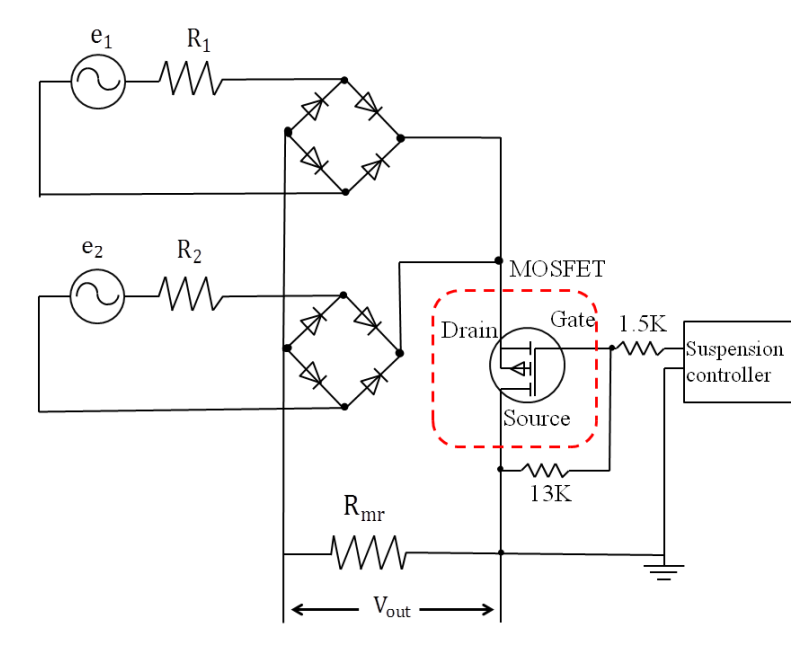


Figure 0.11 Comparison between the experimental results and simulation results

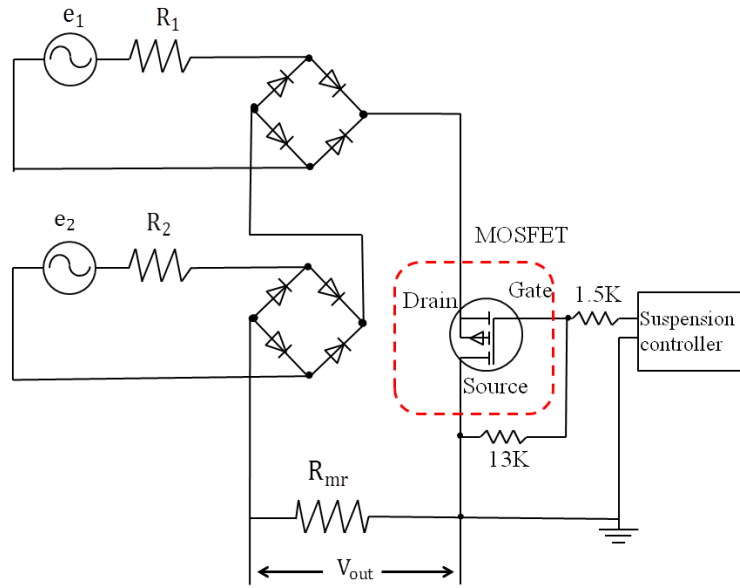
3.4.3 Testing of the self-powered generation capacity

In order to investigate the electricity generating capability of the self-powering component, a series of experiments were done under the harmonic excitation with 0.15Hz frequency and different amplitudes of 10mm, 20mm and 30mm. The generator used in this study is modified from a step motor with four wires (two coil sets). The two coil sets, defined as G_1 and G_2 , will generate electricity under external excitations. During the test, rectifiers are used to rectify the generated electricity. The reason to include the rectifier in our study is illustrated as follows. The direction of the direct supplied voltage changes too quick and will cause control issue because the self-powering circuit exists inductive resistance. Specifically, when the controller sends a control-on signal to the suspension, the self-powered energy will be used to control the MR damper. However, as the direct supplied voltage changes too quick, the conductive resistance of the circuit will delay the current increase of the damper coil and thus delays the response of the suspension system. The voltage changing speed will be significantly reduced with the usage of the rectifier

and the response speed of the suspension will be improved. The two rectifier circuits, parallel scenario and series scenario, are shown in Figure 3.14. A MOSFET switch is also built in the circuit to switch the circuit to be on and off so as to control the MR damper during vibration isolation. However, during this characterization of the self-powering component, the MOSFET is always on and the self-powered energy is always applied to power the MR damper. In the following experiment, the testing case where the MOSFET is on is defined as the closed loop for the self-powered suspension. Otherwise, it is defined as the open loop.



(a)



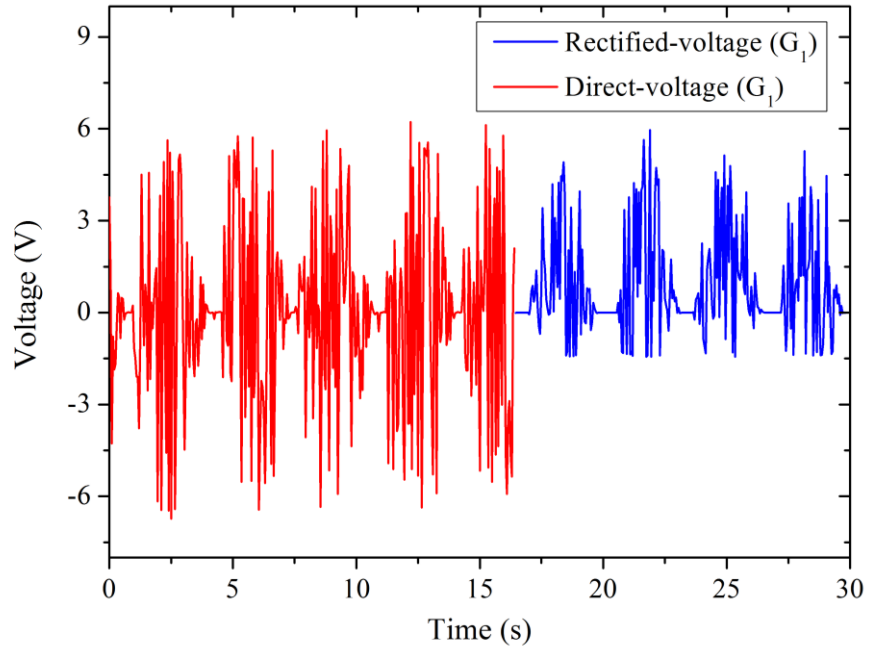
(b)

Figure 0.12 Rectifier circuits of the self-powering component (a) parallel connection (b) series connection

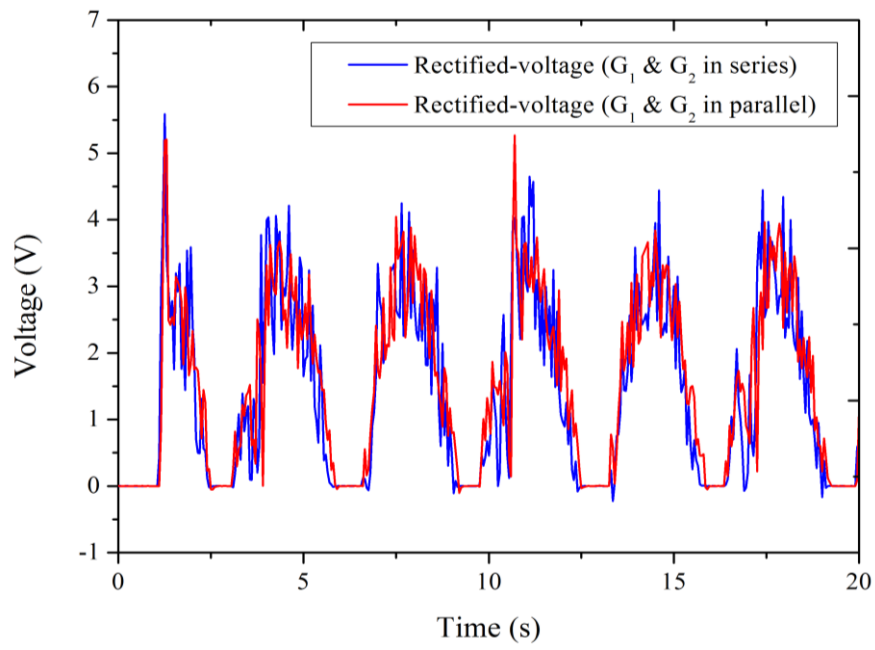
The testing results are shown in Figure 3.15. Figure 3.15 (a) presents the voltage generated by one coil G_1 with and without the rectifier circuit and Figure 3.15 (b) presents the generated power with the two rectified coils connecting in series and parallel, respectively. It should be noticed that the presented voltages in Fig.3.15 and Fig.3.16 are the voltages acting on the MR damper coil. The resistors with $13\text{K}\Omega$ and $1.5\text{K}\Omega$ resistance were chosen according to the operation manual of MOSFET. The harmonic excitation frequency and amplitude are set as 0.15Hz and 20mm , respectively. From Figure 3.15 (b) it can be seen that the self-generated energy of the rectifier circuits connected in parallel is similar to that generated in series. It is decided that the rectifier circuit connecting in parallel is used in our following study.

After the investigation of the influence of the rectifier circuit, the effect of the excitation amplitude is further studied. The two rectifier circuits for G_1 and G_2 are connected in

parallel and the excitation frequency is set as 0.15 Hz. The generated voltage under the excitation amplitudes of 10mm, 20mm and 30mm is shown in Figure 3.16. It can be seen that the generated voltage increases with the increase of the excitation amplitude. The RMS values of the self-generated voltages are 0.92V, 2.48V and 3.34V corresponding to 10mm, 20mm and 30mm, respectively. Additionally, according to the Ohm's Law of $V = IR_{mr}$ ($R_{mr} = 6.5 \Omega$), the RMS values of the self-generated currents can be calculated as 0.014A, 0.382A and 0.514A corresponding to the excitation amplitudes of 10mm, 20mm and 30mm, respectively.



(a)



(b)

Figure 0.13 The effect of the rectifier circuit on the power generation. (a) Directly generated voltage and rectified voltage of G_1 , (b) Rectified voltage of G_1 and G_2 connecting in series and parallel

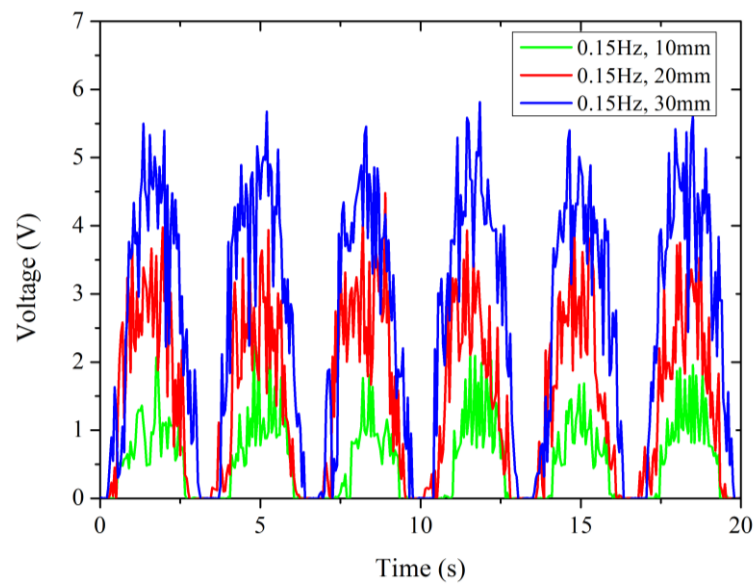


Figure 0.14 Self-generating capability under different amplitude

According to the above modelling and simulation regarding the self-powered component, the comparison between the simulated voltage and the experimentally obtained result is shown in Figure 3.17. According to the figure, the simulated voltages are very close to the experimental results, which means the proposed model can predict the electricity generating performance of the self-powering component well.

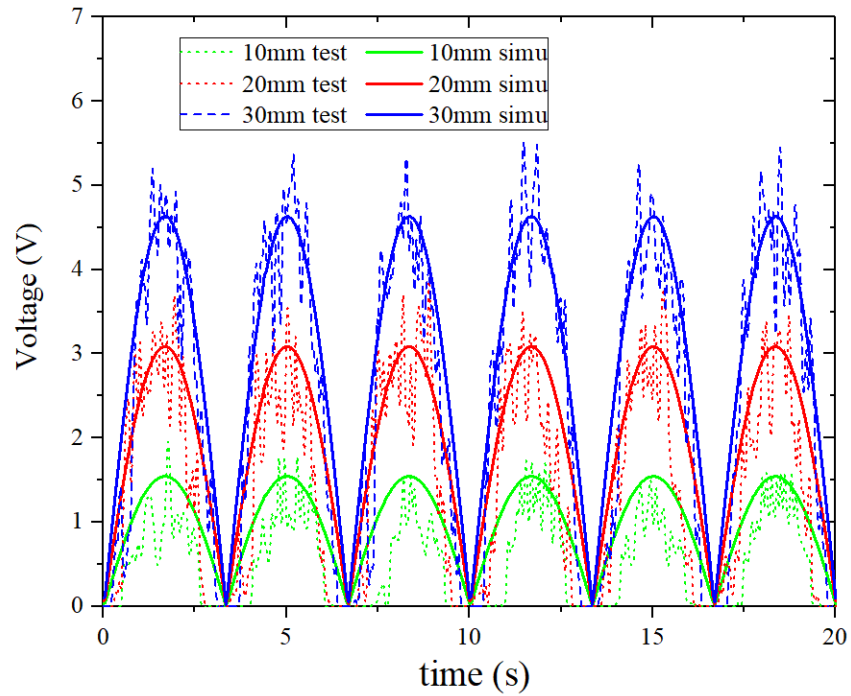


Figure 0.15 Modelling results of the self-powering component

3.5 Conclusion

This chapter presents the successful development of a compact energy free MR vehicle damper with stiffness controllable capability. The stiffness variation mechanism of the new damper was theoretically analyzed. Experimental testing was conducted to evaluate the performance of the MR damper. The stiffness controllability testing demonstrates that the stiffness of the MR damper can vary 70.4% when the applied current increases from 0A to 2A under the harmonic excitation of 0.15Hz frequency and 30mm amplitude. The evaluation results of the self-powering component verify that the effective energy

generated by the MR damper reaches to 2.595 W, which is sufficient to control its MR component.

Chapter 4

Experimental Evaluation of the Self-power Variable Stiffness Damper on a Quarter-car Test Rig

4.1 Introduction

Frequent vibration is detrimental to driver's safety and health, causing drivers' fatigue, which has been a dominate factor in a significant percentage of severe even fatal crashes. Musculoskeletal disorders are very common in jobs that involve driving, especially those required to drive over long hours and distances, and over rough environments with off-road vehicles or machinery operation. To alleviate the adverse impact to the drivers, suspension technology has been increasingly developed to reduce the vehicle vibrations. Hence, a semi-active vehicle suspension is studied for a better vibration suppression.

As presented in Chapter 3, an advanced long stroke stiffness controllable MR damper combining the self-powered capacity, which is the core component of the proposed semi-active suspension, was developed. In the meanwhile, the features including variable stiffness, and self-powered ability were validated via massive property tests in Chapter 3. In this Chapter, several controllers for the new MR suspension were investigated. Besides, the experimental under road excitations were conducted on a quart car test rig to validate the characteristics and effectiveness of the proposed suspension and controllers. The chapter is presented in the following order. Section 4.2 introduces the experimental setup regarding the quarter-car test rig installed with the proposed MR damper. Section 4.3 tells the mathematical model to describe the quarter-car test system and its specifications. Section 4.4 developed the road excitations used in the road tests using white noise generated by MATLAB/Simulink. Section 4.5 demonstrates the transmissibility of the quarter-car test system under different working modes by giving a sweep frequency

excitation. And section 4.6 evaluates the vibration attenuation performance of the MR damper integrated with two controllers on the quarter car test rig. Section 4.7 draws the conclusion.

4.2 Experimental evaluation of the self-powered variable stiffness damper on a quarter-car test rig

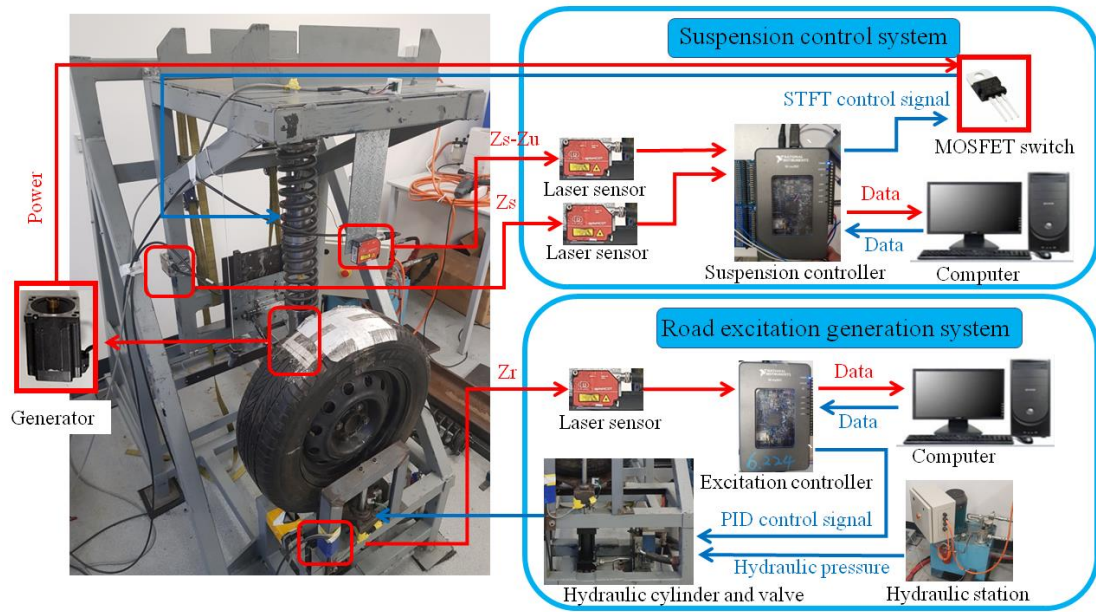


Figure 0.1 Quarter car test system for the novel suspension evaluation

A Quarter-car test system has been built in our lab to evaluate the ride comfort of vehicle suspensions. As shown in Figure 4.1, this quarter-car test system which consists of a car body, suspension system, controller and road excitation generation system was established. The road excitation generation system includes a hydraulic cylinder, a hydraulic valve, a hydraulic station, a laser sensor and a real time excitation controller using PID control algorithm (Model: myRIO-1900 , NI Corp.). Meanwhile, the suspension control system consists of two laser sensors, MOSFET (STP60NF06) switch and a real time suspension controller (Model: myRIO-1900, NI Corp.). Laser sensors are used to collect the displacement of the sprung mass and the stroke of the MR damper.

The MOSFET switch is controlled by the suspension controller and it is used to control the working mode of the self-powering circuit.

The circuit works in the following two modes, switch-on and switch-off. When the input PWM signal from suspension controller is +10V, the MOSFET switch is on, thereby connecting the coil of the MR damper in series with the self-powered component. In this case, the MR damper is energized by the self-powered energy, resulting in the increase of the damping force as well as the stiffness of the device. On the contrary, when the suspension controller sends a 0V signal to the MOSFET, it will be off and the circuit will be open. In this case, the self-powered energy will not be used to power the MR damper.

4.3 The mathematic model for quarter-car test system

The mathematic model for the quarter-car test system was developed considering the road excitation and tyre stiffness, which is shown in Fig. 4.2.

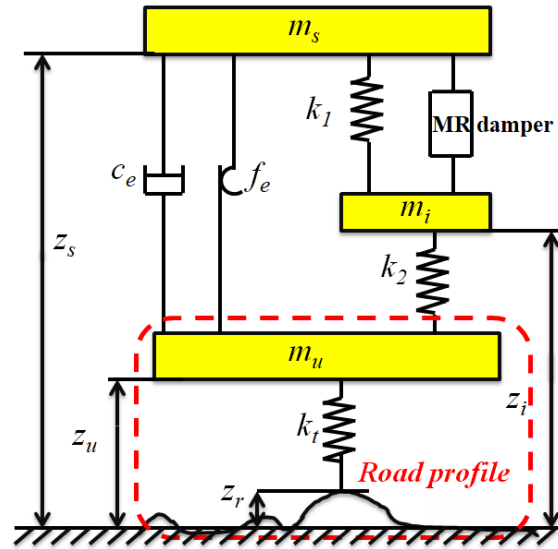


Figure 0.2 Mathematic model for quarter-car test system

The mathematic equation for this model can be expressed as:

$$m_s \ddot{z}_s = -F_m - c_e(\dot{z}_s - \dot{z}_u) - k_1(z_s - z_i) - F_d \quad (4-1)$$

$$m_i \ddot{z}_i = F_d + k_1(z_s - z_i) - k_2(z_i - z_u) \quad (4-2)$$

$$m_u \ddot{z}_u = F_m + k_t(z_r - z_u) + c_e(\dot{z}_s - \dot{z}_u) + k_2(z_i - z_u) \quad (4-3)$$

where, z_r is the displacement of the bottom, can be regarded as the input road excitations. z_s and z_u are the displacements of the sprung mass and unsprung mass. z_i denotes the displacement of the mass m_i . m_s , m_u and m_i represent the mass of sprung, unsprung, and the damper part, respectively. k_1 , k_2 , k_t indicate the stiffness coefficient of the systems. F_d is the damping force provided by the MR damper, and F_m is the force of the motor. The specifications of the quarter-car test rig are listed in Table 4-1.

Table 0-1 Symbol declaration

Symbol	Description	Value
ms	Spring mass	152.30 kg
mu	Unspring mass	30.00 kg
mi	Intermediate mass	3.50 kg
k1	Upper spring stiffness	28015 N/m
k2	Bottom spring stiffness	42428 N/m
kt	Tyre stiffness	100000 N/m

4.4 Road excitations design

In uneven roads, the road signal is completely different from the harmonic excitations. In order to simulate the real road conditions with random and variable amplitudes and frequencies. To present an obvious control affect, the peak of the road signal was set at 1.75Hz. The road excitation is generated via MATLAB/Simulink, which is illustrated in Figure 4.3.

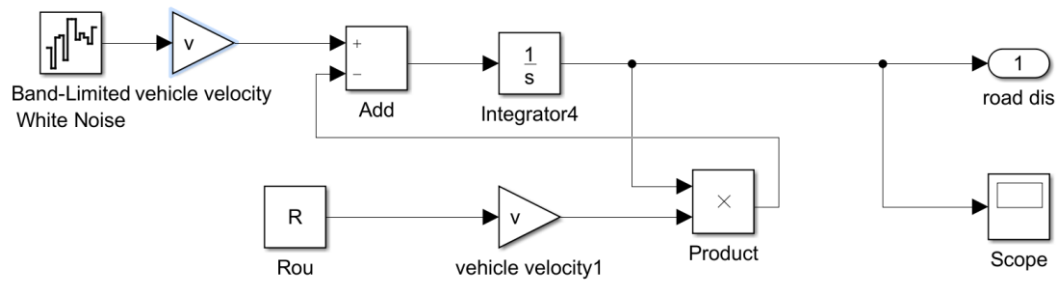


Figure 0.3 Road excitations generator

Where, the ‘band-limited white noise’ block could supply low frequency road excitations. The criteria such as the amplitude, frequency spectrum of the road signal by changing the parameters including vehicle velocity and road coefficient. Figure 4.4 shows the amplitude-time series of the generated random signal, and Figure 4.5 illustrates the frequency spectrum diagram, where, the peak in 1.75Hz could be observed.

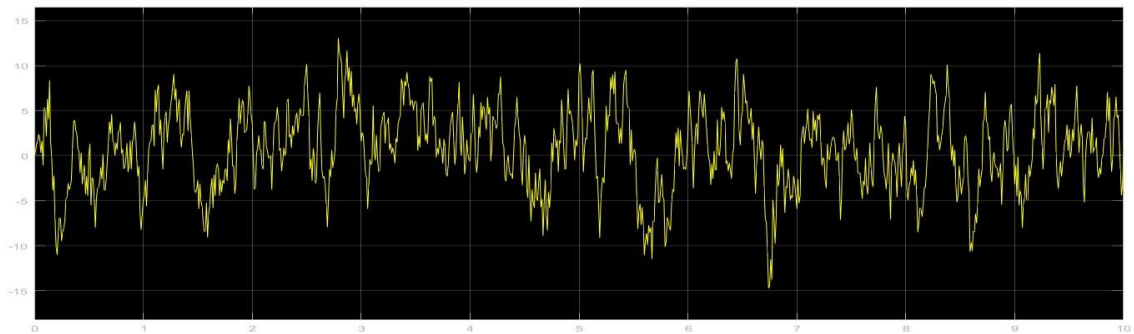


Figure 0.4 The random road signal

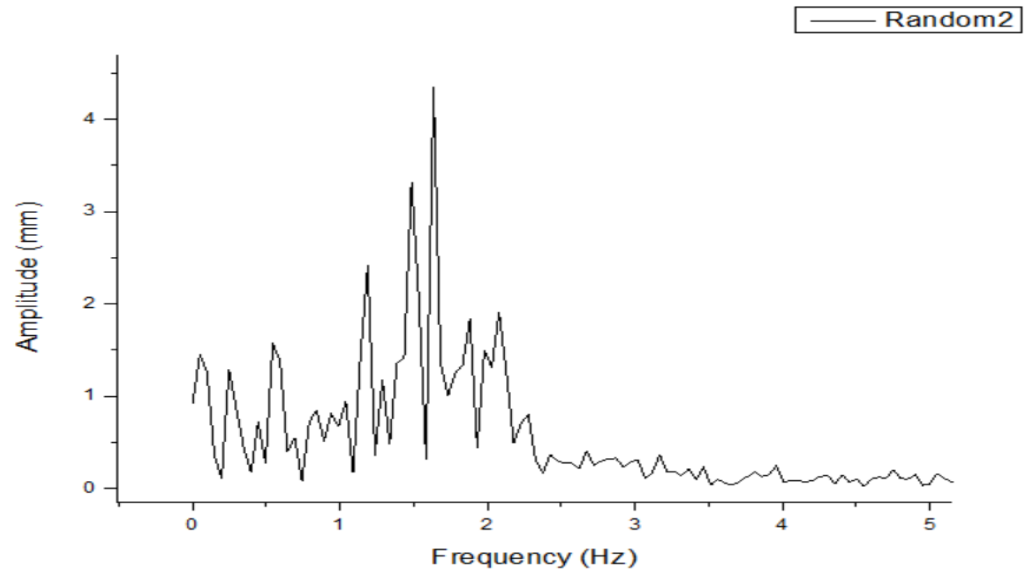


Figure 0.5 The frequency spectrum of the random road signal

4.5 Evaluation under sweep excitation

The harmonic excitation with sweep frequency from 0.5Hz to 2.75Hz was used to excite the quarter car test rig so as to obtain the transmissibility of the vehicle suspension. The transmissibility is the ratio of the car-body displacement to the road excitation displacement with respect to the sweep frequency, the lower the better. Four kinds of suspensions were tested on the quarter-car system: three passive suspensions energized by constant external currents of 0A, 1.2A and 2A, and self-powered suspension using the self-generated energy. For comparison purpose, three vibration transmissibility of the three passive suspensions were measured, presented together with the vibration transmissibility of the self-powered suspension in Figure 4.6. It is observed from the three passive transmissibility that the resonance frequency of the passive suspension increases with the increase of the applied current, indicating the frequency shift property. This is because the increase of the applied current leads to the increase of the damper stiffness. Then comparing the passive transmissibility (0A) to the self-powered one, an intersection is found with the intersecting frequency to be 2.1Hz. Then 2.1Hz is defined as the

threshold frequency. It is seen that if the excitation frequency is within the range from 0.5Hz to 2.1Hz, the transmissibility of self-powered suspension is much lower than the passive one; otherwise, the passive transmissibility is the lower one.

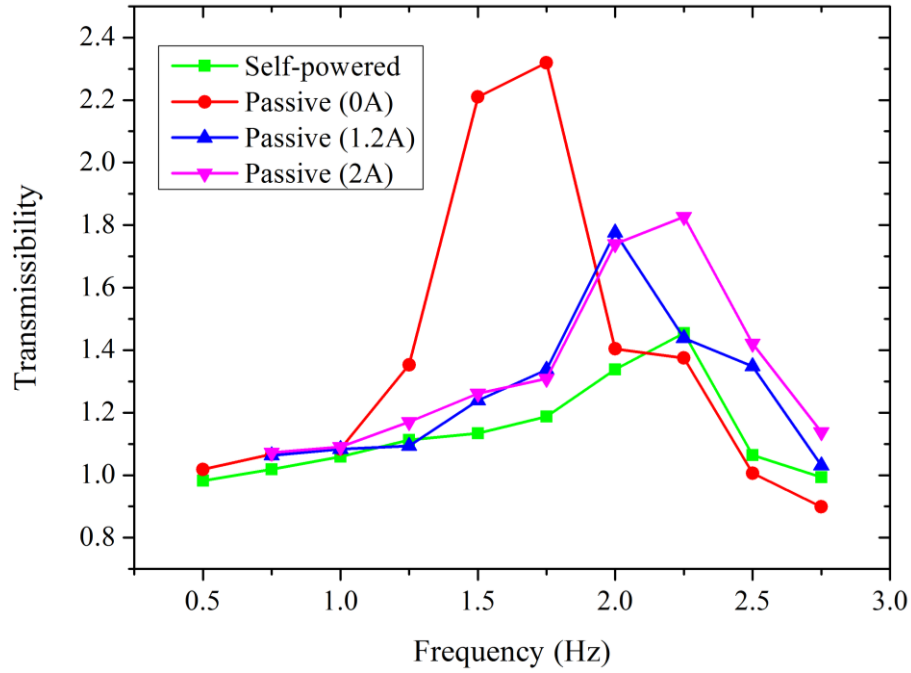


Figure 0.6 Transmissibility comparison under different cases

4.6 Control strategy Development

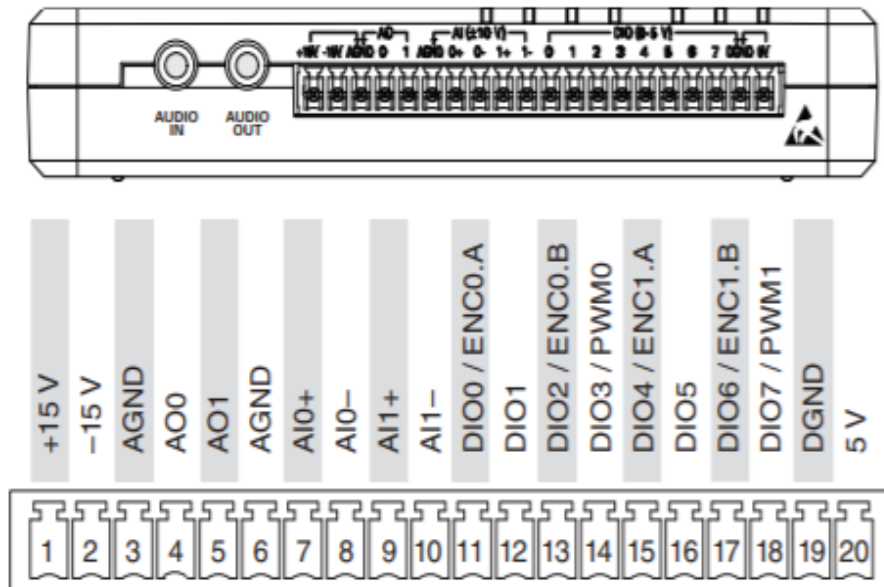
There are various control algorithms which have been employed in semi-active suspension systems, most of which are established on closed-loop feedback control to activate the systems. In this thesis, three control methodologies were developed and discussed, namely, Short Time Fourier Transformation (STFT) control, Skyhook control, and an improvement control algorithm based on Skyhook controller.

4.6.1 The control algorithm preparation

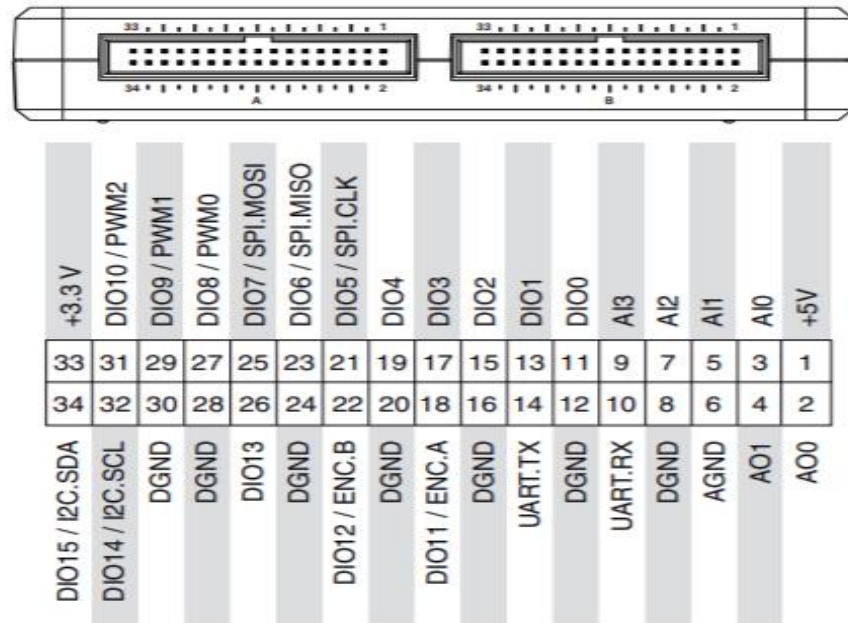
The programming of the control algorithm was developed by the software LabVIEW, which offers a graphical programming method to achieve interaction between the software and hardware configuration. The introduction of NI MyRIO, a real-time

embedded evaluation board, could read the program in LabVIEW, acquire the real-time data, and store the data into connected PC. The pin configuration of MyRIO is shown in Fig. 4.7. The input ports are generally connected to the sensors, while the output ports are connected to the power supply or the actuator of the suspension systems.

The PC could obtain the experimental data and analyse the results under various control strategies via the employment of LabVIEW and MyRIO. Moreover, a PID controller of the input profile is also utilized by a MyRIO board. The two NI MyRIO-1900 applied for data acquisition system and the PID controller is shown in Fig. 4.8.



(a)



(b)

Figure 0.7 MyRIO pin configurations of connectors (a) A, B and (b) C

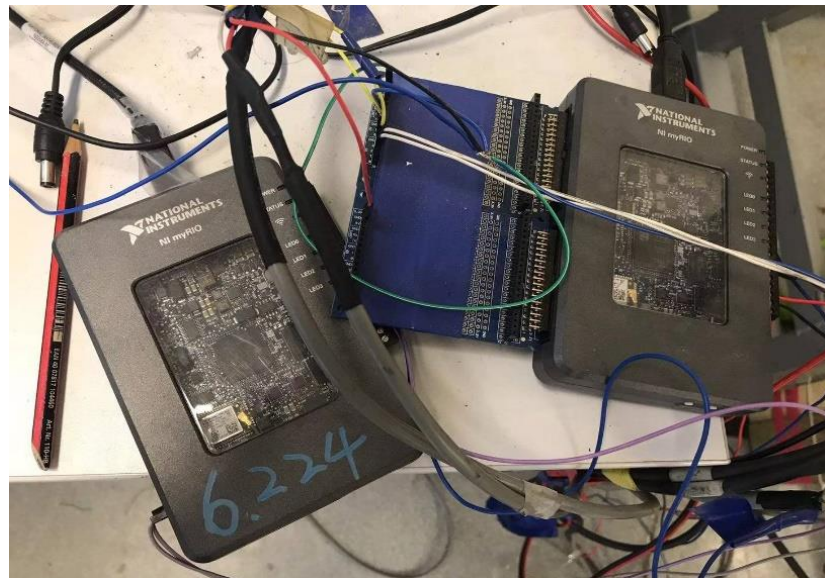


Figure 0.8 NI MyRIO-1900 and PID controllers

The MOSFET (STP60NF06) switch is a component controlled by a 10 V PWM signal. In this thesis, it is applied as a mode transfer switch, whose prototype and circuit diagram is shown in Figure 4.9. The working mechanism of the circuit is when the input PWM

signal from MyRIO board is +10V, the MOSFET switches on, which will connect the rectifier mentioned above, switching the system into self-powered variable stiffness mode. In this case, the damping force and stiffness of the suspension systems will change adaptively according to the various road excitations and reduce seat vibration. By contrast, when the output PWM signal from MyRIO is 0V state, the MOSFET will switch off, the working mode will recover to passive mode. Therefore, the automatical mode switch can be achieved.

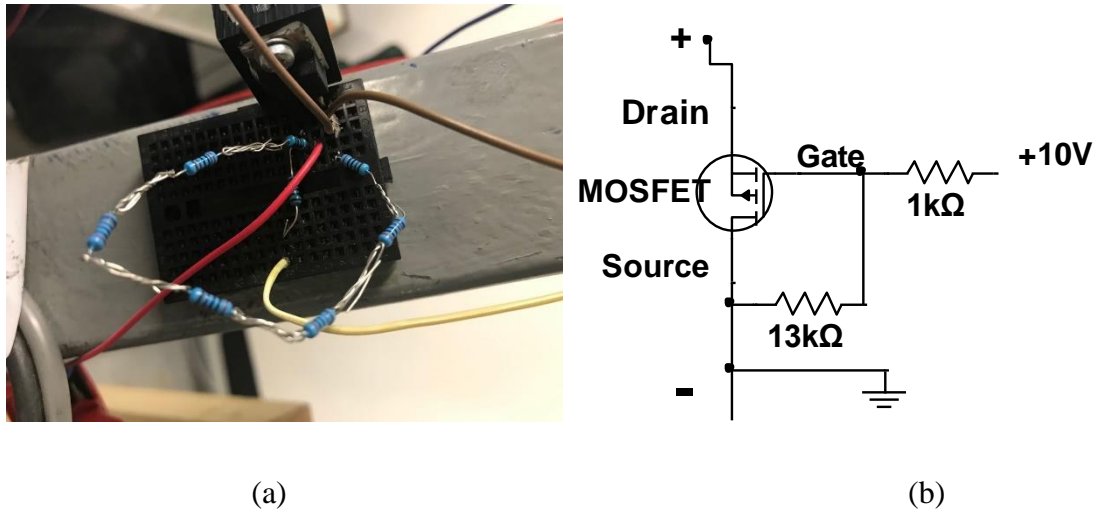


Figure 0.9 (a) Prototype and (b) circuit diagram of the MOSFET

4.6.2. Skyhook control algorithm

- Theoretical introduction

Skyhook control is a typical closed-loop control strategy for semi-active MR damper and its algorithms can improve the system performance to the level of active controls. The mathematical expression of the controller is shown below:

$$\begin{cases} \dot{z}_s * \dot{z}_u \geq 0 & 0V \\ \dot{z}_s * \dot{z}_u < 0 & +10V \end{cases} \quad (4-4)$$

where z_s , z_u is the displacement of the sprung mass and unsprung mass. The derivative of the displacements, \dot{z}_s and \dot{z}_u are the velocities of two sides of the damper, which are the

parameters used to denote the motion of the spring.

From the perspective of real-life scenarios, when \dot{z}_s and \dot{z}_u have the same direction, the spring vertical motion is limited in an acceptable range, which will not have severe negative effect on the drivers. On the other hand, if the directions of the two velocities were opposite, the spring would be compressed or stretched, causing significant vibration of the drivers' seats. Hence, when the product of the two velocities is negative, the MOSFET will activate the self-powering circuit, in this work mode, the suspension will be energized to provide a larger stiffness and damping force for the sake of vibration mitigation. The flow diagram to demonstrate the control process is shown in Fig 4.10. It is worth mentioning that a drawback of the skyhook controller, which is also a common issue for many feedback controllers, is that the feedback delay is not negligible. During vibrations caused by road excitation, the velocities modify instantaneously, so, sometimes the controller even gives a negative effect if the velocity states change.

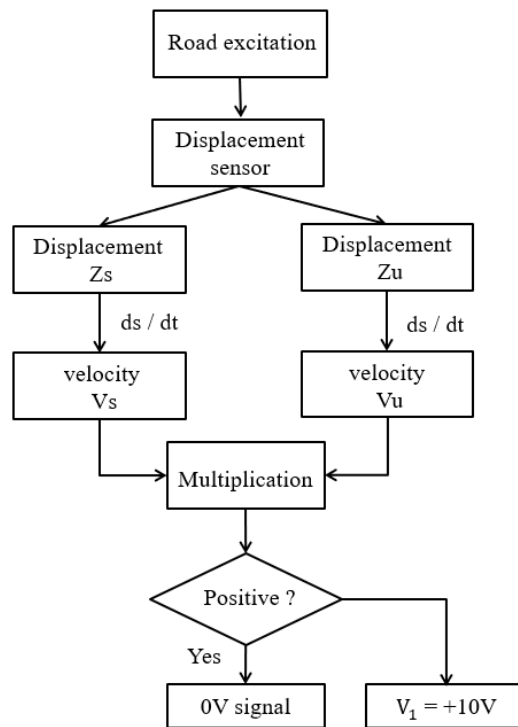


Figure 0.10 Flow diagram of skyhook control

- Programming of the skyhook control algorithm

The LabVIEW graphical program of the skyhook controller is shown in Figure 4.11. A comparison function and a case loop is employed to achieve the control strategy. The velocities were obtained from the derivate of the real-time displacement monitored by the laser sensors.

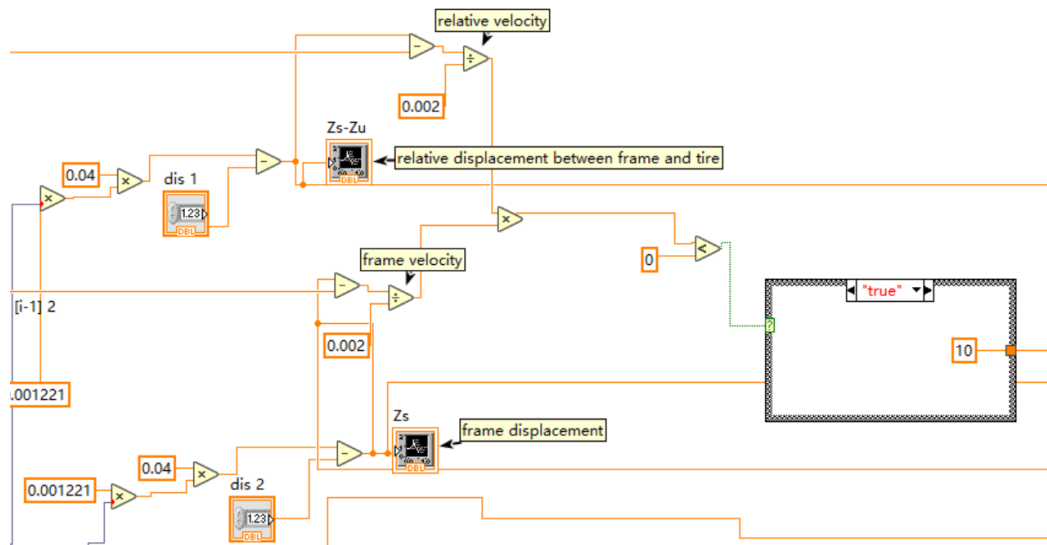


Figure 0.11 The LabVIEW program of the skyhook controller

- Experimental results

The displacement of the seat z_s which could directly reflect the vibration of the drivers' seats and the comfort of the drivers on the road. The experiments were conducted under three cases, namely, passive mode, self-powered mode, and skyhook controlled mode. The comparison among the above three cases are illustrated in Fig. 4.12. From the figure, it can be seen that the skyhook controller could boost the suspension performance dramatically rather than the all-time passive and all-time self-powered modes. Numerically, the seat vibration shaves by 21.3% and 30.5% in skyhook controlled mode than those of all-time self-powered and all-time passive modes, which meets our design expectation.

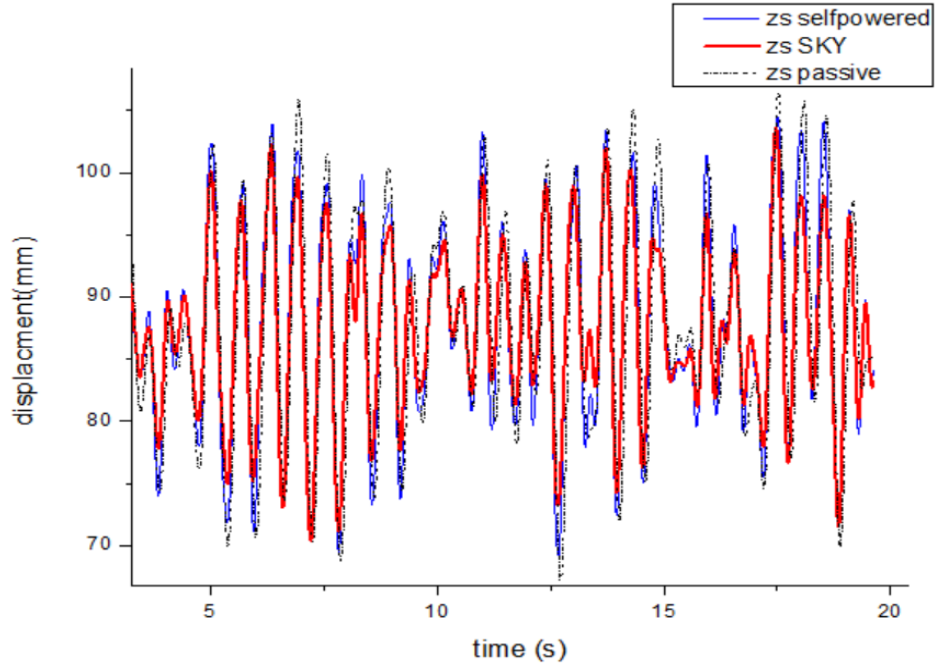


Figure 0.12 Comparison among three above cases.

4.6.3 STFT control algorithm

- Theoretical introduction

For semi-active suspension, the control strategy is also a significant part of the system. STFT control strategy [124, 125] is a popular and effective algorithm for non-resonance vibration control. The STFT algorithm splits the signal into small time segments and then analyses each time segment to find their dominant vibration frequency [110]. The multiplication of a short segment response signal $z_s(\tau)$ and a centred window function $h(\tau - t)$ can obtain the weighted signal. The frequency spectrum is obtained by:

$$z_s(\omega) = \frac{1}{\sqrt{2\pi}} \int e^{-j\omega\tau} z_s(\tau) d\tau = \frac{1}{\sqrt{2\pi}} \int e^{-j\omega\tau} z_s(\tau) h(\tau - t) d\tau \quad (4-5)$$

After attaining the frequency spectrum, the transmissibility T of the system on the frequency domain can be calculated by:

$$T = z_s(\omega)/z_r(\omega) \quad (4-6)$$

where $z_s(\omega)$, $z_r(\omega)$ is the displacement function of the seat and road surface.

After obtaining the dominant frequency, it will be compared with a threshold frequency.

The threshold frequency is the frequency corresponding to the intersection point of the transmissibility of the passive mode (0A) and self-powered mode as mentioned in section 4.3.

The transmissibility plots were obtained by giving a sweep frequency road signal.

Fig 4.13 and Fig 4.14 illustrate the theoretical and measured transmissibility plots of the above two working modes.

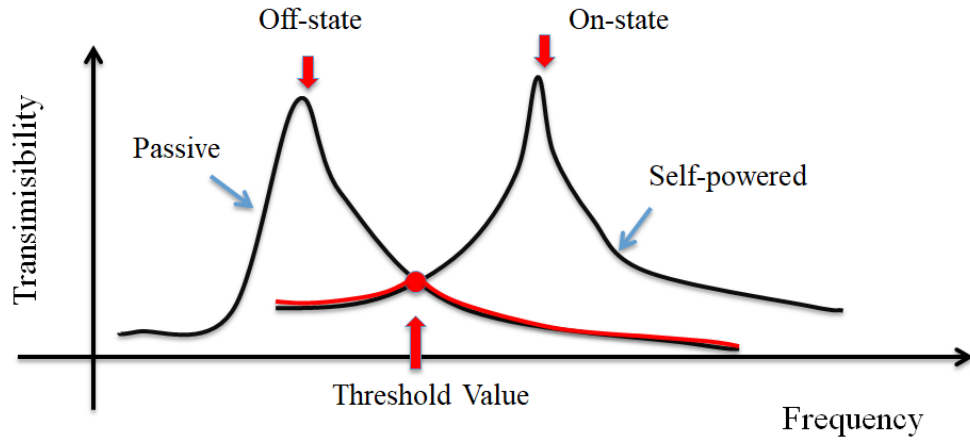


Figure 0.13 The ideal transmissibility graph of the two working modes

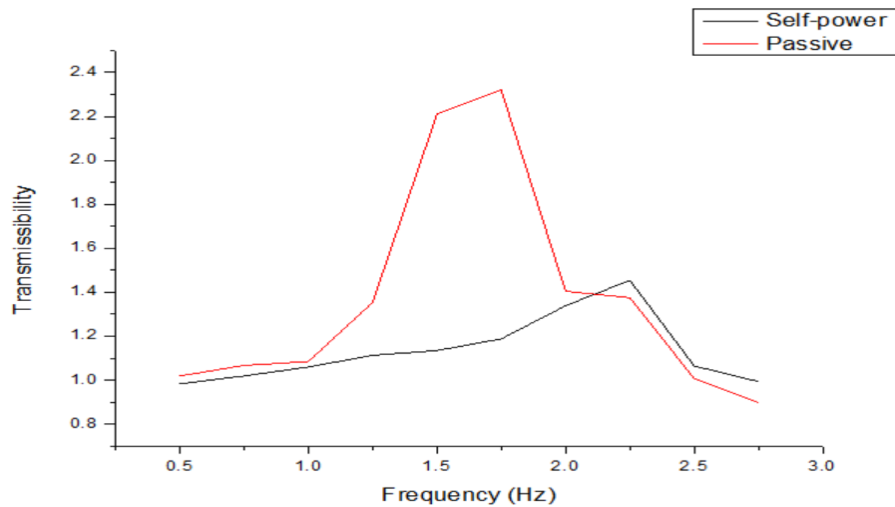


Figure 0.14 The measured transmissibility graph

From the figure, it can be seen that the intersection of the two graphs lies in 2.1Hz. Before 2.1Hz, the on-state (self-powered mode) has lower transmissibility, while when the frequency is larger than 2.1Hz, the off-state (passive mode) will provide lower transmissibility. Upon comparing the dominant frequency with the threshold frequency, the controller will send a control signal to the MOSFET switch so that the stiffness of the self-powered MR damper can be adjusted to avoid the resonance. To sum up, a mode switch is essential at the frequency of 2.1Hz to mitigate the transmissibility for all the time.

The judgment sentence of STFT control strategy can be written as:

$$\begin{cases} f > 2.1 & 0V \\ f \leq 2.1 & +10V \end{cases} \quad (4-7)$$

And the control flow chart of STFT control method is shown in Fig. 4.15.

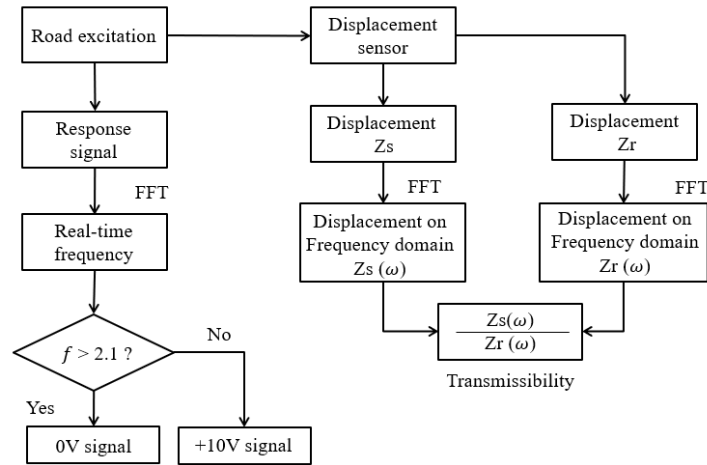


Figure 0.15 The flow diagram of STFT control strategy

- Programming of the STFT control algorithm

According to the LabVIEW graphic program of the STFT control algorithm shown in Fig 4.16, a filter, a conversion and an algorithm for calculating the real-time frequencies were utilized. The mentioned filter was set up High-pass to filter the undesired noises in the

input road excitations. The input road signal was converted from time domain to frequency domain by the conversion. After obtaining the real-time frequency, a comparison and a case loop were built to switch the working modes of the MR suspensions.

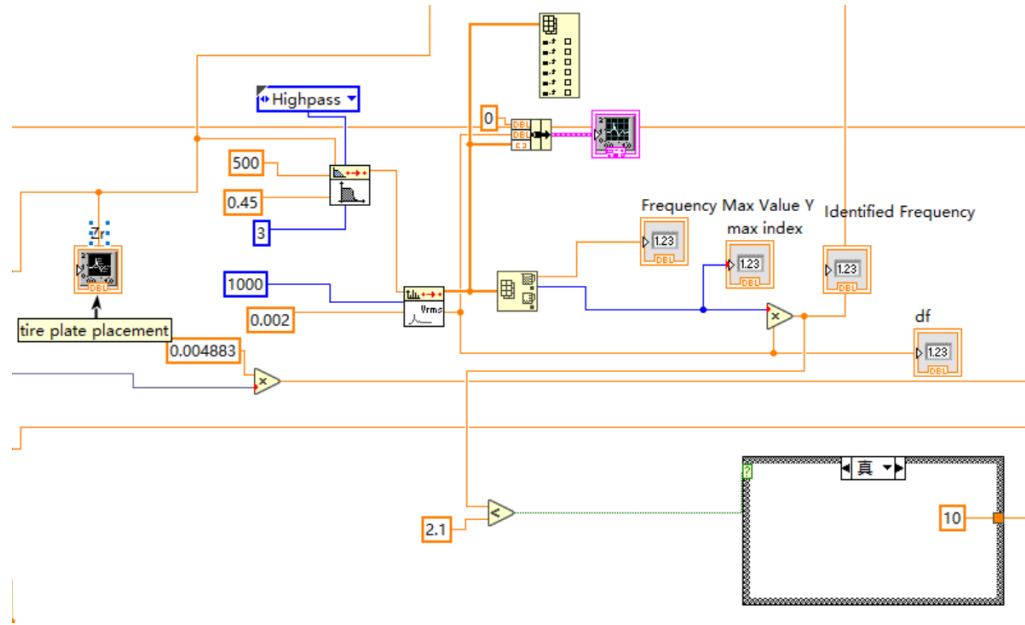


Figure 0.16 The LabVIEW program of the STFT control algorithm

- Experimental results

The displacement and acceleration responses of the sprung mass are important indications of the ride comfort achieved by a vehicle suspension system. These indexes are the core evaluation criteria and will be applied to the subsequent analysis. Figure 4.17 presents the comparison of accelerations between the passive open loop suspension (0A) and the self-powered closed loop suspension using STFT control. It can be seen that the acceleration of the controlled case is much lower than that of the passive suspension. Figure 4.18 indicates the control signal (voltage) and the self-powered energy during the STFT control. The generated power changes consistently with the control signal, i.e. when the control signal is 10V, the electric energy can be collected and used to power the MR damper; otherwise, no energy was applied to the MR damper. Figure 4.19 (a) and Figure

4.19 (b) present the displacement comparison between the passive suspension and self-powered suspension in time domain and frequency domain, respectively. For both the time domain and the frequency domain, the self-powered suspension under STFT control performs better than the passive suspension in reducing the displacement. The RMS values for both acceleration and displacement are calculated and listed in Table 4-2. The quantitative analysis results demonstrate that the STFT controlled self-powered MR damper reduces the acceleration and displacement by 16.8% and 21.4% respectively compared to the passive suspension.

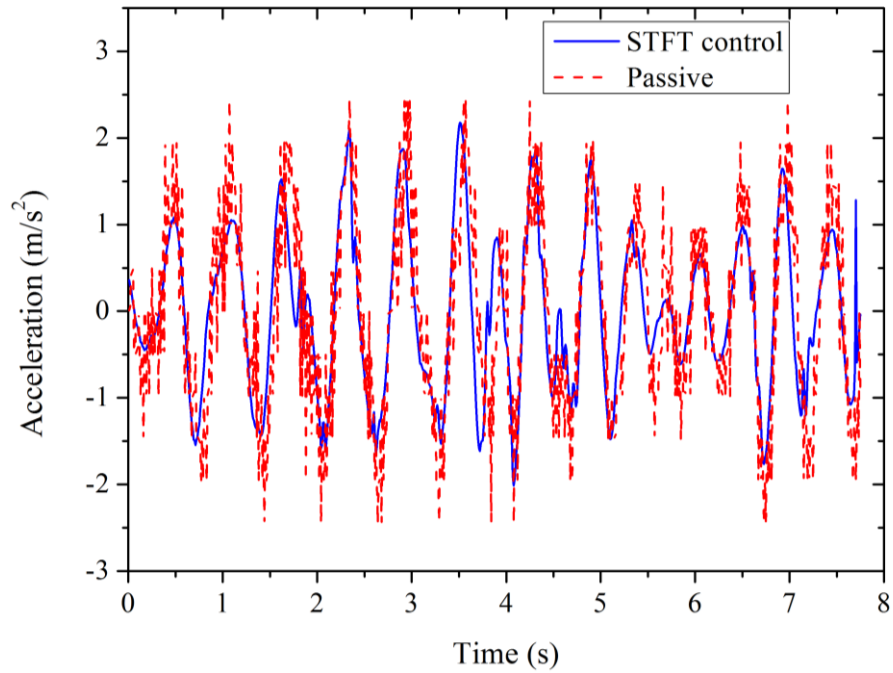


Figure 0.17 Acceleration comparison between the controlled MR damper and passive MR damper

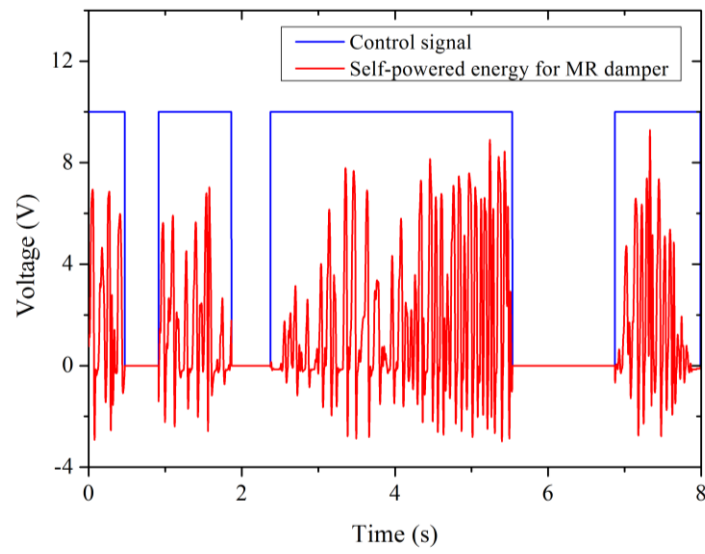
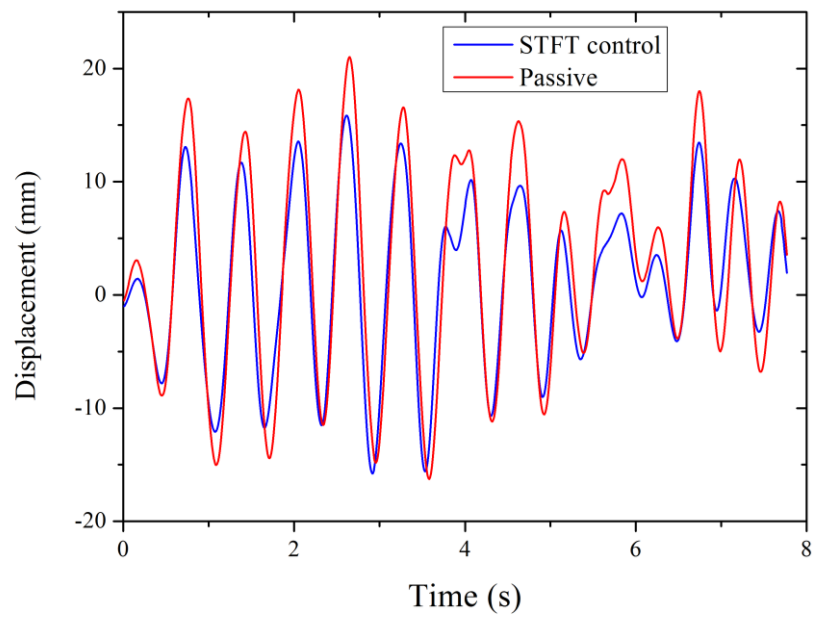
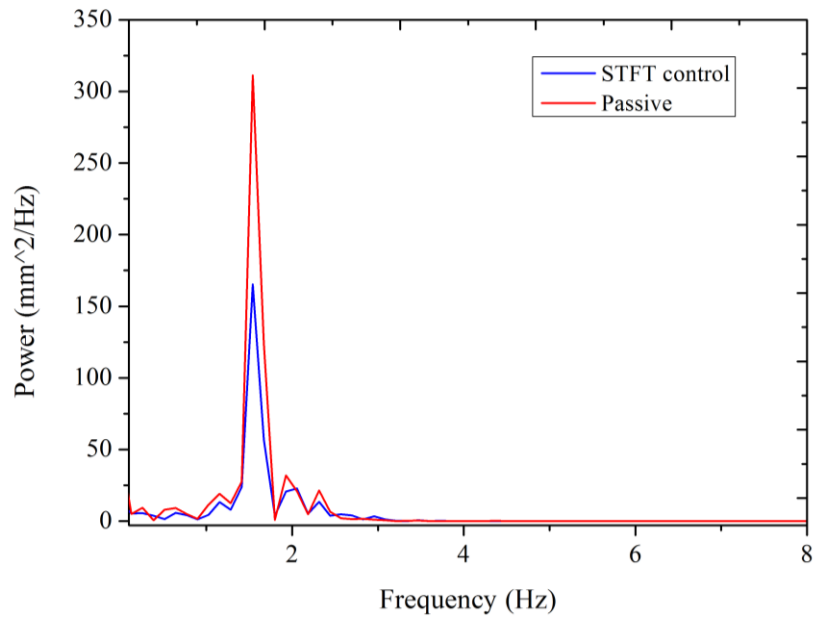


Figure 0.18 The control signal and self-powered energy of the MR damper under random excitation



(a) Time domain



(b)

Figure 0.19 Displacement response comparison between passive suspension and controlled MR suspension (a) Time domain, (b) Frequency domain

Table 0-2 RMS value

Object	STFT control	Passive	Reduction against passive
Acceleration RMS (m/s ²)	0.938	1.128	16.8%
Displacement RMS (mm)	7.411	9.429	21.4%

4.7 Conclusion

In this chapter, the STFT controller and the skyhook controller of a semi-active vehicle suspension which can provide variable stiffness and self-generate electric power was successfully developed. Experimental tests have been conducted to evaluate the performance of above two controllers. Regarding the skyhook controller, the results

illustrate the effectiveness of vibration mitigation as well. Nevertheless, this control principle could possibly have a counter effect due to the time delay of the feedback. Thus, an improvement is required for further study. The evaluation results of the self-powered MR damper on a quarter car test rig demonstrate that the self-powered suspension controlled by the STFT controller outperforms the passive suspension, with the acceleration reduced by 16.8% and displacement reduced by 21.4% compared with the passive case.

Chapter 5

Design, Modelling, and Testing of Semi-active Impact Absorber

5.1 Introduction

It has been a popular topic to mitigate the shock or impact such as the crash landings of aircrafts, the gun recoils in wars, and the explosions of weapons. All of which could be harmful to human beings especially spine parts, induce structural failure of the devices like helicopters, boats, vehicles, and gun systems. Thus, various impact absorber and shock mitigation devices were proposed. For passive devices, once they are manufactured, the properties are unchangeable, which will be undeniably effective for the investigated scenarios. However, in real-life shock, the situations would change frequently, in some cases, the passive device will work well, but in some other situation, the passive one would be a failure or even detrimental. Regarding the active devices, the performance facing various scenarios could be improved, but the energy consumption is striking. In addition, the device scale and assembly requirement are too high to be widely used in different fields. Therefore, the semi-active devices were put forward which combine the strength of passive and active devices, specifically, low energy requirement, flexible performance and compact structure.

Magnetorheological fluid (MRF), as a new kind of smart material which could reversibly modify its mechanical properties by providing or removing a magnetic field, has been investigated and utilized extensively. For conventional MR damper, the MRF is accommodated in two chambers, the MRF in one chamber will be pressed and pushed into another through a narrow bypass when shock/impact occurs. This design requires much MRF, while, the MRF that works during impact only occupies a small proportion

of all of the MRF. Besides, if the impact velocity was pretty large, at the impact moment, the velocity of MRF would be extremely large, causing an enormous damping force, which could put both passengers and the objective (helicopters, vehicles) in severe danger.

Therefore, in this thesis, a semi-active damper with a creative mechanical structure is proposed, which is an impact absorber, generally, employed in helicopters for soft landing. The main advantages are as following: 1) less velocity dependent. In this structure, an invariable channel is designated to accommodate the MRF instead of the chamber in the conventional MR damper. For the conventional damper, the difference between the chamber cross-section area and the MRF bypass cross-section area would generate pressure difference, subsequently induce the excessive velocity, by contrast, the proposed design avoids this drawback. 2) More MRF working areas and less MRF consumption. Due to the employment of multiple groups of electrical coils, the MRF working area has been enlarged dramatically. And the total amount of the MRF also decreases largely. By multiple impact tests, the new impact absorber integrated with a control algorithm is validated to be effective to maintain the peak damper force at around 500N over the impact velocities from 2m/s to 5m/s.

5.2 Design, analysis, and prototype of the impact absorber

5.2.1 Structure prototype of the impact absorber

The proposed new MR damper consists of an inner coil shaft, multiple electromagnetic coils, a steel shell, an outer cylinder, and MRF. The coils are connected in series, which are evenly distributed around the coil shaft. Besides, any adjacent coils should have reversed winding direction to prevent the generated magnetic field from being cancelled. There are 11 sets of coils, each set has 150 turns. The structural schematic of the new damper is shown in Fig. 5.1 (a). From the figure, it can be seen that the MRF is

accommodated between the steel shell and the cylinder, in which the cylinder is affixed on the ground, the steel shell is connected with the coil shaft using multiple screws. On the top of the shaft, there is a lid as a cover of the cylinder and MRF which is not shown in the figure. An O-ring is placed inside the lid to avoid the leakage of the MRF so that the gap between the cylinder and the steel shell is full of the MRF, and even the damper is experiencing a severe shock, the MRF will not have a high velocity. When the damper is experiencing a shock, the steel shell will move in a vertical direction, causing the MRF to work in shear mode.

Additionally, a conventional double-ended MR damper is designed as well as a control group to validate the effectiveness of the novel MR damper. The structural comparison between the two dampers is shown in Fig. 5.1. The top end of the damper is threaded.

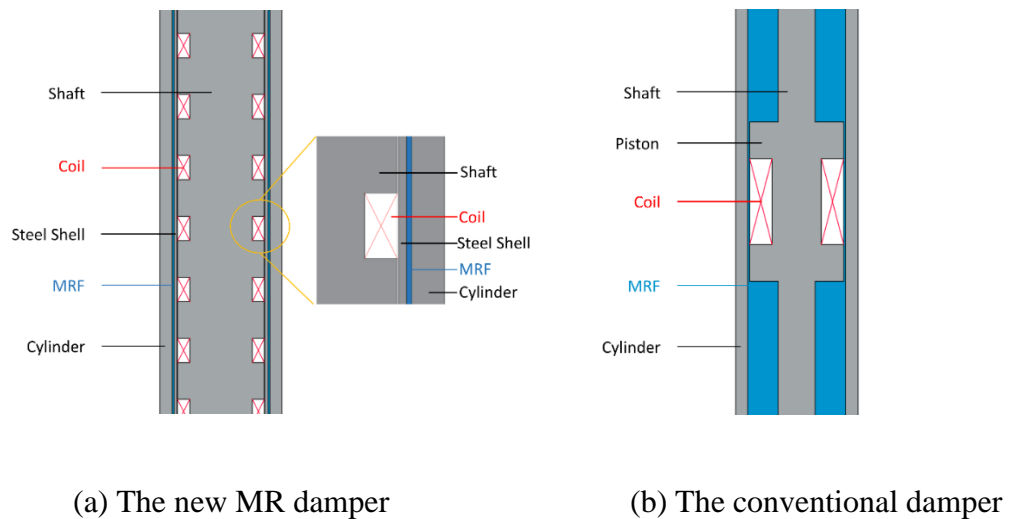


Figure 0.1 The structural comparison between the new MR damper and the conventional one.

The impact absorber generally consists of the proposed MR damper, a spring, a load cell, a laser sensor. The prototype of the impact absorber is shown in Fig. 5.2. The top end of the damper is threaded, from Figure 5.2, the thread is connected with a circular plate,

which is fixed together with a square disc by five positioning screws to have a uniform force. For the square disc, four holes are designed to connect with four smooth rods via ball bearings to guide the path of impact, making the impact structure a 1-DOF structure. The advantage of the 1 DOF structure is that only vertical force should be considered, which decrease the difficulty of experimental data analysis, and improve the accuracy of the further experiments.



Figure 0.2 The prototype of the impact absorber

5.2.2 Magnetic field simulation

In order to understand the effect of the given current on the magnitude of the induced magnetic field flux density, a magnetic field simulation is developed by employing the software COMSOL Multiphysics. The modelled damper in magnetic field simulation is shown in Fig. 5.3. The segment from point A to point G can reflect the magnetic field strength of the MRF working area because the damper can be regarded as an axisymmetric cylinder.

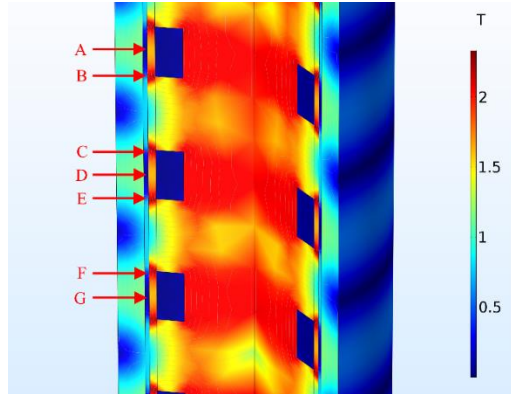


Figure 0.3 Magnetic field simulation

Figure 5.4 illustrates the corresponding magnetic flux density along the segment from point A to point G under different given currents. It can be clearly seen that the region of segment BC and EF, (i.e. the part between the adjacent coils) have the strongest magnetic field strength owing to more magnetic lines. By contrast, the magnetic flux density of the region which is adjacent to the coils is much lower. More importantly, the induced magnetic field intensity increases as the applied current increases, the maximum magnetic field intensity increases from 0.35T with 0.5A current to 0.76T with 3A current. To illustrate, a plot of averaged magnetic flux density with different current will be shown in Figure 5.5.

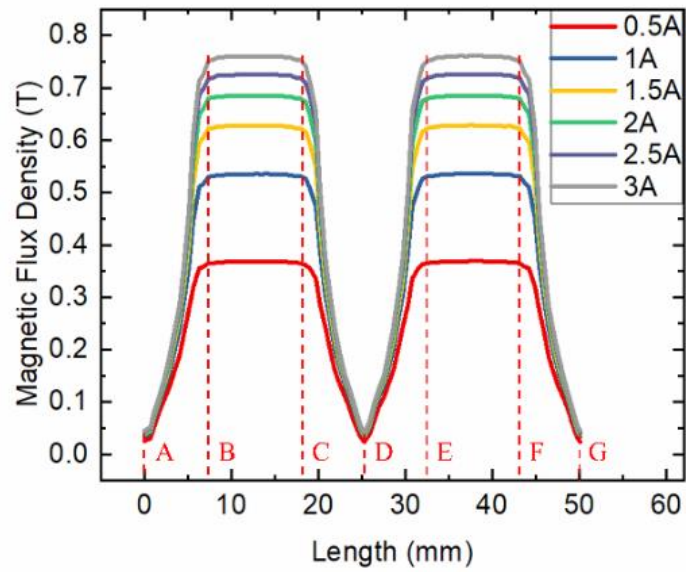


Figure 0.4 The magnetic flux density

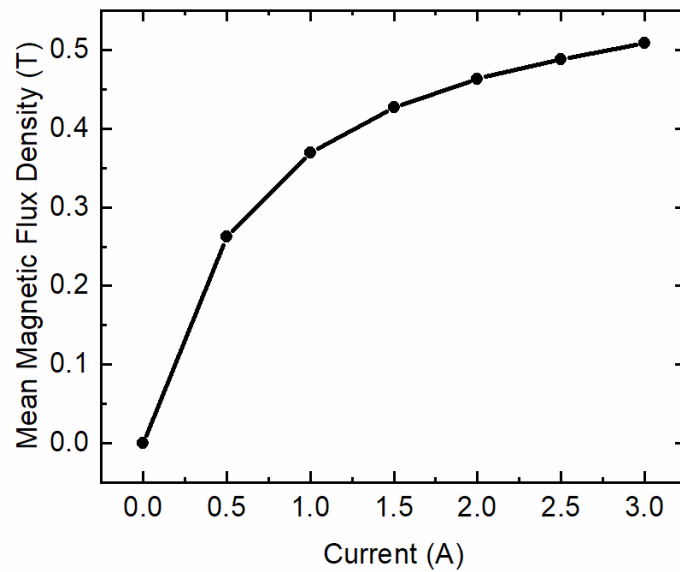


Figure 0.5 The averaged magnetic flux density

In order to provide strong evidence that the given current can activate the MRF, a data analysis was developed. In this thesis, the MRF applied is MRF-140CG, a kind of high concentration MRF, whose typical properties could be found from ‘LORD TECHNICAL

DATA' and listed in Table 5-1. Besides, the yield stress (kPa) versus magnetic field strength (kAmp/m or H), and B-H curve are given as well in Fig. 5.6 and 5.7.

Table 0-1 Typical properties of MRF-140CG (From Lord company)

Appearance	Dark Gray Liquid
Viscosity (Pa·s) @ 40 °C	0.280+/-0.070
Density (g/cm ³)	3.54-3.74
Solids Content by Weight (%)	85.44
Flash Point (°C)	>150
Operating Temperature (°C)	-40 to +130

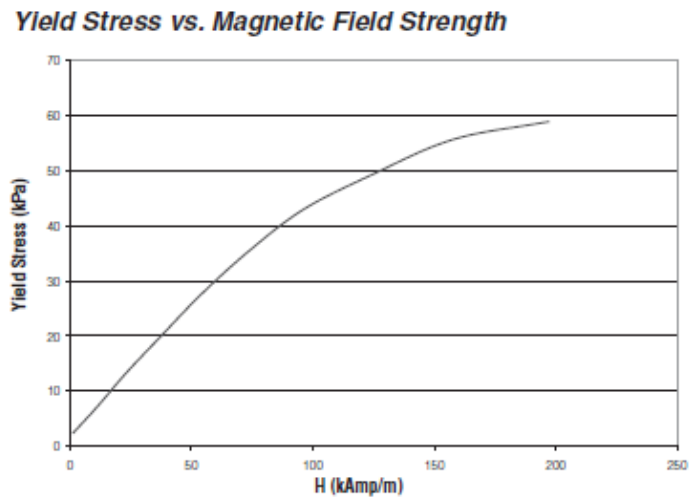


Figure 0.6 Yield Stress vs. Magnetic field strength

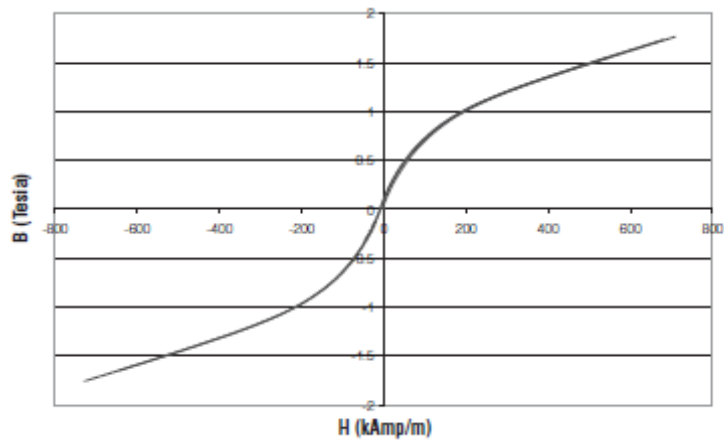


Figure 0.7 B-H curve

Therefore, the ‘Image digitizing tool’ in ORIGIN was used to obtain a discrete set of data that fit in the above graphs. Then these attained data were utilized for polynomial fitting. The fitted graphs were compared the original graphs shown in Figure 5.8 and figure 5.9. From the figures, the actual figure and fitted figure have a very high fitting precision. The fitted function can be expressed as following:

$$\tau_y = -7.02363 * 10^{-6} * H^3 - 1.15895 * 10^{-4} * H^2 + 0.50451 * H + 1.58401 \quad (5-1)$$

$$H = 116.56012 * B^2 + 65.72684 * B - 4.35269 \quad (5-2)$$

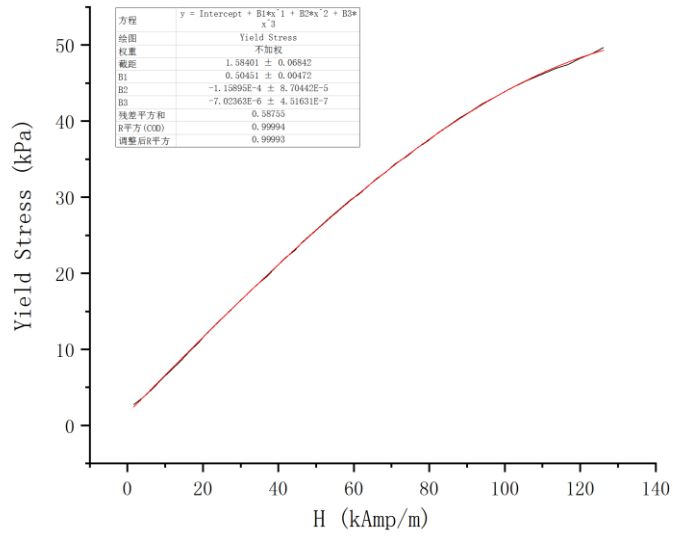


Figure 0.8 Comparison for yield stress

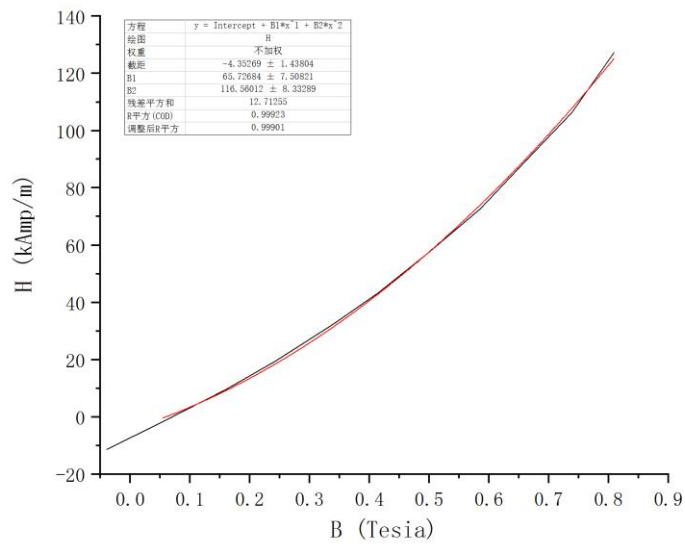


Figure 0.9 Comparison for B-H curve

Subsequently, from Fig. 5.4, the magnetic flux density increases from 0T to 0.75T when the current boosts from 0A to 3A, the corresponding yield stress is 1.584kPa and 46.442kPa. It is clear that the yield stress of the MRF enlarges significantly, enough to improve the performance of the MR damper.

5.3 Simulation

In this section, a simulation of the shock (impact) process was proposed based on MATLAB/Simulink. This simulation aims to obtain the required results of the shock such as displacements and forces, and compare them with the experimental data. The block diagram is built under the shear stress and the damping force formulas. Finally, by giving a current, the corresponding damper force and displacement can be calculated.

5.3.1 Block diagram building

- Damping force calculation

According to the above formulas,

$$\tau_y = -7.02363 * 10^{-6} * H^3 - 1.15895 * 10^{-4} * H^2 + 0.50451 * H + 1.58401 \quad (5-3)$$

$$H = 116.56012 * B^2 + 65.72684 * B - 4.35269 \quad (5-4)$$

The magnetic flux density is the input of the whole function regarding the damping force calculation, which can be obtained from COMSOL. The ‘user defined function’ (as shown in Figure 5.10) was applied to attain the theoretical damping force by the following formula.

$$\tau(y) = \tau_y + \frac{\mu v_0}{d} \quad (5-5)$$

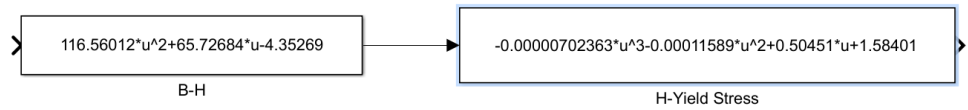


Figure 0.10 Yield stress calculation

Regarding the input, i.e., the magnetic flux density, the magnitude is various with the different locations in the magnetic field, and the relationship is not linear. Thus an averaged flux density is not accurate. Instead, a differential method is utilized. In the magnetic flux density graph (Figure 5.4), the magnetic field distribution is composed by

multiple repeating units. As shown in Figure 5.4, the part from ‘A’ to ‘G’ is a unit. The graph was sketched by 47 groups of data, which will be imported into the Simulink program.

After building the block diagram of the yield stress calculation, the effective area of the MRF should be calculated, which will be divided into 46 parts. In this thesis, the contact working area can be represented as the area of a rectangle, whose length is the circumference of the circle, width is the height in the structure. However, the diameters of the two sides of MRF is unequal, so the average diameter is selected. The basic specifications are listed in the below table. The Simulink program is shown in Figure 5.11.

Table 0-2 Parameters of effective area

Inner diameter	38.4 mm
Outer diameter	40.0 mm
Averaged diameter	39.2 mm
Height for one unit	25.241 mm
Number of differentials	46
Area for one part	0.00006757 m ²
Total Height	240 mm

‘Integrator’ block (Figure 5.13). Among these parameters, the parameter velocity has a changeable initial value for different release heights. And the momentum conservation theory is applied. During the calculation, there is an assumption that once the drop mass touches the impact structure, they will move together without relative motion. The calculation principle can be expressed by the following equations:

$$m_1 * g * h = \frac{1}{2} * m_1 * (v_1)^2 \quad (5-6)$$

$$m_1 * v_1 = (m_1 + m_2) * v_2 \quad (5-7)$$

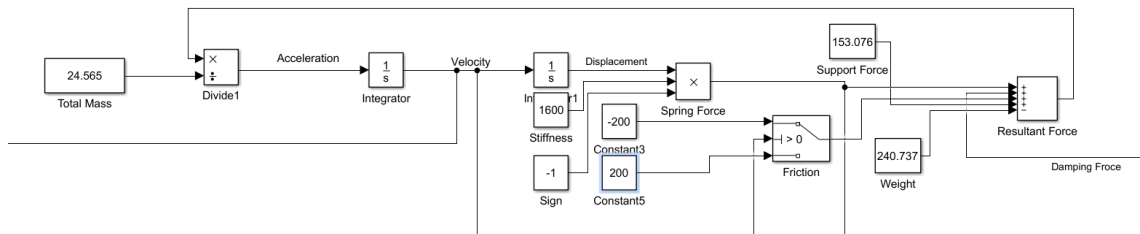


Figure 0.13 The acc-velocity-displacement relationship

From the above graph, the resultant force contains five parts, namely, friction, spring force, damping force, weight, and the support force. And the overall block diagram could be constructed by the combination of all above parts.

5.3.3 Simulation results

By running the block diagram with different given initial velocity and current, the simulated displacement, velocity and force graphs could be gained. The simulation was conducted by two parts, current dependency and velocity dependency.

The displacement, velocity, and force versus time graphs are as shown in the below figure (Fig. 5.14, 5.15, 5.16). For current dependency, the current ranges from 1A, 2A to 3A.

When the release height is 0.2m:

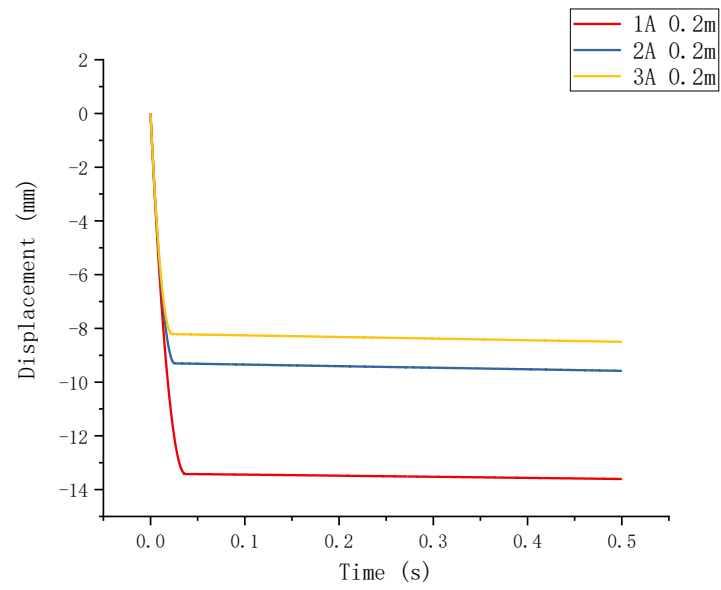


Figure 0.14 Displacements under different currents with 2m/s impact velocity

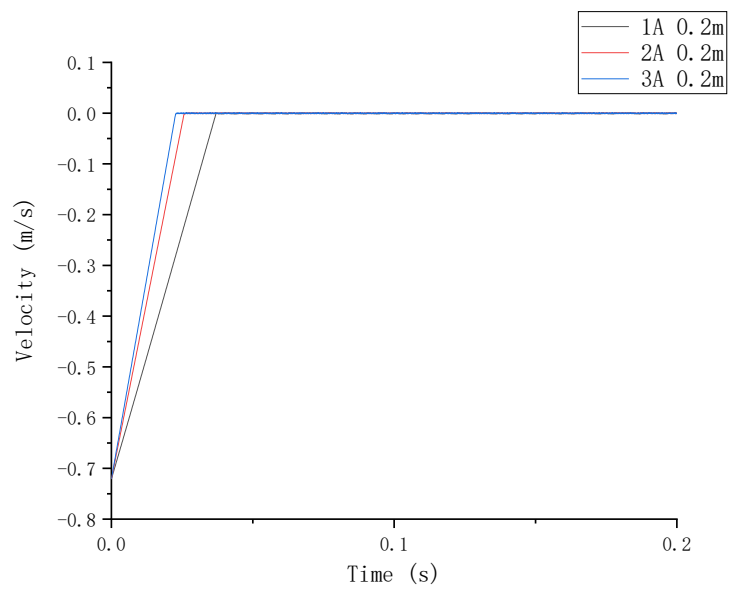


Figure 0.15 Real-time velocities under different currents with 2m/s impact velocity

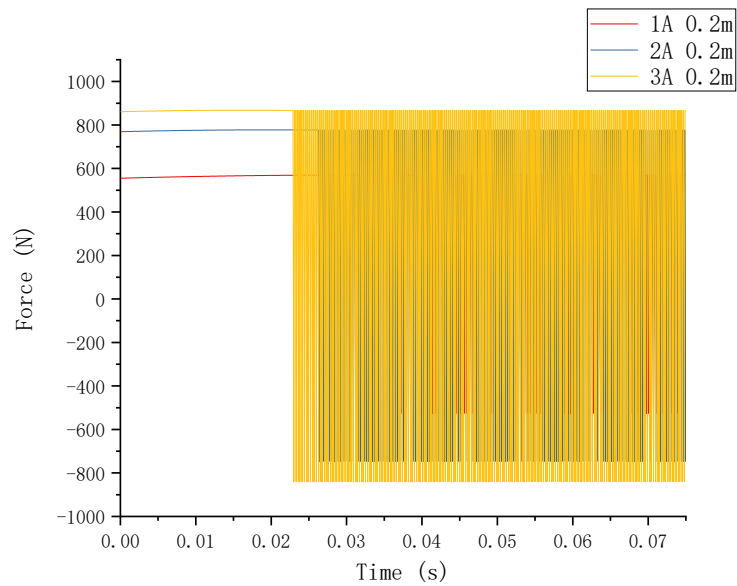


Figure 0.16 Forces under different currents with 2m/s impact velocity

As for the Displacement-Time graph, the tendency, generally, is similar to that of the drop hammer tests: the displacement decreases as the current increases. In terms of the Velocity-Time graph, it took shorter time period for the cases with larger applied current to reduce the velocity to zero. The velocity reduction rate (i.e. the slope of the graph) looks like a straight line, but actually not. The velocity reduction rate is the acceleration of the impact structure, which is directly decided by the resultant force, as mentioned before, the damping force will be determined by the velocity and the magnetic flux density, and the velocity only takes a minor part of that. So, when the current is constant, the magnetic will also be stable, so the damping force would only change slightly, thus the acceleration modifies as well, hard to distinguish from the figure. In addition, in the stable stage, the velocity also fluctuated frequently (Figure below) until all the energy is dissipated. The direction of force is decided by the direction velocity, so it keeps switching.

For the simulation, all the tendencies of displacement, velocity, force are as expected. The

force increases sharply as the given current enlarges, and also increases slightly when the impact velocity is getting larger. And the displacement will decrease as the current increases, increases as the impact velocity increases. But the specific data is obviously different from the experimental data, which may be due to several reasons:

- The initial impact velocity is not accurate.
- The friction generated by the ball bearings is not accurate.
- The actual simulated magnetic flux density might be less than the simulated one due to the external interruption.

According to those reasons, the further improvement will be proposed in the future, obtaining the consistent simulation results with the experiments.

5.4 Experimental tests

5.4.1 Property test of the proposed linear impact absorber

To validate the effect of the given current on the damper force, the property test was conducted using MTS machine as shown in Fig. 5.17. And Fig 5.18 shows the damping force tendency under different given current from 0A, 1A, 2A to the maximum value 3A. The frequency is 0.5Hz and the amplitude is 10mm. It can be seen from the figure, when no current is provided, the original damping force is around 100N, while there is a surge in damping force when a current is given. For one displacement, there are two corresponding forces, forward and backward, respectively. The mathematical expression is shown below:

$$\begin{cases} F_t = k(x_0 - 10) - F_{mrf} + mg & \text{For Forward} \\ F_t = k(x_0 - 10) + F_{mrf} + mg & \text{For Backward} \end{cases} \quad (5-8)$$

It is clear that when the displacement is -10mm, the difference of the above two forces is $2F_{mrf}$, so we can obtain that the damping force increases to approximately 300N, 415N, 510N when the currents are 1A, 2A, and 3A, respectively. Hence, a larger current truly

leads to a larger damping force.



Figure 0.17 MTS test system

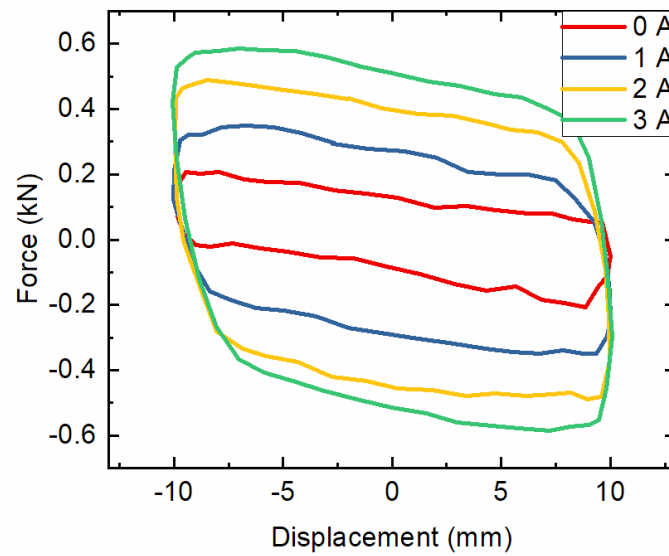


Figure 0.18 Force-displacement plots under different currents

5.4.2 Constant current impact tests

For this section, multiple drop hammer tests (impact tests) were conducted to simulate the real-life impacts, and obtain the controllable damping range of the proposed MR damper. The current varies from 0A to 3A. And the impact velocity could be controlled

and adjusted by changing the release height of the hammer, where the release height is selected as 0.2m, 0.3125m, 0.45m, 0.6125m, 0.8m, 1.0125m, and 1.25m, reflecting the impact velocity changing from 2m/s to 5m/s with 0.5m/s increment slot.

The experimental setup is shown in Fig 5.19, which demonstrates the process of data and command transferring during the tests. First of all, the DC power supply provide 24V voltage to activate the load cell. Besides, the power amplifiers are employed to give variable currents to the coils in the damper, contributing to the controllable magnetic field. During the tests, the laser sensor and the load cell could monitor the dynamic performance (real-time displacement and force signals) of the proposed MR damper, then transfer the data into NI myRIO for recording, which could be looked up and analyzed via a computer.

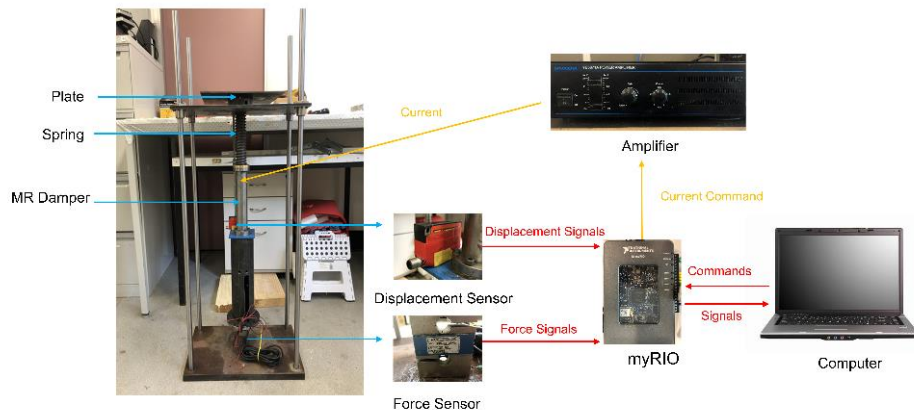


Figure 0.19 The experimental setup for impact tests.

Figure 5.20 and 5.21 are sample experimental results for illustration. The initial impact speed is 3m/s, and the supplied currents are 0A, 1A, 2A and 3A. It can be clearly seen that displacement shaves sharply after giving a larger current, when the current is 3A, the displacement is approximately 25mm, which is nearly one third of that of 0A current. Besides, large currents result in large damper forces. The force increases by over 300N as current climbs, which proves the properties (magnetic field sensitive property) of the

MRF.

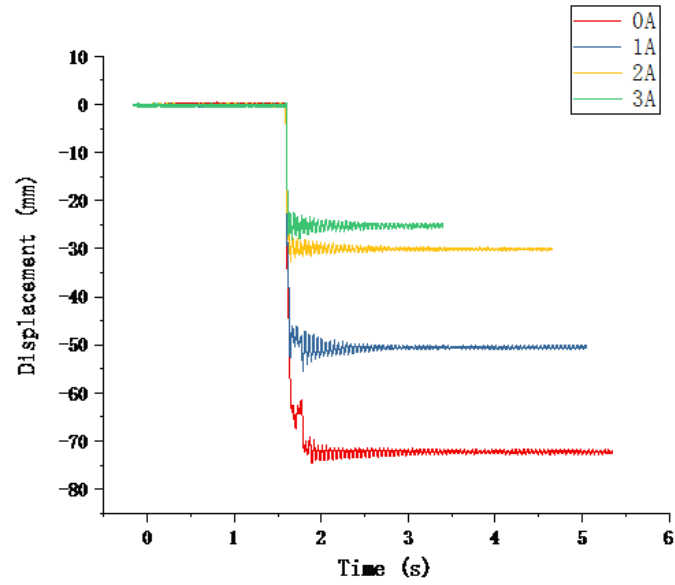


Figure 0.20 Displacement-time plot

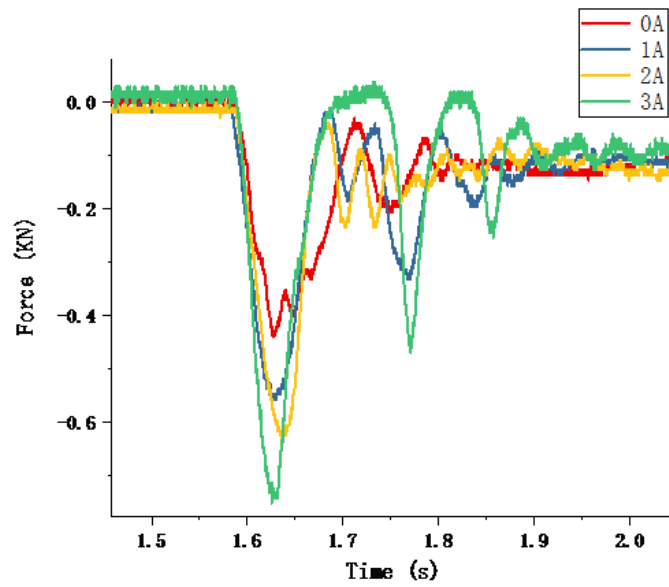
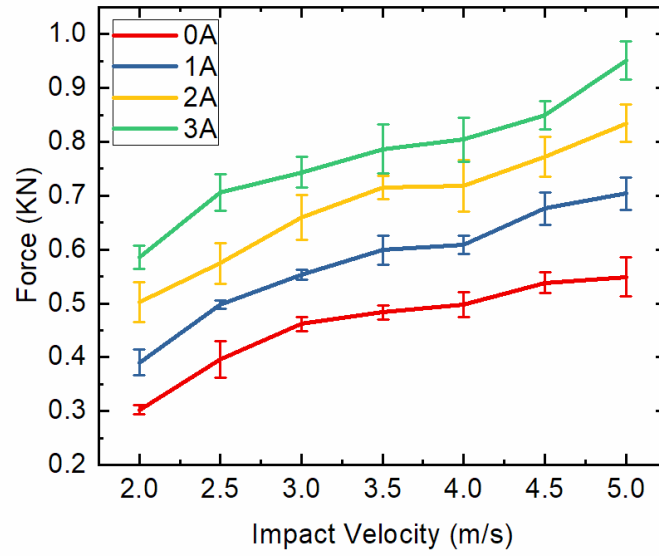


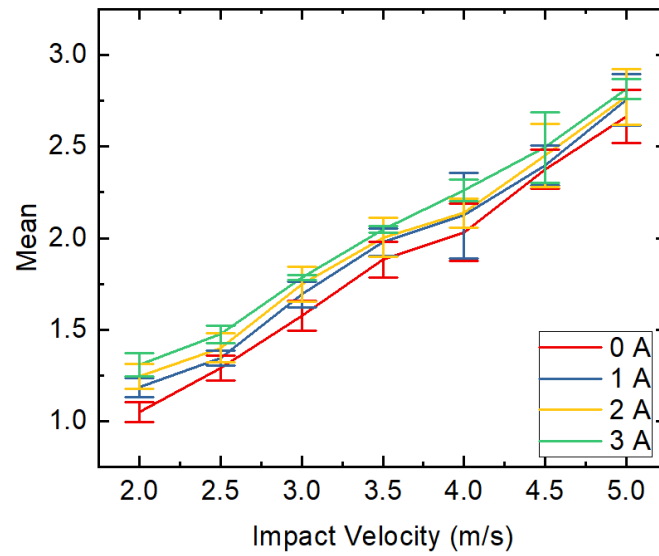
Figure 0.21 Force-time plot

In order to attain the dynamic control range of the new MR damper, the peak damper force versus impact velocity graph is generated as shown in Fig. 5.22 (a). As mention above, as a control group, the same graph is generated in Fig. 5.22 (b) as well. From the

figure, it is clear that regarding the proposed new MR damper, the peak damper force surge due to the increment of the impact velocity is much smaller than that of the traditional MR damper. Numerically, the range of force variation is about 200N in terms of the proposed damper. By contrast, the number of the conventional damper is 1500N. The excessive force generated by the conventional damper will be detrimental to passengers and mechanical structure of the target object like helicopters. Although the proposed damper could limit the growth of the peak damper force effectively, 200N is still considerable in many venues. Therefore, a control algorithm is put forward and validated in next section.



(a)



(b)

Figure 0.22 (a) The proposed MR damper; (b) The conventional damper

5.4.3 Controlled current impact tests

A bang-bang current control is integrated to a force feedback control methodology to

obtain a stable peak damper force in various impact velocities. The objective of the control method is to switch the on/off state of the given current by comparing the real-time damper force with the desired damper force, as a result, the peak damper force could almost keep stable although impact velocities change from 2m/s to 5m/s. The mathematical expression of the control algorithm could be written as:

$$Current(t) = \begin{cases} 0A & \text{if } F_{real-time}(t) > kF_{target} \\ 3A & \text{if } F_{real-time}(t) < kF_{target} \end{cases} \quad (5-9)$$

where $F_{real-time}$ denotes the real time damper force recorded by the load cell, the coefficient k represents the control gain of the control methodology, normally ranges from 0 to 1, the error generated by the MRF and current response time can be compensated by adjusting this parameter, and the F_{target} means the target damper force.

The peak damper force is supposed to retain at the target force, which means the target force must be available under any impact velocities from 2m/s to 5m/s. Hence, according to Fig. 5.22 (a), the target force must be larger than the peak damper force with 0A current and 5m/s impact velocity, smaller than the peak damper force when the current is 3A, and the impact speed is 2m/s. Otherwise, the target force cannot be achieved. Therefore, the target force was selected as 500N.

However, in real scenarios, the absolute stable force cannot be reached, some minor deviations are acceptable. Specifically, by setting an error bound of 40N, in other word, the peak damper force can be viewed as satisfied as long as it lies in the interval between 480N and 520N. By adjusting the parameter k , the peak damper force could be stable over the impact velocity from 2m/s to 5m/s. The real-time control process could be illustrated in Fig 5.23. From the figure, when impact/shock occurs, the current keeps switching the on/off state as the real time force change.

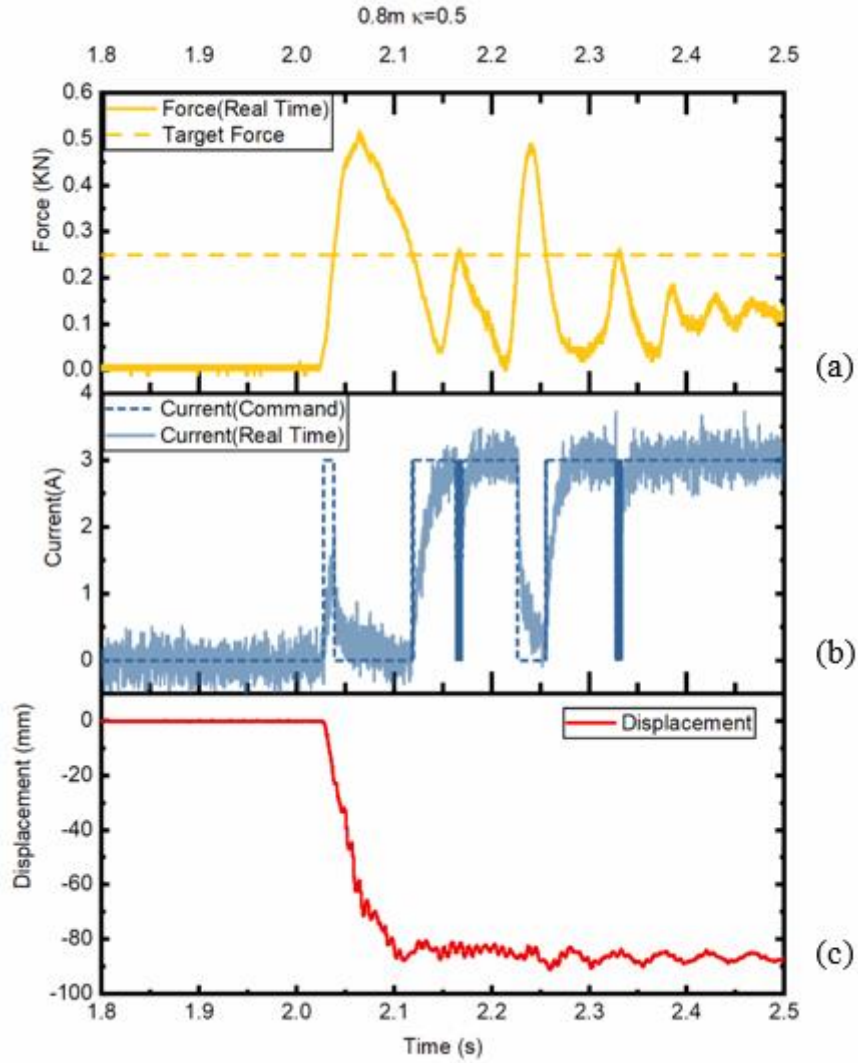


Figure 0.23 Real-time (a) Force (b) Current (c) Displacement of the control process with 4m/s impact velocity.

Besides, there is delay for current command response. Theoretically, given a fixed impact velocity, the enlargement of the coefficient k increases the peak damper force. Multiple tests have been done to confirm that under 4m/s impact velocity, the results are shown in Fig 5.24. As expected, large gain k lead to large peak damper force. Therefore, a small gain could be considered to compensate the time delay due to command response. To be specific, for a high impact velocity, the force goes up faster, (i.e. the acceleration is larger), a smaller control k could give the current command earlier to limit the peak

damper force. And the control gain selection in various impact velocities is demonstrated in Fig. 5.25. Finally, the peak damper force is almost a constant in various impact velocities, which could be seen in Fig 5.26.

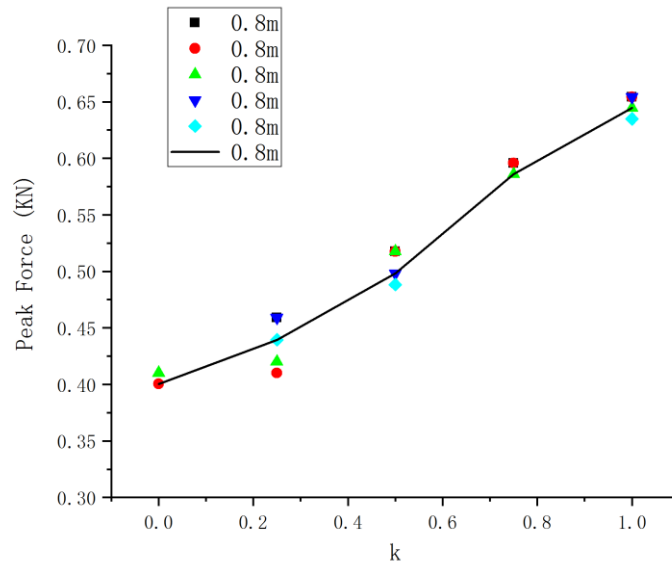


Figure 0.24 The effect of control gain k

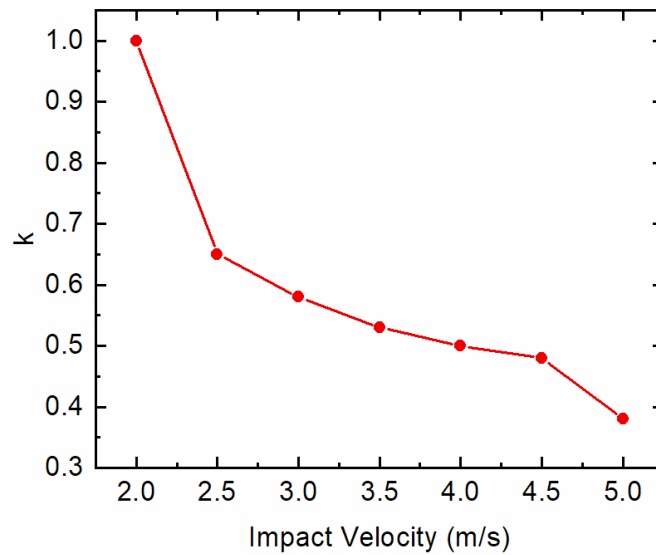


Figure 0.25 The control gain k selection

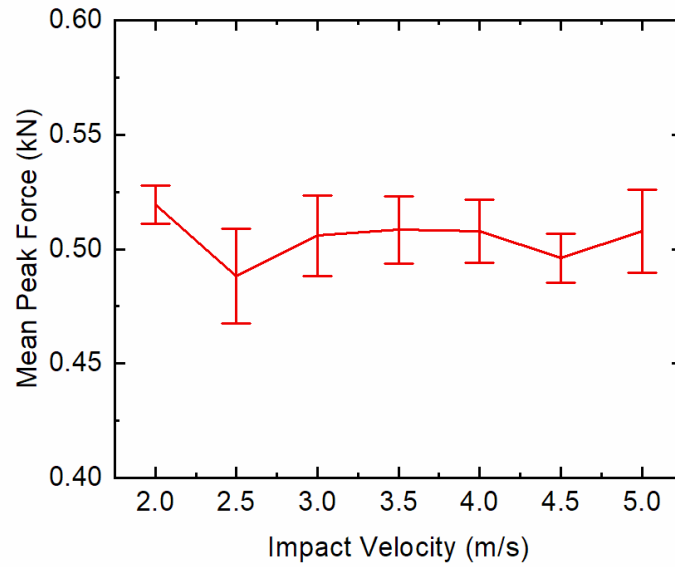


Figure 0.26 The mean peak force versus impact velocity

5.5 Conclusion

In this chapter, a new impact absorber with a low sensitivity of velocity is proposed, in accordance with MR dampers. Multiple tests have been conducted to prove the effectiveness of the MR damper. Besides, a control algorithm based on bang-bang current control to improve the capacity of the MR damper, specifically, to get a stable peak damper force in various impact velocities, in the meanwhile, capitalize on the stroke of the impact structure as far as possible, for example, 80% of the stroke. Also, comparing this novel MR damper with a conventional linear damper to validate its low sensitivity to velocity.

Chapter 6

Conclusions and future work

6.1 Summary of the semi-active MR suspension with self-powered capacity

This thesis proposed an MR damper with self-generated ability installed in a semi-active vehicle suspension. The mathematical model of the MR vehicle suspension was developed and simulated to describe the dynamic properties of the MR damper. The simulation results preliminarily demonstrate the feasibility of the concept. After the prototype of the new MR damper, the stiffness controllability and the energy generating ability were validated using a hydraulic Instron test system. To be specific, the stiffness increased by over 70% when the given current increases from 0A to 2A. In addition, under a harmonic excitation with 0.15Hz frequency and 30mm displacement, the test results show that the self-powered component could generate 2.595W effective power, which is capable to activate the MRF of the damper. Subsequently, a quarter-car test rig was built in our lab installed with the MR suspension, in order to avoid resonance and obtain the lowest transmissibility, i.e. the best damping effect, two controllers, namely, skyhook controller and STFT controller were applied to switch the on/off state of the self-powered mode. Specially, when a moderate stiffness is required to achieve a better mitigation performance, the self-powered circuit will be disconnected. Otherwise, the self-powered mode will be switched on, offering a large stiffness. Regarding the skyhook controller, the relative direction of the sprung mass velocity and the unsprung mass velocity whether the self-powered component is working or not. Multiple tests were conducted under road excitations, the evaluation results illustrate the skyhook controller could effectively reduce the response displacements and accelerations comparing with the passive mode and all-time self-powered mode. Nevertheless, the decision condition of the skyhook

controller cannot reflect the state of the suspension system accurately, besides, the velocity changes instantaneously under road excitations, the time delay of the feedback could possibly have a negative effect on the mitigation performance. Thus, the STFT controller was introduced into the suspension system, under sweep frequency excitations, a critical frequency was obtained to control the on/off of the energy generating component. Then, the evaluation results under road excitations show that the proposed MR damper integrated with STFT controller can shave the displacements and accelerations dramatically.

6.2 Summary of the semi-active MR landing gears

This thesis proposed an MR damper with a novel structure, comparing with the conventional damper, the multiple-coils structure of the new damper offers a strong controllability regarding the damping force. The MRF was accommodated in the narrow gap between the outer cylinder and the inner cylinder, although the amount of the MRF was rather less than that of the conventional dampers, the actual working amount of MRF was more on the contrary. When the structure experiences severe shock, the both sides of the MRF will move in reversed direction, causing the MRF work in shear mode. In addition, a magnetic field simulation was developed to verify that the induced magnetic field could activate the MRF. After the prototype of the MR damper, the property tests were conducted using Instron test system, the evaluation results demonstrate that the dramatic damping controllability. The mathematic model of the landing gear system was built by MATLAB/Simulink to further describe the MRF property. Moreover, an impact structure consists the proposed MR damper, supporting frame, laser sensor, and load cell was established. Multiple impact tests were carried on to obtain the damping force variation under varied velocities and currents. The experimental results illustrate that the increment of damping force due to the increase of the impact velocities is smaller than

that of conventional MR damper, which gives a relatively smooth damping growth to protect the passengers and the aircraft structures from severe damage. In order to keep the damping force constant under distinct impact velocity, based on bang-bang current control, a control algorithm was proposed to introduce a parameter called control gain. By adjusting the control gain, an almost constant damping force at diverse impact velocities was realized. The evaluation results validate the feasibility of the proposed MR damper with the control algorithm, the damping force could be kept at approximately 500N over the sink rate from 2m/s to 5m/s.

6.3 Future work of the semi-active MRF vehicle suspension

As presented in Chapter 4.7, the proposed skyhook controller may have a negative effect due to feedback time delay. Thus, an improved skyhook control strategy, a new optimized method on the basis of the skyhook strategy should be proposed. As it can be seen from above that the skyhook control strategy uses the speed sensor to identify the relative movement trend (same direction or different direction) of the objects at both ends of the spring to determine whether to adjust the suspension system mode, thereby changing the spring stiffness to adapt to the environmental conditions. Following this line of thought, we increased the working mode of the system from the original two to a variety of types (three in this thesis) and increase the condition of relative motion correspondingly. Doing so can not only reduce the switching steps of each condition, which can reduce the delay time and make the system more stable during mode switching, but also make full use of the two sets of coil power supply characteristic of the new damper used in this thesis. To be more specific, the two sets of coil power supply can be selected to provide half power supply or full power supply, the idea is to find the average value of the negative velocity product data ($-0.0037\text{m}^2/\text{s}^2$) and use full power supply mode when the product of velocity is negatively large while transform to half power supply if the negative velocity product

value is relatively small.

To achieve this theory, another MOSFET switch is used in the experiment so that each switch can control one certain group of coil power supply, the prototype of the entire circuit for the MOSFET switch is displayed in Figure 4.20. As soon as the product of velocity meet the condition, the DAQ will provide 10V PWM signal to the MOSFET switch so that it will be triggered on and half of the voltage produced by the self-powered generation part will supply to the system and adjust the spring stiffness.

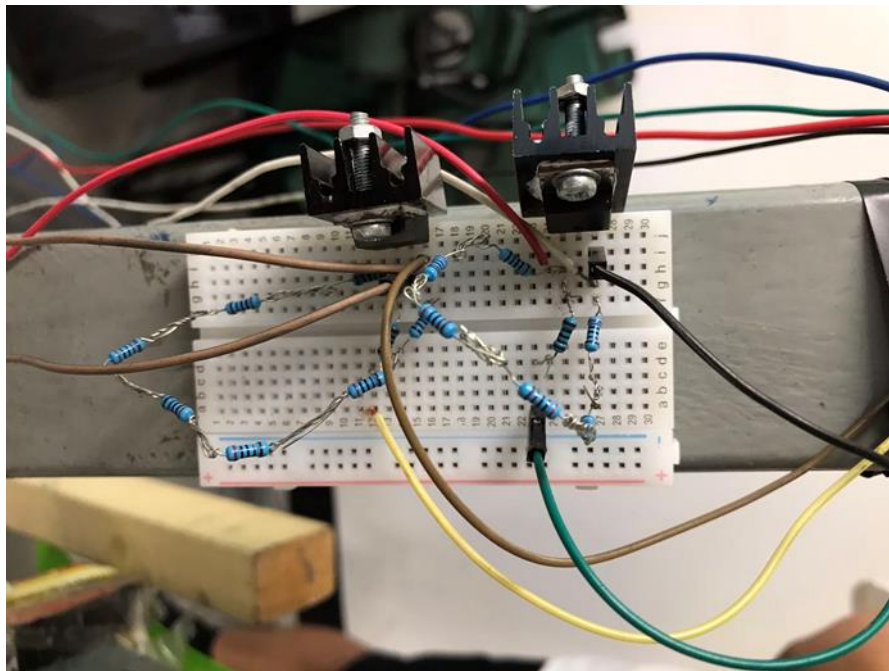


Figure 0.1 Prototype of the MOSFET switch circuit in improved Skyhook control strategy

So, the judgment sentence of improved Skyhook control strategy can be expressed as:

$$\left\{ \begin{array}{ll} \dot{z}_s * \dot{z}_u \geq 0 & 0V \\ -0.0037 < \dot{z}_s * \dot{z}_u < 0 & V_1 = +10V \\ \dot{z}_s * \dot{z}_u < -0.0037 & V_1 = +10V, V_2 = +10V \end{array} \right. \quad (6-1)$$

where z_s, z_u is the displacement of the sprung mass and unsprung mass. The derivative of the displacements are the speeds of two sides of the damper, which are the parameters

used to record the motion of the spring. V_1, V_2 are two 10V PWM signals to control the working mode of the suspension system. And the operation flow diagram of the improved Skyhook control strategy is shown in Figure 4.21.

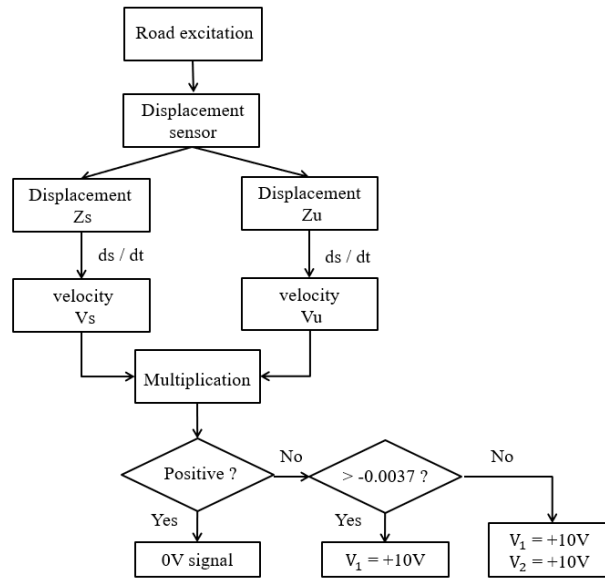


Figure 0.2 Operation flow diagram of the improved Skyhook control strategy

To sum up, in further investigation, the feasibility of the improved skyhook controller will be evaluated by both simulation and experimental results.

6.4 Future work of the semi-active MRF landing gear

For the semi-active MRF landing gear, the control gain values under different impact velocities were obtained by plenty of impact tests and manual adjustments. When this design is applied in a real scene, the values of the control gain requires abundant measurements and tunings using large-scale landing gears, which will consume lots of manpower, time, and money. Therefore, the expectation of the next study is to obtain the relationship between control gain and impact velocities through more lab-scale experiments to achieve an automatic control gain tuning according to the impact velocities.

References

- [1] A. Naude, J. Snyman, Optimisation of road vehicle passive suspension systems. Part 1. Optimisation algorithm and vehicle model, *Applied Mathematical Modelling*, 27 (2003) 249-261.
- [2] M. Nagai, A. Moran, Y. Tamura, S. Koizumi, Identification and control of nonlinear active pneumatic suspension for railway vehicles, using neural networks, *Control Engineering Practice*, 5 (1997) 1137-1144.
- [3] S. Sun, X. Tang, W. Li, H. Du, Advanced vehicle suspension with variable stiffness and damping MR damper, 2017 IEEE International Conference on Mechatronics (ICM), IEEE, 2017, pp. 444-448.
- [4] G. Priyandoko, M. Mailah, H. Jamaluddin, Vehicle active suspension system using skyhook adaptive neuro active force control, *Mechanical systems and signal processing*, 23 (2009) 855-868.
- [5] M. Jonasson, F. Roos, Design and evaluation of an active electromechanical wheel suspension system, *Mechatronics*, 18 (2008) 218-230.
- [6] K.-G. Sung, Y.-M. Han, J.-W. Cho, S.-B. Choi, Vibration control of vehicle ER suspension system using fuzzy moving sliding mode controller, *Journal of Sound and Vibration*, 311 (2008) 1004-1019.
- [7] X. Tang, H. Du, S. Sun, D. Ning, Z. Xing, W. Li, Takagi–Sugeno fuzzy control for semi-active vehicle suspension with a magnetorheological damper and experimental validation, *IEEE/ASME transactions on mechatronics*, 22 (2016) 291-300.
- [8] U. Solomon, C. Padmanabhan, Semi-active hydro-gas suspension system for a tracked vehicle, *Journal of Terramechanics*, 48 (2011) 225-239.
- [9] T. Gordon, Non-linear optimal control of a semi-active vehicle suspension system, *Chaos, Solitons & Fractals*, 5 (1995) 1603-1617.

- [10] W. Hongjun, T. Ailing, T. Qian, C. ZHILI, L. BINGCAI, Research on rheological property of magnetorheological fluid, Proceedings of SPIE, the International Society for Optical Engineering, 2008, pp. 672230.672231-672230.672235.
- [11] P. Kuzhir, M. López-López, G. Bossis, Abrupt contraction flow of magnetorheological fluids, Physics of Fluids, 21 (2009) 053101.
- [12] C. Miao, K.M. Bristol, A.E. Marino, S.N. Shafrir, J.E. DeGroote, S.D. Jacobs, Magnetorheological fluid template for basic studies of mechanical-chemical effects during polishing, Optical Manufacturing and Testing VII, International Society for Optics and Photonics, 2007, pp. 667110.
- [13] S.-W. Cho, H.-J. Jung, I.-W. Lee, Smart passive system based on magnetorheological damper, Smart Materials and Structures, 14 (2005) 707.
- [14] J.D. Carlson, M.R. Jolly, MR fluid, foam and elastomer devices, mechatronics, 10 (2000) 555-569.
- [15] J.D. Carlson, Critical factors for MR fluids in vehicle systems, International Journal of Vehicle Design, 33 (2003) 207-217.
- [16] G. Tsampardoukas, C.W. Stammers, E. Guglielmino, Hybrid balance control of a magnetorheological truck suspension, Journal of Sound and Vibration, 317 (2008) 514-536.
- [17] M. Yu, X. Dong, S.B. Choi, C. Liao, Human simulated intelligent control of vehicle suspension system with MR dampers, Journal of Sound and Vibration, 319 (2009) 753-767.
- [18] J.N. Potter, S.A. Neild, D.J. Wagg, Quasi-active suspension design using magnetorheological dampers, Journal of sound and vibration, 330 (2011) 2201-2219.
- [19] X. Dong, Design and characterization of axial flux permanent magnet energy harvester for vehicle magnetorheological damper, Smart Materials and Structures, 25

(2015) 015024.

[20] L. Segel, X. Lu, Vehicular resistance to motion as influenced by road roughness and highway alignment, *Australian road research*, 12 (1982) 211-222.

[21] S. Choi, M. Seong, K. Kim, Vibration control of an electrorheological fluid-based suspension system with an energy regenerative mechanism, *Proceedings of the Institution of Mechanical Engineers, Part D: Journal of Automobile Engineering*, 223 (2009) 459-469.

[22] B. Sapiński, Vibration power generator for a linear MR damper, *Smart Materials and Structures*, 19 (2010) 105012.

[23] Y.-T. Choi, N.M. Wereley, Self-powered magnetorheological dampers, *Journal of Vibration and Acoustics*, 131 (2009).

[24] B. Sapiński, Energy-harvesting linear MR damper: prototyping and testing, *Smart Materials and Structures*, 23 (2014) 035021.

[25] K.-M. Choi, H.-J. Jung, H.-J. Lee, S.-W. Cho, Feasibility study of an MR damper-based smart passive control system employing an electromagnetic induction device, *Smart Materials and Structures*, 16 (2007) 2323.

[26] S. Sun, H. Deng, W. Li, Variable stiffness and damping suspension system for train, *Active and Passive Smart Structures and Integrated Systems 2014*, International Society for Optics and Photonics, 2014, pp. 90570P.

[27] G.Y. Pan, F.Q. Fan, Research on semi-active suspension system with variable stiffness and damping, *Applied Mechanics and Materials*, Trans Tech Publ, 2012, pp. 584-589.

[28] K.K. Walsh, K.D. Grupenhof, K.L. Little, A. Martin, C.A. Moore Jr, Development and testing of a newly proposed continuously variable stiffness/damping device for vibration control, *Sensors and Smart Structures Technologies for Civil, Mechanical,*

and Aerospace Systems 2012, International Society for Optics and Photonics, 2012, pp. 83452N.

[29] J. Rabinow, The magnetic fluid clutch, *Electrical Engineering*, 67 (1948) 1167-1167.

[30] N. Wereley, A. Chaudhuri, J.-H. Yoo, S. John, S. Kotha, A. Suggs, R. Radhakrishnan, B. Love, T. Sudarshan, Bidisperse magnetorheological fluids using Fe particles at nanometer and micron scale, *Journal of Intelligent Material Systems and Structures*, 17 (2006) 393-401.

[31] D. Lee, Y. Nam, R. Yamane, M. Park, Performance evaluation on vibration control of MR landing gear, *Journal of Physics: Conference Series*, IOP Publishing, 2009, pp. 012068.

[32] F.D. Goncalves, J.D. Carlson, Investigating the time dependence of the MR effect, *International Journal of Modern Physics B*, 21 (2007) 4832-4840.

[33] F.D. Goncalves, J.-H. Koo, M. Ahmadian, A review of the state of the art in magnetorheological fluid technologies--Part I: MR fluid and MR fluid models, *The Shock and Vibration Digest*, 38 (2006) 203-220.

[34] K.D. Weiss, T.G. Duclos, Controllable fluids: the temperature dependence of post-yield properties, *International Journal of Modern Physics B*, 8 (1994) 3015-3032.

[35] Q.-H. Nguyen, S.-B. Choi, Optimal design methodology of magnetorheological fluid based mechanisms, *Smart Actuation and Sensing Systems--Recent Advances and Future Challenges*, DOI (2012) 347-382.

[36] A. Farjoud, R. Cavey, M. Ahmadian, M. Craft, Magneto-rheological fluid behavior in squeeze mode, *Smart Materials and Structures*, 18 (2009) 095001.

[37] M.T. Avraam, MR-fluid brake design and its application to a portable muscular rehabilitation device, *Universite Libre de Bruxelles*, DOI (2009).

- [38] R. Ahamed, S.-B. Choi, M.M. Ferdous, A state of art on magneto-rheological materials and their potential applications, *Journal of Intelligent Material Systems and Structures*, 29 (2018) 2051-2095.
- [39] D. Wang, W.H. Liao, Magnetorheological fluid dampers: a review of parametric modelling, *Smart materials and structures*, 20 (2011) 023001.
- [40] M.R. Jolly, J.W. Bender, J.D. Carlson, Properties and applications of commercial magnetorheological fluids, *Journal of intelligent material systems and structures*, 10 (1999) 5-13.
- [41] R. Stanway, J. Sproston, A. El-Wahed, Applications of electro-rheological fluids in vibration control: a survey, *Smart Materials and Structures*, 5 (1996) 464.
- [42] K. Wilson, A. Thomas, Analytic Model of Laminar-Turbulent Transition for Bingham Plastics, *The Canadian Journal of Chemical Engineering*, 84 (2006) 520-526.
- [43] X. Wang, F. Gordaninejad, Flow analysis and modeling of field-controllable, electro-and magneto-rheological fluid dampers, *Journal of Applied Mechanics*, 74 (2005) 13-22.
- [44] Y. Choi, J. Cho, S. Choi, N. Wereley, Constitutive models of electrorheological and magnetorheological fluids using viscometers, *Smart materials and structures*, 14 (2005) 1025.
- [45] Z. Parlak, T. Engin, İ. Şahin, Optimal magnetorheological damper configuration using the Taguchi experimental design method, *Journal of Mechanical Design*, 135 (2013).
- [46] B. Avinash, S.S. Sundar, K. Gangadharan, Experimental study of damping characteristics of air, silicon oil, magneto rheological fluid on twin tube damper, *Procedia Materials Science*, 5 (2014) 2258-2262.
- [47] Q. Wang, M. Ahmadian, Z. Chen, A novel double-piston magnetorheological

damper for space truss structures vibration suppression, *Shock and Vibration*, 2014 (2014).

[48] J.C. Poynor, Innovative designs for magneto-rheological dampers, Virginia Tech, 2001.

[49] J.W. Sohn, J.-S. Oh, S.-B. Choi, Design and novel type of a magnetorheological damper featuring piston bypass hole, *Smart Materials and Structures*, 24 (2015) 035013.

[50] H. Hong, S. Tang, Y. Sheng, Q. Cui, Magnetic circuit design and computation of a magnetorheological damper with exterior coil, 2015 IEEE international conference on mechatronics and automation (ICMA), IEEE, 2015, pp. 60-64.

[51] K. Kim, Z. Chen, D. Yu, C. Rim, Design and experiments of a novel magneto-rheological damper featuring bifold flow mode, *Smart Materials and Structures*, 25 (2016) 075004.

[52] N. Wereley, J. Cho, Y. Choi, S. Choi, Magnetorheological dampers in shear mode, *Smart Materials and Structures*, 17 (2007) 015022.

[53] A. Alghamdi, A. Olabi, Novel design concept of magneto rheological damper in squeeze mode, *International conference on experimental mechanics*, 2012.

[54] I.I. Yazid, S.A. Mazlan, T. Kikuchi, H. Zamzuri, F. Imaduddin, Magnetic circuit optimization in designing magnetorheological damper, *Smart Structures and Systems*, 14 (2014) 869-881.

[55] S. Ali, A. Ramaswamy, Testing and modeling of MR damper and its application to SDOF systems using integral backstepping technique, *Journal of Dynamic Systems, Measurement, and Control*, 131 (2009).

[56] G. Hu, F. Liu, Z. Xie, M. Xu, Design, analysis, and experimental evaluation of a double coil magnetorheological fluid damper, *Shock and Vibration*, 2016 (2016).

[57] H.J. Singh, N.M. Wereley, Optimal control of gun recoil in direct fire using

magnetorheological absorbers, *Smart materials and Structures*, 23 (2014) 055009.

[58] X.-X. Bai, N.M. Wereley, W. Hu, Maximizing semi-active vibration isolation utilizing a magnetorheological damper with an inner bypass configuration, *Journal of Applied Physics*, 117 (2015) 17C711.

[59] M. Unsal, Semi-active vibration control of a parallel platform mechanism using magnetorheological damping, University of Florida 2006.

[60] Y. Lau, W. Liao, Design and analysis of magnetorheological dampers for train suspension, *Proceedings of the Institution of Mechanical Engineers, Part F: Journal of Rail and Rapid Transit*, 219 (2005) 261-276.

[61] M. Brigley, Y.-T. Choi, N.M. Wereley, S.-B. Choi, Magnetorheological isolators using multiple fluid modes, *Journal of Intelligent Material Systems and Structures*, 18 (2007) 1143-1148.

[62] M. Schwartz, *Smart materials*, CRC press 2008.

[63] Y.-J. Nam, M.-K. Park, Performance evaluation of two different bypass-type MR shock dampers, *Journal of intelligent material systems and structures*, 18 (2007) 707-717.

[64] W. Hu, R. Robinson, N.M. Wereley, A design strategy for magnetorheological dampers using porous valves, *Journal of Physics: Conference Series*, IOP Publishing, 2009, pp. 012056.

[65] H. Sodeyama, K. Sunakoda, H. Fujitani, S. Soda, N. Iwata, K. Hata, Dynamic tests and simulation of magneto-rheological dampers, *Computer-Aided Civil and Infrastructure Engineering*, 18 (2003) 45-57.

[66] H. Sodeyama, K. Suzuki, K. Sunakoda, Development of large capacity semi-active seismic damper using magneto-rheological fluid, *J. Pressure Vessel Technol.*, 126 (2004) 105-109.

- [67] G. Yang, B. Spencer Jr, J. Carlson, M. Sain, Large-scale MR fluid dampers: modeling and dynamic performance considerations, *Engineering structures*, 24 (2002) 309-323.
- [68] J.A. Norris, M. Ahmadian, Behavior of magneto-rheological fluids subject to impact and shock loading, *ASME International Mechanical Engineering Congress and Exposition*, 2003, pp. 199-204.
- [69] F.D. Goncalves, M. Ahmadian, J. Carlson, Investigating the magnetorheological effect at high flow velocities, *Smart Materials and Structures*, 15 (2005) 75.
- [70] J.D. Carlson, W. Matthis, J.R. Toscano, Smart prosthetics based on magnetorheological fluids, *Smart structures and materials 2001: industrial and commercial applications of smart structures technologies*, International Society for Optics and Photonics, 2001, pp. 308-316.
- [71] Q.-H. Nguyen, S.-B. Choi, N.M. Wereley, Optimal design of magnetorheological valves via a finite element method considering control energy and a time constant, *Smart Materials and Structures*, 17 (2008) 025024.
- [72] I. Maciejewski, T. Krzyżyński, Control design of semi-active seat suspension systems, *Journal of Theoretical and Applied Mechanics*, 49 (2011) 1151-1168.
- [73] W.S. Aboud, S.M. Haris, Y. Yaacob, Advances in the control of mechatronic suspension systems, *Journal of Zhejiang University SCIENCE C*, 15 (2014) 848-860.
- [74] L. Zuo, P.-S. Zhang, Energy harvesting, ride comfort, and road handling of regenerative vehicle suspensions, *Journal of Vibration and Acoustics*, 135 (2013).
- [75] P.W. Nugroho, W. Li, H. Du, G. Alici, J. Yang, An adaptive neuro fuzzy hybrid control strategy for a semiactive suspension with magneto rheological damper, *Advances in Mechanical Engineering*, 6 (2014) 487312.
- [76] K. Yi, B. Song, A new adaptive sky-hook control of vehicle semi-active

suspensions, Proceedings of the Institution of Mechanical Engineers, part D: Journal of automobile engineering, 213 (1999) 293-303.

[77] C. Poussot-Vassal, C. Spelta, O. Sename, S.M. Savaresi, L. Dugard, Survey and performance evaluation on some automotive semi-active suspension control methods: A comparative study on a single-corner model, Annual Reviews in Control, 36 (2012) 148-160.

[78] M. Crosby, D.C. Karnopp, The active damper: a new concept for shock and vibration control, Shock and Vibration Bulletin, 43 (1973) 119-133.

[79] H.E. Tseng, D. Hrovat, State of the art survey: active and semi-active suspension control, Vehicle system dynamics, 53 (2015) 1034-1062.

[80] E. Guglielmino, T. Sireteanu, C.W. Stammers, G. Ghita, M. Giuclea, Semi-active suspension control: improved vehicle ride and road friendliness, Springer Science & Business Media 2008.

[81] O. Altet, X. Moreau, M. Moze, P. Lanusse, A. Oustaloup, Principles and synthesis of hydractive CRONE suspension, Nonlinear Dynamics, 38 (2004) 435-459.

[82] R. Gehm, Delphi improves cadillac's ride, Automotive Engineering International, 109 (2001) 32-33.

[83] R.N. Jazar, Vehicle dynamics: theory and application, Springer 2017.

[84] J.-K. Ok, D.-W. Park, W.-S. Yoo, J.-H. Sohn, Development of a new bushing model for vehicle suspension module design, Transactions of the Korean Society of Automotive Engineers, 14 (2006) 143-150.

[85] A. Giua, C. Seatzu, G. Usai, A mixed suspension system for a half-car vehicle model, Dynamics and Control, 10 (2000) 375-397.

[86] K.-S. Hong, D.-S. Jeon, W.-S. Yoo, H. Sunwoo, S.-Y. Shin, C.-M. Kim, B.-S. Park, A new model and an optimal pole-placement control of the Macpherson

suspension system, SAE transactions, 108 (1999) 2452-2461.

[87] J. Hurel, A. Mandow, A. García-Cerezo, Nonlinear two-dimensional modeling of a McPherson suspension for kinematics and dynamics simulation, 2012 12th IEEE International Workshop on Advanced Motion Control (AMC), IEEE, 2012, pp. 1-6.

[88] J. Hurel, A. Mandow, A. García-Cerezo, Kinematic and dynamic analysis of the McPherson suspension with a planar quarter-car model, Vehicle System Dynamics, 51 (2013) 1422-1437.

[89] A. Mahir, S.P. Deng, Y. Qi, Gantry robot dynamic analysis based on Lagrange's motion equation, Key Engineering Materials, Trans Tech Publ, 2016, pp. 1741-1746.

[90] M. Ahmadian, C.A. Pare, A quarter-car experimental analysis of alternative semiactive control methods, Journal of Intelligent Material Systems and Structures, 11 (2000) 604-612.

[91] S. Türkay, H. Akçay, A study of random vibration characteristics of the quarter-car model, Journal of sound and vibration, 282 (2005) 111-124.

[92] H. Jung, D. Jang, S. Cho, J. Koo, Experimental verification of sensing capability of an electromagnetic induction system for an MR fluid damper-based control system, Journal of Physics: Conference Series, IOP Publishing, 2009, pp. 012058.

[93] H.-J. Jung, D.-D. Jang, H.-J. Lee, I.-W. Lee, S.-W. Cho, Feasibility test of adaptive passive control system using MR fluid damper with electromagnetic induction part, Journal of engineering mechanics, 136 (2010) 254-259.

[94] C. Chen, W.-H. Liao, A self-powered, self-sensing magnetorheological damper, 2010 IEEE International Conference on Mechatronics and Automation, IEEE, 2010, pp. 1364-1369.

[95] L.G. Horta, R.H. Daugherty, V.J. Martinson, Modeling and validation of a Navy A6-Intruder actively controlled landing gear system, DOI (1999).

- [96] I. Ross, An electronic control for an electrohydraulic active control landing gear for the F-4 aircraft, DOI (1982).
- [97] Y. Kushida, S. Hara, M. Otsuki, Y. Yamada, T. Hashimoto, T. Kubota, Robust landing gear system based on a hybrid momentum exchange impact damper, *Journal of Guidance, Control, and Dynamics*, 36 (2013) 776-789.
- [98] H. Wang, J. Xing, W. Price, W. Li, An investigation of an active landing gear system to reduce aircraft vibrations caused by landing impacts and runway excitations, *Journal of Sound and vibration*, 317 (2008) 50-66.
- [99] J.-Y. Yoon, B.-H. Kang, J.-H. Kim, S.-B. Choi, New control logic based on mechanical energy conservation for aircraft landing gear system with magnetorheological dampers, *Smart Materials and Structures*, 29 (2020) 084003.
- [100] Y.-T. Choi, N.M. Wereley, Vibration control of a landing gear system featuring electrorheological/magnetorheological fluids, *Journal of aircraft*, 40 (2003) 432-439.
- [101] C. Han, B.-H. Kang, S.-B. Choi, J.M. Tak, J.-H. Hwang, Control of landing efficiency of an aircraft landing gear system with magnetorheological dampers, *Journal of Aircraft*, 56 (2019) 1980-1986.
- [102] X. Dong, G. Xiong, Vibration attenuation of magnetorheological landing gear system with human simulated intelligent control, *Mathematical Problems in Engineering*, 2013 (2013).
- [103] A.A. Gharapurkar, A.F. Jahromi, R.B. Bhat, W.-F. Xie, Semi-active control of aircraft landing gear system using H-infinity control approach, 2013 International Conference on Connected Vehicles and Expo (ICCVE), IEEE, 2013, pp. 679-686.
- [104] D. Karnopp, Active damping in road vehicle suspension systems, *Vehicle System Dynamics*, 12 (1983) 291-311.
- [105] H.-S. Lee, S.-B. Choi, Control and response characteristics of a magneto-

rheological fluid damper for passenger vehicles, *Journal of Intelligent Material Systems and Structures*, 11 (2000) 80-87.

[106] D.E. Simon, Experimental evaluation of semiactive magnetorheological primary suspensions for heavy truck applications, Virginia Tech, 1998.

[107] C.A. Pare, Experimental evaluation of semiactive magneto-rheological suspensions for passenger vehicles, Virginia Tech, 1998.

[108] F.D. Goncalves, M. Ahmadian, A hybrid control policy for semi-active vehicle suspensions, *Shock and Vibration*, 10 (2003) 59-69.

[109] E. Sejdić, I. Djurović, J. Jiang, Time–frequency feature representation using energy concentration: An overview of recent advances, *Digital signal processing*, 19 (2009) 153-183.

[110] S. Narasimhan, S. Nagarajaiah, A STFT semiactive controller for base isolated buildings with variable stiffness isolation systems, *Engineering structures*, 27 (2005) 514-523.

[111] Z.-D. Xu, Y.-Q. Guo, J.-T. Zhu, F.-H. Xu, *Intelligent Vibration Control in Civil Engineering Structures*, Academic Press 2016.

[112] L. Palkovics, J. Bokor, P. Venhovens, Design problems of the semi-active wheel suspension system and a possible way of their elimination, DOI (1994).

[113] M. Yokoyama, J.K. Hedrick, S. Toyama, A model following sliding mode controller for semi-active suspension systems with MR dampers, *Proceedings of the 2001 American Control Conference*.(Cat. No. 01CH37148), IEEE, 2001, pp. 2652-2657.

[114] S. Choi, Y.T. Choi, D. Park, A sliding mode control of a full-car electrorheological suspension system via hardware in-the-loop simulation, *J. Dyn. Sys., Meas., Control*, 122 (2000) 114-121.

- [115] L.A. Zadeh, Fuzzy sets, *Information and control*, 8 (1965) 338-353.
- [116] A.M. Tusset, M. Rafikov, J.M. Balthazar, An intelligent controller design for magnetorheological damper based on a quarter-car model, *Journal of Vibration and Control*, 15 (2009) 1907-1920.
- [117] M.N. Khajavi, V. Abdollahi, Comparison between optimized passive vehicle suspension system and semi active fuzzy logic controlled suspension system regarding ride and handling, *Proceedings of world academy of science, engineering and technology*, 2007, pp. 57-61.
- [118] D.S. Joe, N. Al-Holou, Development and evaluation of fuzzy logic controller for vehicle suspension systems, *Proceedings of the Twenty-Seventh Southeastern Symposium on System Theory*, IEEE, 1995, pp. 295-299.
- [119] M.J. Craft, Design optimization of MagneShock magnetorheological shock absorbers and development of fuzzy logic control algorithms for semi-active vehicle suspensions, North Carolina State University, 2004.
- [120] A. Hać, Stochastic optimal control of vehicles with elastic body and active suspension, *Trans. ASME, Dynamic Systems, Measurement, and Control*, 108 (1986) 106-110.
- [121] N.T. Nguyen, Model-reference adaptive control, *Model-Reference Adaptive Control*, Springer 2018, pp. 83-123.
- [122] X. Feng, C.-F. Lin, T.-J. Yu, N. Coleman, X. Feng, C.-F. Lin, T.-J. Yu, N. Coleman, Intelligent control design and simulation using neural networks, *Guidance, Navigation, and Control Conference*, 1997, pp. 3528.
- [123] S. Sun, J. Yang, W. Li, H. Deng, H. Du, G. Alici, Development of a novel variable stiffness and damping magnetorheological fluid damper, *Smart Materials and Structures*, 24 (2015) 085021.

- [124] S. Nagarajaiah, N. Varadarajan, Short time Fourier transform algorithm for wind response control of buildings with variable stiffness TMD, *Engineering Structures*, 27 (2005) 431-441.
- [125] G.K. Sharma, A. Kumar, C.B. Rao, T. Jayakumar, B. Raj, Short time Fourier transform analysis for understanding frequency dependent attenuation in austenitic stainless steel, *NDT & E International*, 53 (2013) 1-

Publications during the PhD candidature

- 1 **X. Zhu**, L. Deng, S. S. Sun, T. Yan, J. Yu, Z. Ma, and W. H. Li, Development of a variable stiffness magnetorheological damper with self-generation capacity, *Journal of Intelligent Material Systems and Structures*, 31, 209-219, 2019.
- 2 **X. Zhu**, D. Ning, Z. Hao, H. Huang, Y. Z. Sun, H. Jia, S. S. Sun, T. Yan, and W. H. Li, Modelling and experimental evaluation of a variable stiffness MR suspension with self-powering capability, *Journal of Intelligent Material Systems and Structures*, DOI 10.1045389X2098699, 2021.
- 3 Y. Yang, Y. Pan, **X. Zhu**, M. Gao, J. Zhang, and D. Tao, A human-like dual-forklift collaborative mechanism for container handling, *IEEE Transactions on Industrial Electronics*, DOI 10.1109/TIE.2020.3044788, 2020.
- 4 S. S. Sun, J. Yang, T. Yildirim, D. Ning, **X. Zhu**, H. Du, S. Zhang, M. Nakano, and W.H. Li, A magnetorheological elastomer rail damper for wideband attenuation of rail noise and vibration, *Journal of Intelligent Material Systems and Structures*, 31, 220-228, 2019.
- 5 L. Deng, S. S. Sun, MD. Christie, J. Yang, D. Ning, **X. Zhu**, H. Du, S. Zhang, and W. H. Li, Experimental testing and modelling of a rotary variable stiffness and damping shock absorber using magnetorheological technology, *Journal of Intelligent Material Systems and Structures*, 30, 1453-1465, 2019.
- 6 Poster ‘Design, modelling, and testing of semi-active MRF impact absorber’, Poster session, The 17th international conference on electroheological fluid and magnetorheological suspensions (ERMRS 2019).